December 2021

Toward Carbon Neutrality: The Modeling and Implementation of an Algal Carbon Capture System

Elizabeth Zanin Flanagan
Clemson University, ezanin@g.clemson.edu

TOWARD CARBON NEUTRALITY: THE MODELING AND IMPLEMENTATION OF AN ALGAL CARBON CAPTURE SYSTEM

A Thesis
Presented to
the Graduate School of
Clemson University

In Partial Fulfillment
of the Requirements for the Degree
Master of Science
Biosystems Engineering

---

by
Elizabeth Zanin Flanagan
December 2021

Accepted by:
Dr. Caye Drapcho, Chair
Dr. William Bridges
Dr. Terry Walker
Dr. Mary Katherine Watson

ABSTRACT

Carbon dioxide (CO_2) emissions from anthropogenic sources are causing widespread ecological disruptions. The uptake of CO_2 by aquatic photoautotrophs is one strategy for carbon capture to mitigate these emissions. The objectives of this thesis were to investigate carbonate chemistry and algal growth equations to improve MATLAB model predictive capability in a closed-reactor system and to develop, design, and evaluate a non-fossil fuel technology and strategy for operation of the Algal Carbon Capture System (ACCS).

A dynamic growth model based on carbon-limited algal specific growth rate with Monod kinetics, considering CO_2, bicarbonate (HCO_3), and carbonate (CO_3^{2-}) as substitutable substrates, provided the best estimates for algal biomass in closed-reactors. Total inorganic carbon (TIC), CO_2, HCO_3^-, CO_3^{2-}, pH, and alkalinity were also well predicted. This model improves upon those reviewed by incorporating kinetic rates of inorganic carbon species interconversion instead of the equilibrium assumption. Discrepancies in rate constants of the bicarbonate hydroxylation reaction indicate more exploration of these parameters is needed. Here is proposed the use of the geometric mean (2.25×10^8 $M^{-1} \cdot s^{-1}$) for the forward rate constant. Underprediction of algal biomass and improved response of $CO_2/HCO_3^-/CO_3^{2-}$ substitutable model over the CO_2/HCO_3^- substitutable may indicate an unknown biological pathway for the use of carbonate for growth.

An airlift pump prototype was designed, built, implemented, and tested at the ACCS to create water flow in one raceway channel as a demonstration of the concept.

The airlift operates solely on available solar power and provides at its outlet a water velocity of 12.5 cm/s, and an average channel velocity of 1.02 ± 0.15 cm/s as the surface kinetic energy is distributed throughout the channel depth.

DEDICATION

This thesis is dedicated to my husband, William Flanagan, for his continued love and support of my every endeavor. As well as my parents, Frank and Kathy Zanin for their constant encouragement and commitment to my education. And lastly, to Mother Earth, thank you for sustaining me, and I hope this work brings us all one step closer to restoring your balance.

ACKNOWLEDGEMENTS

Thank you to my committee members for your contributions to my thesis work and master's education. Especially to my committee chair, Dr. Caye Drapcho, thank you for sharing your guidance, knowledge, and passion throughout my undergraduate and graduate studies. I feel very fortunate to have had the opportunity to study under your advisership. To Dr. Mary Katherine Watson, whose work preceded this thesis, thank you for setting a crucial foundation for this work and your words of advice.

I want to thank the Department of Environmental Engineering and Earth Sciences and the National Science Foundation's Resilient Infrastructure and Environmental Systems Program for their financial support. For technical support, I would like to thank Rodney Morgan and Rodney Merck of the Department of Environmental Engineering and Earth Sciences for their crucial fabrication skills. I want to thank Gianfranco Esteves, Mary Fran Burnett, and Alex Kasko, undergraduate students in Biosystems Engineering, for research support. To Scott Brame, for the instruction and use of his pygmy meter. And lastly, I would like to thank William Flanagan for his fabrication support.

TABLE OF CONTENTS

Page

Table of Contents (Continued)

Page

Table of Contents (continued)

Page

LIST OF TABLES

LIST OF FIGURES

List of Figures (Continued)

Figure Page

List of Figures (Continued)

Figure Page

List of Figures (Continued)

Figure Page

List of Figures (Continued)

Figure Page

CHAPTER I: INTRODUCTION

Introduction

Carbon dioxide (CO_2) emissions from anthropogenic sources are causing widespread ecological disruptions. The diffusion of gaseous CO_2 into seawater has caused an oceanic decrease of 0.1 pH unit since the last 1980s due to the formation of carbonic acid (IPCC, 2019). The uptake of CO_2 by terrestrial and aquatic photoautotrophs is a strategy for carbon capture to mitigate these emissions (Sayre, 2010). One strategy is the cultivation of algal biomass in alkaline ponds, where increased CO_2 hydration rates at high pH may maximize inorganic carbon availability to cultures for biofixation (Reichle et al., 1999). However, since biomass decay releases CO_2 into the atmosphere, biomass must be strategically stored or utilized to mitigate carbon. For instance, biomass could be harvested, converted to biofuels, and used to reduce fossil fuel use (Ono & Cuello, 2003).

Phytoplankton provides critical primary productivity and their growth requires dissolved inorganic carbon, nitrogen, and phosphorous, with phosphorous being the growth rate-limiting nutrient in freshwater environments when inorganic carbon is not considered. In a classic work, Redfield (1963) presented a balanced equation for algal biomass that led to the formation of the balanced growth equation (1). When nitrate is the nitrogen source for growth, 18 moles of hydrogen ion are consumed per mole of algal biomass produced which creates a pH rise.

$$106\ CO_2 + 16\ NO_3^- + HPO_4^{2-} + 122\ H_2O + 18\ H^+ \rightarrow C_{106}H_{263}O_{110}N_{16}P + 138\ O_2 \quad (1)$$

The Redfield cell composition for mixed cultures of marine phytoplankton is presented as a C:N:P ratio of 106:16:1; however, this ratio is highly dependent on the

concentration of C, N and P in the aqueous environment and the species of phytoplankton. Some species have been shown to create nitrogen reservoirs which could lead to deviations from Redfield's ratio (Caperon, 1968; Nyholm, 1977). Media composition has been shown to impact cell composition (Watson & Drapcho, 2016) and dominant species present (Goldman & Stanley, 1974).

Clemson University's emissions fall into three categories. The first scope is from sources owned by the university, such as the on-campus natural gas plant and vehicle fleet. The second scope is the electricity purchased by the University. The third scope is from sources not directly controlled by the University. Scope 3 is considered the most difficult to mitigate as it includes things like student and faculty travel. Scope 3 also makes up about a third of Clemson Universities' emissions (Sightlines Report, 2019). This project will aim to capture a portion of Scope 3 emissions of Clemson University in the Algal Carbon Capture System (ACCS).

Objectives

1) Investigate carbonate chemistry and algal growth equations used in MATLAB model to improve model predictive capability
2) Develop, design, and evaluate a non-fossil fuel technology for the operation of the ACCS

Objective 1) Closed-System Algal Growth Model

A dynamic growth model based on complete carbonate chemistry for freshwater algal culture was produced at Clemson University by Dr. Mary Katherine Watson in 2009. Often models for marine cultures only include the use of carbon dioxide (CO_2) as the carbon source for growth (Lee et al., 2015). However, this model is flexible to incorporate the use of CO_2, bicarbonate (HCO_3), and carbonate (CO_3) by the algae. The model produced by Watson (2009) had minimum residual biomass when all three carbon species were considered as substitutable but largely underpredicted TIC, specifically CO_3, as can be seen in Figure 1.1 below.

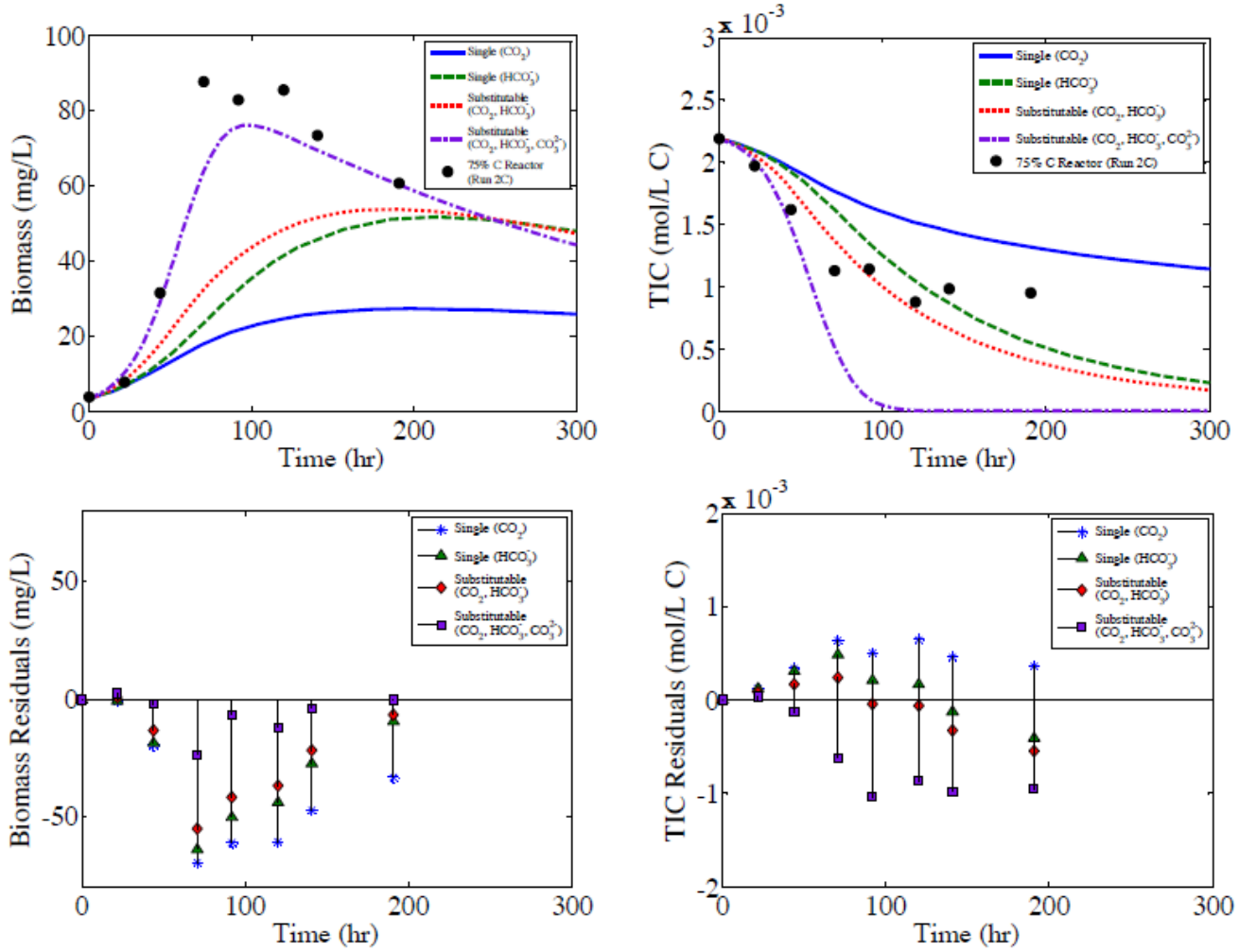

Figure 1.1: Biomass and TIC Residuals for 75% Media Carbon Run 2C (Watson, 2009)

Kinetic Rate Constants

Many model changes were incorporated to improve the accuracy of the model. First a literature review of kinetic constants of the inorganic carbon reactions was conducted. As can be seen in the summary Table 2.3. This literature review uncovered the wide variability in the literature of reported kinetic constants for the hydroxylation of bicarbonate reaction, equation 2 below.

$$HCO_3^- + OH^- \rightleftharpoons CO_3^{2-} + H_2O \quad (2)$$

The reported forward rate constants for this reaction vary by three orders of magnitude. The reported value in Eigen (1964) is 6×10^9 $M^{-1} \cdot s^{-1}$ and the reported value in Buxton and Elliot (1986) is 8.5×10^6 $M^{-1} \cdot s^{-1}$. This reaction is very rapid and often considered to be at equilibrium so very few sources were found that had a reaction rate constant. Given the rate of this reaction it is also likely that there could be significant error in their measurement. The reaction rate constant was changed to be the geometric mean of the two constants, calculated using equation 3 below.

$$\prod_{i=1}^{n} x_i = \sqrt[n]{x_1 x_2 \ldots x_n} \quad (3)$$

Where Π is the geometric mean, n is the number of values, and x are the values.

The geometric mean of these reaction rate constants comes to 2.25×10^8 $M^{-1} \cdot s^{-1}$. Previously this reaction had been removed from the model code and final mass balances due to matrix scalding that created unrealistic jumps in model predictions, however at the experimental pH this reaction is significant (Eigen, 1964; Kern, 1960; Patel et al., 1973; Zeebe & Wolf-Gladrow, 2001). The reaction was reincorporated into the code and final mass balances with the new rate constant. This change removed the issues that were

generating matrix scalding in some solutions. While more values were gathered for all other reaction rate constants none were significantly different than values previously in use or those generated from temperature dependent relationships, so all other reaction rate constants remained unchanged, after considerable verification.

Light Modeling

Sensitivity analysis of the model indicated that the predictions were highly dependent on photosynthetic oxygen production (p_r) and biomass light attenuation coefficients (K_B) (Watson, 2009). Models for light and p_r were further investigated. The relationship between light and photosynthetic rate is known as the PI relationship. There are three regimes in this relationship. One below light saturation (usually I_K) where the rate of photosynthesis is proportional to the intensity is known as light-limited growth, which can be found in low light environments (Béchet et al., 2013). Next between light saturation and light inhibition there is light saturated growth where the rate of photosynthesis is at its max and is independent of light intensity (Crill, 1977). The last regime is past the inhibitory light threshold (I_{inhib}) where the increase in light intensity starts to denature proteins required for photosynthesis and p_r begins to decrease (Camacho Rubio et al., 2003). Another important factor in this relationship is known as the hysteresis effect, where previous exposure to high or low levels of light and sudden change can decrease the photosynthetic rate of the algal cells (Beardall & Morris, 1976). In well mixed cultures where cells are experiencing rapid changes in light as they are moved from the bottom to the top of the reactor the rate of photosynthesis can be increased due to the flashing light effect. The short cycles give the photosynthetic units of

the algae cell time to turn captured photons into NADPH and ATP before starting the next cycle (Grobbelaarl et al., 1996).

An additional model included the combination of Andrews (1968) proposed model with Beer-Lamberts Law and the Monod model, which produced the optimum lighting profile for high biomass concentrations and light intensities (Koller et al., 2017), equation 4 below.

$$\mu = \mu_{max} \left\{ \frac{I_{avg}}{K_{S,I} \cdot I_{avg} \cdot \frac{I_{avg}^2}{K_{I,I}}} \right\} \qquad (4)$$

Where $K_{S,I}$ is the half-saturation constant for light (μmol/m^{2}s), I_{avg} is the average scalar irradiance (μmol/m^2-s), and $K_{I,I}$ is the light inhibition coefficient (μmol/m^{2}s).

Reported values for $K_{S,I}$ vary from 39 – 237 μmol/m^{2}s and $K_{I,I}$ from 1152 – 4780 μmol/m^{2}s (Koller et al., 2017). These effects will vary based on species sensitivity to photo-inhibition. For example, *Scenedesmus almeriensis* is tolerant to high irradiances, showing no signs of photoinhibition up to 1625 μmol/m^2-s (Sánchez et al., 2008). Since the parameters $K_{S,I}$ and $K_{I,I}$ vary so greatly, the addition of this light model did not improve results and added more unnecessary unknowns. Other models tested include the Sanchez model (2008) and the hyperbolic Beer-Lambert (Béchet et al., 2013) with no model improvement.

Given that the system modeled here has low light intensity and culture density (121 μmol/m^{2}s and under 100 mg TSS/L) it is possible that no hysteretic or flashing lights are affecting the cells. The original light model of average light found from integrating the Beer-Lambert Law (equation 5) over the reactor depth (equation 6) was incorporated as a

complimentary limiting nutrient in the Monod model. Example displayed in equation 7 for growth on carbon dioxide.

$$I_z = I_0 e^{-K \cdot z} \qquad (5)$$

$$I_{avg} = \frac{I_0 \left(1 - e^{-K \cdot d}\right)}{K \cdot d}. \quad (6) \text{ (Benson \& Rusch, 2006; Sánchez et al., 2008)}$$

$$\mu_{CO2} = \mu_{max,CO2} \left\{ \left(\frac{[CO_2(aq)]}{K_{CO_2} + [CO_2(aq)]} \right) \left(\frac{I_{avg}}{K_{S,I} + I_{avg}} \right) \right\} \quad (7)$$

Alkalinity Adjustments

Alkalinity is defined as the acid-absorbing capacity of water is a critical parameter due to its use in calculating the total inorganic carbon. Alkalinity in natural freshwater is presented with the following equation 8.

$$ALK = [HCO_3^-] + 2[CO_3^{2-}] + [OH^-] - [H^+] \qquad (8)$$

Roughly this refers to the number of weak bases in the solution that can be changed to uncharged species by an acid, where the moles of the base are multiplied by the charge of the ion. Some ions are not considered such as: Na^+, K^+, Ca^{2+}, Mg^{2+}, Cl^-, SO_4^{2-}, and NO_3^- because their concentrations are not changed with changes in pH (Drever, 1982). In sea water, it expands to the following equation 9.

$$ALK = [HCO_3^-] + 2[CO_3^{2-}] + [B(OH)_4^-] + [OH^-] + 2[PO_4^{3-}] + [HPO_4^{2-}] + [SiO(OH)_3^-] - [H^+] - [HSO_4^-] - [HF] \qquad (9)$$

In seawater, up to 5 percent of alkalinity can be due to borate, whereas HF, HSO_4^-, phosphates, and silica are typically negligible and at typical seawater pH values (Zeebe et al., 2001). In algal culture systems, considerations must be made for the concentrations of these ions in the growth medium to ensure accurate total inorganic

carbon concentrations. In this system BG-11 growth medium was used (Watson & Drapcho, 2016), the high concentration of ions cause changes to measurable alkalinity. Individual BG-11 media alkalinity components were measured following Standard Method 2320, with results shown in in Table 1.1 below.

Table 1.1: Measured Alkalinity Contribution of BG-11 Media Components

Compound	Concentration in Modified BG-11 (g/L)	Measured ALK (mmol equiv/L)
$NaNO_3$	1.5	0.06 ± 0.01
K_2HPO_4	0.04	0.3 ± 0.01
$MgSO_4$ $7H_2O$	0.075	0.02
$CaCl_2$ $2H_2O$	0.036	0.02
Ferric ammonium citrate	0.006	0.003
EDTA	0.001	0.002
Na_2CO_3	0.2	3.72 ± 0.02
Trace Metal Mix A5	1.0 mL/1L	0.02 ± 0.004

Therefore, data collected by Dr. Watson was adjusted for non-carbonate alkalinity due to media. The initial amount of sodium carbonate added was converted to an equivalent alkalinity and the non-carbonate alkalinity was determined using equation 10 below.

$$ALK_{non-carbonate} = ALK_{measured,initial} - ALK_{CalculatedCarbon,initial} \quad (10)$$

The non-carbonate alkalinity was then removed from measured alkalinity at all time points. The new corrected alkalinity was used to recalculate carbonate species concentrations for experimental data values, described further in Chapter 2. These new concentrations were loaded into the model for comparison to predicted results for all carbon media concentrations.

Various Other Corrections

Other corrections and additions were made through out model verification that improved model completeness. The water mass balance was completed by adding in the water utilization from growth on bicarbonate that had previously been omitted. This mass balance was checked, and water maintains balance at 55.5 mol/L. A nitrogen utilization term was introduced to verify that nitrogen was not becoming a limiting nutrient. The maximum growth rates of algae based on CO_2, HCO_3, CO_3 replaced the overall maximum growth rate in the Monod calculations for each carbon species. The values were adjusted to be the average across both methods used for the determination of maximum growth rate by Watson (2009) shown in Table 1.2 below.

Table 1.2: Maximum Growth Rate (1/hr)

Substrate	Run 2C, Excel	Run 3C, Excel	Run 2C, SAS	Run 3C, SAS	Average, Excel Values	Average, SAS Vales	Average All Values
CO_2	0.0737	0.0967	0.0756	0.07	0.0852	0.0728	0.079
HCO_3	0.0738	0.095	0.0756	0.073	0.0844	0.0743	0.07935
CO_3	0.0704	0.0689	0.0728	0.0691	0.06965	0.071	0.0703

Lastly plots were created to demonstrate the growth rate on each carbon species and the decay rate through the model run. An example is shown below for 75% Media Carbon Content for both substitutable models in Figure 1.2.

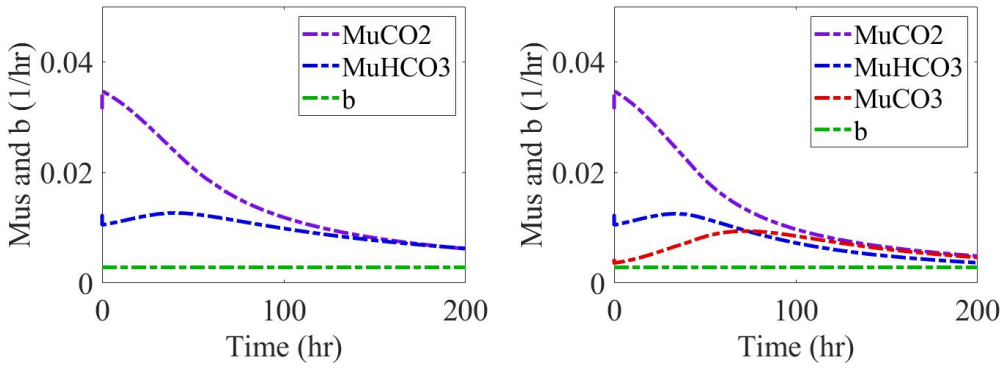

Figure 1.2: Specific Growth Rates (Mu) and Decay Rates (b) for 75% Media Carbon Content (L) HCO_3/CO_2 Substitutable (R) $CO_3/HCO_3/CO_2$ Substitutable

The two models depicted here will be compared based on Root Mean Square Error in Chapter 2.

Objective 2) Develop, design, and evaluate a non-fossil fuel technology for operation of the ACCS - Airlift Pump Fabrication

The Partitioned Aquaculture System (PAS), Figure 1.3 below, at Clemson University was originally designed to optimize oxygen dynamics in aquaculture systems through management of photosynthetic oxygen production by freshwater algae (Drapcho & Brune, 2000). The original design incorporated raceway ponds for algae cultivation for nutrient removal and oxygen production. Adjacent tanks for the were used for fish production. The system is now being revitalized through a variety of projects, including this one, to become an Algal Carbon Capture System (ACCS).

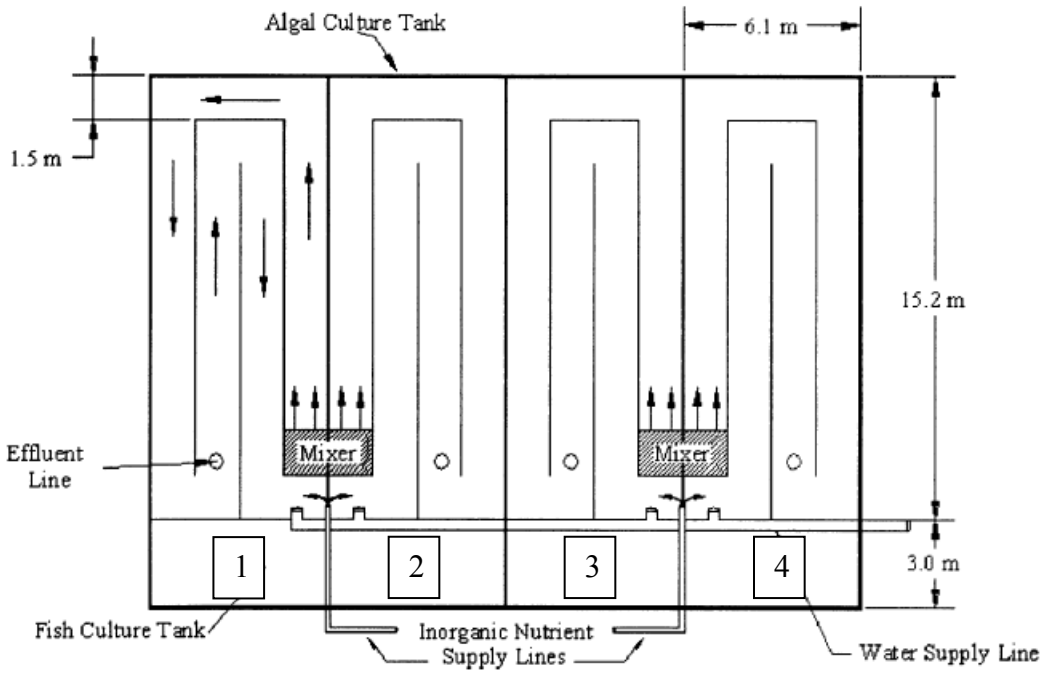

Figure 1.3: Partitioned Aquaculture System Schematic (Drapcho & Brune, 2000)

A key component of the system is the movement of water, depicted in Figure 1.3 as the

"Mixer." Mixing in the ponds allows for the algae on the bottom to be moved to the top where the cells can receive sunlight. This reduces the light inhibition of growth and increases productivity. Increasing water velocity was found to increase algal productivity up to a water velocity of 12.5 cm/s (Drapcho & Brune, 2000). In the past, mixing has been accomplished with the use of paddle wheels powered by electrical motors. This system of creating water movement have ultimately failed due to the harsh conditions and exposure to the elements at the ACCS.

Air lift pumps provide an alternative method for the mixing water that has high reliability and low maintenance (Clark & Dabolt, 1986). The simplicity and low cost of

air lift pump systems makes them suitable to provide water flow and mixing in the ACCS (Parker, 1991). Airlift pumps provide the added benefit of facilitating gas transfer and creating water flow simultaneously. This may be beneficial in the conversion to an Algal Carbon Capture System as compressed CO_2 or flue gas could be used as the feed gas. Flue gas has been shown to increase biomass productivity by 30% compared to compressed CO_2 due to the presence of supplemental nutrients like sulfur and nitrate that are present in flue gas (Douskova et al., 2009; Sayre, 2010). Compressed CO_2 alone elevates biomass yields up to three times (Jeong et al., 2003).

In chapter 3, an airlift pump prototype is described that was designed, built, implemented, and tested at the ACCS to create water flow in one raceway channel as demonstration of concept. The airlift operates solely on available solar power and provides at its outlet a water velocity of 12.5 cm/s, and an average channel velocity of 1.02 ± 0.15 cm/s as the surface kinetic energy is distributed throughout the channel depth.

CHAPTER II: MANUSCRIPT

KINETIC MODELING OF INORGANIC CARBON-LIMITED FRESHWATER ALGAL GROWTH AT HIGH PH

Abstract

A dynamic growth model based on carbon-limited algal specific growth rate with Monod kinetics, considering carbon dioxide (CO_2), bicarbonate (HCO_3^-), and carbonate (CO_3^{2-}) as substitutable substrates, provided the best estimates for algal biomass growth in closed-reactors. Total inorganic carbon (TIC), CO_2, HCO_3^-, CO_3^{2-}, pH, and alkalinity were also well predicted, with the only better predictions of the CO_2/HCO_3^- model being CO_2, HCO_3^-, and pH. This model improves upon those reviewed by incorporating kinetic rates of carbon species interconversion instead of the equilibrium assumption. Discrepancies in rate constants of the bicarbonate hydroxylation reaction indicate more exploration of these parameters is needed. Here is proposed the use of the geometric mean (2.25×10^8 $M^{-1} \cdot s^{-1}$) for the forward rate constant. Underprediction of algal biomass and improved response of $CO_2/HCO_3^-/CO_3^{2-}$ substitutable model over a CO_2/HCO_3^- substitutable alone may indicate an unknown biological pathway for the use of carbonate for growth.

Keywords: Algae, Monod kinetics, Carbonate System Kinetics, Carbonate Rate Constants

Introduction

Carbon dioxide (CO_2) emissions from anthropogenic sources are causing widespread ecological disruptions. The diffusion of gaseous CO_2 into seawater has caused an oceanic decrease of 0.1 pH unit since the late 1980s, due to formation of carbonic acid

(IPCC, 2019). The uptake of CO_2 by terrestrial and aquatic photoautotrophs is a strategy for carbon capture to mitigate these emissions (Sayre, 2010). One strategy is cultivation of algal biomass in alkaline ponds, where increased CO2 hydration rates at high pH may maximize availability of inorganic carbon to cultures for biofixation (Reichle et al., 1999). However, since the decay of algal biomass would release CO_2 into the water algal biomass must be strategically stored or utilized to ensure carbon mitigation. Biomass could be harvested, converted to biofuels, and used to reduce fossil fuel use (Ono & Cuello, 2003).

Phytoplankton provide critical primary productivity and their growth requires dissolved inorganic carbon, nitrogen, and phosphorous; with phosphorous being the growth rate limiting nutrient in freshwater environments when inorganic carbon is not considered. In a classic work, Redfield (1963) presented a molecular formula for marine phytoplankton, which led to the development of a balanced equation for growth with nitrate as the nitrogen source indicating that 18 moles of hydrogen ion are consumed per mole of algal biomass produced. (Equation 1). This proton consumption causes the pH rise in photoautotrophic growth of algae culture when pH is not controlled.

$$106\ CO_2 + 16\ NO_3^- + HPO_4^{2-} + 122\ H_2O + 18\ H^+ \rightarrow C_{106}H_{263}O_{110}N_{16}P + 138\ O_2 \qquad (1)$$

The Redfield cell composition for mixed cultures of marine phytoplankton is presented as a C:N:P ratio of 106:16:1; however, this ratio is highly dependent on the concentration of C, N and P in the aqueous environment and the species of phytoplankton. Some species create nitrogen reservoirs that could lead to deviations from Redfield's ratio (Caperon, 1968; Nyholm, 1977; Sommer, 1991). Medium inorganic carbon content has been shown to impact cell composition (Watson & Drapcho, 2016)

and dominant species present (Goldman & Stanley, 1974, Drapcho & Brune 2000). The goal of this paper is to present a dynamic algal growth model considering inorganic carbon substrates to predict algal biomass and carbonate species concentrations in closed systems. This model will aid in design of carbon mitigation biosystems and indicate important shortcomings of available carbonate system kinetic rate constants.

Algal Growth Models

Existing algal growth models can be broken into categories based on the factors considered. Growth kinetic models can consider a single substrate, multiple substrates, light, temperature, salinity, or a combination of these factors. For single substrate models both the Monod model and the Droop model are used to model algal growth. The Monod model offers simplicity as it relies on the measurement of external nutrients. The Droop model is a function of the cell quota of the limiting nutrient (Lemesle & Mailleret, 2008). The cell quota is an internal measurement of the limiting nutrient. The internal measurement inside the cell is technologically difficult to determine although has been found to be more accurate in outdoor conditions (Sommer, 1991). Models that are a function of light intensity may consider light limitations on growth rate, the attenuation by cells, the attenuation by the medium, and photoinhibition. Models that look at a combination of factors often consider nitrogen or phosphorus to be limiting nutrients and will also include a function of light intensity (Lee et al., 2015). Often models for cultures only include the use of carbon dioxide as the carbon source for growth (Spijkerman et al., 2011; Lee et al., 2015; Park & Li, 2015); however, CO_2 and HCO_3^- can be used (Sayre, 2010). Additionally, there is evidence to suggest the use of all three carbon species by an

undetermined mechanism (Watson & Drapcho, 2016). A short review of some available models is included in Table 2.1 below.

Table 2.1: Review of Algal Kinetic Growth Models

Source	Experiment Setting	Carbon Nutrient Modeled	Limiting Nutrient	Media Used	pH range	Model and Software Used
(Casagli, Zuccaro, Bernard, Steyer, & Ficara, 2021)	Raceway	Y	Minimum of TIC, Nitrogen, and Phosphorous	Synthetic Wastewater, (starch, milk powder, yeast, peptone)	7.2 - 11	ALBA model on AQUASIM, mixed algae and bacteria culture
(Feng et al., 2021)	Lab	N	Light	Synthetic Wastewater	-	MatLab®, reactor broken into layers with Beer-Lamberts Law for light
(Gao et al., 2018)	Raceway	N	Salinity, Nitrogen, and Light	CO_2 gas	7.8	Huesemann Algae Biomass Growth, included shading from walls
(Banks et al., 2017)	Lab	N	-	-	-	Logistic Population Growth Model, curve fitting
(Park & Li, 2015)	Field	Y	CO_2, Inorganic Nitrogen, and Light	0.075 g/L CO_2 flu gas	7.5 - 8.5	Commercial Computational Fluid Dynamics software, ANSYS-Fluent 14.5, Monod
(Ruiz et al., 2013)	Lab	N	-	CO_2 in Synthetic Wastewater, Wastewater, and Combo two-fold medium containing sodium bicarbonate	8.4 - 6.3	Wastewater photobiotreatment with microalgae (PhBT model) using Verhulst growth model, predicts nutrient removal of N and P
(Spijkerman et al., 2011)	Lab	Y	CO2 and Phosphorous	Aerated Woods Hole Medium	2.7	Monod with Liebigs Law of the minimum

Table 2.1 (Continued)

Source	Experiment Setting	Carbon Nutrient Modeled	Limiting Nutrient	Media Used	pH range	Model and Software Used
(Quinn, de Winter, & Bradley, 2011)	Field with maintained temperature	N	Nitrogen	CO_2 gas	7.3 +/- 0.1	MatLab®, Growth rate as function of photosynthetic rate, respiration rate, and specific uptake of nitrogen, Droop model, Predicts lipid production
(Hsueh, Li, Chen, & Chu, 2009)	Lab	Y	TIC	gaseous CO_2 and dissolved inorganic carbon, DIC	5.5-7	Monod, TIC: mu_{max} 3.5 d^{-1} and K_S 1.9 mM
(Lemesle & Mailleret, 2008)	Lab	N	Vitamin B12	Simulation Only	-	Droop
(Wijanarko et al., 2008)	Lab	Y	HCO3	CO2 gas	5.5-6.5	Haldane found to fit better than Monod or Ierusalemsky
(Sommer, 1991)	Field	N	Silicate and Nitrogen	-	-	Droop
(Goldman, Jenkins, & Oswald, 1974)	Lab	Y	TIC	PAAP medium, Sodium Carbonate and Bicarbonate	7.05-7.61	Monod

A 2015 review article by Lee et al. (2015) of algal growth kinetic models reviewed 55 models. Of these 55 models, 13 considered some form of carbon as limiting nutrient, but only 3 considered TIC or HCO_3 where the rest modeled using CO_2 alone. No models in this review mentioned the incorporation of rates of inorganic carbon transformation; instead, carbon species are assumed to be at equilibrium.

Carbonate Chemistry

Inorganic carbon in natural waters can derive from dissolved carbon dioxide gas and dissolved mineral rock such as calcium carbonate. Dissolved inorganic carbon compounds include dissolved (aqueous) carbon dioxide ($CO_{2(aq)}$) , carbonic acid (H_2CO_3) , bicarbonate (HCO_3^-) and carbonate (CO_3^{2-}). The traditional representation of the reversable carbonate reactions are given below, equations 2-4 (Kern 1960):

$$CO_2(aq) + H_2O \rightleftharpoons H_2CO_3 \quad (2)$$

$$H_2CO_3 \rightleftharpoons H^+ + HCO_3^- \quad (3)$$

$$HCO_3^- \rightleftharpoons H^+ + CO_3^{2-} (4)$$

Since reaction 2 has an equilibrium very far to the left, $H_2CO_3^*$ is often used to represent the sum of carbonic acid and aqueous carbon dioxide. Equations 2 and 3 are therefore often combined into the following equation 5.

$$H_2CO_3^* \rightleftharpoons H^+ + HCO_3^- \quad (5)$$

This reaction is also displayed as a summary reaction as shown in equation 6 by Johnson (1982) and Zeebe and Wolf-Gladrow (2001).

$$CO_2(aq) + H_2O \rightleftharpoons H^+ + HCO_3^- \quad (6)$$

While these are presented as the traditional reactions, they are not the only reactions present in aqueous systems. Ho and Sturtevant (1963) presented that the above reactions (equations 2-6) are not found experimentally instead the following scheme in Figure 2.1 is presented for carbon hydration.

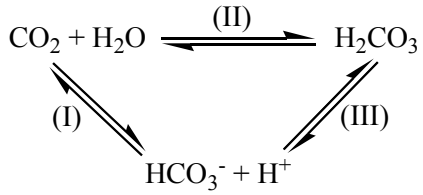

Figure 2.1: Carbon dioxide hydration (Watson, 2009)

Hydroxylation of carbon dioxide, show in equation 7 below, becomes important at pH of 7.5 and dominates at pH over 10 (Pinsent & Pearson, 1956; Sirs, 1957; Kern, 1960; Hikita et al., 1976; Stumm et al., 1996; Schulz et al., 2006).

$$CO_2(aq) + OH^- \rightleftharpoons HCO_3^- \quad (7)$$

Bicarbonate is in acid-base equilibrium and can undergo protolysis and hydrolysis in the following scheme as presented by Eigen (1964) in Figure 2.2.

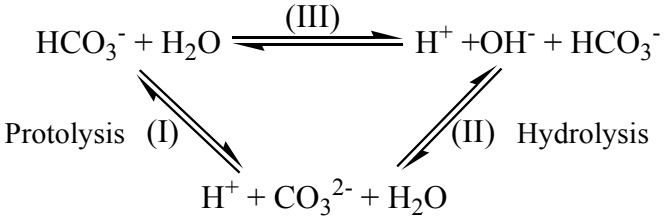

Figure 2.2: Bicarbonate Acid-Base Equilibrium Reactions (Watson, 2009)

Path I, equation 4, shows bicarbonate dissociation to carbonate, with the release of a proton. Path II, equation 8 below, shows hydrolysis to form carbonate. Path III, equation 9 below, is the dissociation of water. Not all sources show path II but it is supported by (Eigen, 1964; Kern, 1960; Patel et al., 1973; Zeebe et al., 2001).

$$HCO_3^- + OH^- \rightleftharpoons CO_3^{2-} + H_2O \quad (8)$$

$$H_2O \rightleftharpoons H^+ + OH^- \quad (9)$$

These reactions are summarized with their corresponding rate and equilibrium constants in Table 2.2.

Table 2.2: Carbonate System Equations with Constants Defined

Equation	Forward Rate Constant	Reverse Rate Constant	Equilibrium Constant	Equilibrium pK Value	Source
$CO_2(aq) + H_2O \rightleftharpoons H_2CO_3$ (2)	k_{+2}	k_{-2}	K_h	2.59	(Edsall, 1969)
$H_2CO_3 \rightleftharpoons H^+ + HCO_3^-$ (3)	k_{+3}	k_{-3}	K_{H2CO3}	3.76	(Wissbrun, French, & Patterson, 1954)
$HCO_3^- \rightleftharpoons H^+ + CO_3^{2-}$ (4)	k_{+5}	k_{-5}	K_2	10.315	(Greenwood & Earnshaw, 1997)
$CO_2(aq) + H_2O \rightleftharpoons H^+ + HCO_3^-$ (6)	k_+	k_-	K_1	6.352	(Harned & Davis, 1943)
$CO_2(aq) + OH^- \rightleftharpoons HCO_3^-$ (7)	k_{+4}	k_{-4}	K_4	-7.645	K_1/K_W
$HCO_3^- + OH^- \rightleftharpoons CO_3^{2-} + H_2O$ (8)	k_{+6}	k_{-6}	K_3	-3.667	K_2/K_W
$H_2O \rightleftharpoons H^+ + OH^-$ (9)	k_{+7}	k_{-7}	K_W	14.01	(Eigen, 1964)

Kinetic Constants

A literature review of kinetic constants of the above inorganic carbon reactions was conducted. As can be seen in the summary Table 2.3, there is wide variability in the literature of reported kinetic constants. Temperature dependent relationships were used when available. Equations included in model are 4, 6, 7, 8 and 9. Rate constants used in the model are denoted with an asterisk (*).

Table 2.3: Summary of kinetic constants for carbonate system reactions at 25ºC

Kinetic Rate Constant	Corresponding Equation	Value at 25°C	Units	Source	Mean Kinetic Rate Constant[12]
k_{+}	6	*3.55×10^{-2}	s^{-1}	(Portielje & LiJklema, 1995)[1]	
k_{+}	6	3.7×10^{-2}	s^{-1}	(K. S. Johnson, 1982)	
k_{+}	6	$2.5\text{-}4 \times 10^{-2}$	s^{-1}	(Stumm & Morgan, 1996)	3.54×10^{-2}
k_{+}	6	4×10^{-2}	s^{-1}	(Zeebe & Wolf-Gladrow, 2001)	
k_{-}	6	*7.983×10^{4}	$M^{-1} \cdot s^{-1}$	calculated[2]	
k_{-}	6	2.66×10^{4}	$M^{-1} \cdot s^{-1}$	(Zeebe & Wolf-Gladrow, 2001)	4.44×10^{4}
k_{-}	6	2.67×10^{4}	$M^{-1} \cdot s^{-1}$	(Schulz et al., 2006)	
k_{+3}	3	0.9×10^{7}	s^{-1}	calculated[3]	1.2×10^{7}
k_{+3}	3	1.5×10^{7}	s^{-1}	(Knoche, 1980)	
k_{-3}	3	4.7×10^{-10}	$M^{-1} \cdot s^{-1}$	(Eigen & Hammes, 1963)	5.6×10^{-10}
k_{-3}	3	6.5×10^{-10}	$M^{-1} \cdot s^{-1}$	(Knoche, 1980)	
k_{+4}	7	*8.053×10^{3}	$M^{-1} \cdot s^{-1}$	(Sirs, 1957) [4]	
k_{+4}	7	2.23×10^{3}	$M^{-1} \cdot s^{-1}$	(Schulz et al., 2006)[5]	
k_{+4}	7	8.5×10^{3}	$M^{-1} \cdot s^{-1}$	(Stumm & Morgan, 1996; Kern, 1960)	5.71×10^{3}
k_{+4}	7	4.05×10^{3}	$M^{-1} \cdot s^{-1}$	(K. S. Johnson, 1982)	
k_{-4}	7	*18.24×10^{-5}	s^{-1}	calculated[6]	
k_{-4}	7	17.6×10^{-5}	s^{-1}	(Zeebe & Wolf-Gladrow, 2001)	
k_{-4}	7	9.71×10^{-5}	s^{-1}	(Schulz et al., 2006)	9.19×10^{-5}
k_{-4}	7	0.188×10^{-5}	s^{-1}	(Ho & Sturtevant, 1963)	
k_{-4}	7	0.20×10^{-5}	s^{-1}	(Stumm & Morgan, 1996)	
k_{+5}	4	*2.344	s^{-1}	calculated[7]	
k_{+5}	4	59	s^{-1}	(Zeebe & Wolf-Gladrow, 2001)	30.67
k_{-5}	4	*5×10^{10}	$M^{-1} \cdot s^{-1}$	(Zeebe & Wolf-Gladrow, 2001)[8]	-
k_{+6}	8	6×10^{9}	$M^{-1} \cdot s^{-1}$	(Eigen, 1964)[9]	3×10^{9}
k_{+6}	8	8.5×10^{6}	$M^{-1} \cdot s^{-1}$	(Buxton & Elliot, 1986)	
k_{-6}	8	*0.48×10^{5}	s^{-1}	calculated[10]	
k_{-6}	8	3×10^{5}	s^{-1}	(Zeebe & Wolf-Gladrow, 2001)	7.95×10^{5}
k_{+7}	9	*1.410×10^{-3}	$M \cdot s^{-1}$	calculated[11]	-
k_{-7}	9	*1.4×10^{11}	$M^{-1} \cdot s^{-1}$	(Eigen, 1964)	-

[1]Calculated using $k_{+} = 10^{(10.685-3618/T)}$, where T is absolute temperature (K).
[2]Calculated using $K_1 = k_{+}/k_{-}$, where K_1 is the equilibrium constant for equation 6 and $pK_1 = 6.352$ (Harned & Davis, 1943).
[3]Calculated using $K_{H2CO3} = k_{+3}/k_{-3}$, where K_{H2CO3} is the equilibrium constant for equation 3 and
$pK_{H2CO3} = 3.71$ (Wissbrun et al., 1954).
[4]Calculated using $k_{+4} = 10^{(13.589-2887/T)}$, where T is absolute temperature (K)
[5]Value measured at ionic strength of 1.0M, discussion on ionic strength effects found in Zeebe and Wolf-Gladrow (2001).
[6]Calculated using $k_{-4} = k_{+4} \cdot K_W/K_1$, where K_W is the equilibrium constant for equation 9 and
$pK_W = 13.997$ (Edsall, 1969).
[7]Calculated using $K_2 = k_{+5}/k_{-5}$, where K_2 is the equilibrium constant for equation 4 and $pK_2 = 10.329$ (Harned & Davis, 1943).
[8]Value for k_{-5} assumed to be approximately equal to k_{-3} since no experimental data available.
[9]Value measured by Eigen (1964) at ionic strength of 1.0M. No value for freshwater found in literature.
[10]Calculated using $K_3 = k_{+6}/k_{-6}$, where K_3 is the equilibrium constant for equation 8 and $pK_3 = -3.667$ (Hikita et al., 1976).
[11]Calculated using $K_W = k_{+7}/k_{-7}$.
[12]Note the order of magnitude difference in the given rate constants for k_{+6}, geometric mean of $*2.25 \times 10^8$ $M^{-1} \cdot s^{-1}$ is used in model

Algal Carbon Concentration Mechanisms

Algae have been shown to allow for the passing of CO_2 and HCO_3 across their cell membranes. The cell membrane is permeable to CO_2, and it can passively diffuse across the cell membrane. HCO_3 however is moved across by active transporters, likely hydrogen ion pumps (Ludden et al., 1985; Amoroso et al., 1998; Chrachri et al., 2018).

At neutral pH, the concentration of CO_2 compared to that of HCO_3 is negligible. To combat this, algae use an enzyme called external carbonic anhydrase (eCA) to catalyze the conversion of HCO_3 to CO_2 at its cell surface. This zone of higher carbon

dioxide concentration around the cells allows for passive diffusion into the cells and counters the limitations of diffusion from cell size (Chrachri et al., 2018).

Bicarbonate is moved into the cell via an active hydrogen ion pump, which requires ATP. This energy demand to use this substrate would make it not preferable over carbon dioxide (Moroney & Somanchi, 1999). In the absence or inhibition of eCA the active pump is used (Chrachri et al., 2018). This same mechanism is deployed in the chloroplasts of algal cells (Amoroso et al., 1998).

Although there is no known mechanism of CO_3 transport across the cell membrane the concentration is expected to decline. This is because the equilibrium between HCO_3 and CO_3 is very rapid, so as HCO_3 is pumped into the cell the external concentration declines. After this decline equilibrium is quickly reached and some CO_3 is converted to HCO_3 (Chrachri et al., 2018). When algae are not significantly light limited or inhibited and rates of photosynthesis are high large amounts of CO_2 and HCO_3 are removed from the water. Since the hydration of CO_2 and dehydration of HCO_3 are fairly slow processes (Johnson, 1982) the carbonate system should not be assumed to be at equilibrium (Ludden et al., 1985).

Monod Model for Algae Growth

The algal growth model described below was developed to represent the growth of the freshwater alga *Scenedesmus* cultured in closed, batch reactors using an inorganic carbon modified BG-11 medium under artificial lights as described in Watson & Drapcho (2016). The single-substrate Monod (Monod, 1949) model (equation 10) can be used to model inorganic-carbon limited algal growth with CO_2, HCO_3, CO_3^{2-} or TIC as substrate.

Phosphorous is usually taken as the rate limiting nutrient in freshwater systems, when inorganic carbon is not considered; however many references report a Monod response with CO_2 (King, 1970; Novak & Brune, 1985; Park & Li, 2015) or TIC (Goldman et al., 1974; Watson & Drapcho, 2016).

$$\mu_C = \frac{\mu_{max}[C]}{K_C + [C]}, \quad (10)$$

Where, μ_C = inorganic-carbon-limited specific growth rate (hr^{-1}), μ_{max} = maximum specific growth rate (hr^{-1}), C = CO_2, HCO_3^-, CO_3^{2-}, or TIC (mol/L C), and K_C = half-saturation constant for inorganic-carbon-limited growth (mol/L C).

Simultaneous use of multiple carbonate species may be modeled through expansion of the Monod equation for substitutable substrates (Grady et al, 1999). A preferred substrate (C_{pfd}) is used when available; however, as C_{pfd} becomes depleted, cells use an alternative substrate (C_{alt}). Growth rate on C_{pfd} is modeled by equation 10, while growth rate on C_{alt} (μ_C) is inhibited by presence of C_{pfd} (equation 11).

$$\mu_C = \mu_{max}\left(\frac{[C_{alt}]}{K_{C,alt} + [C_{alt}]}\right)\left(\frac{K_{C,pfd}}{[C_{pfd}] + K_{C,pfd}}\right). \quad (11)$$

This equation was deployed with the use of $CO_{2(aq)}$ as the C_{pfd} and HCO_3 or CO_3 as C_{alt} as shown in equations 12 - 14 below.

$$(12) \quad \mu_{CO2} = \mu_{max,CO2}\left(\frac{[CO_2(aq)]}{K_{CO_2} + [CO_2(aq)]}\right)$$

$$(13) \quad \mu_{HCO3} = \mu_{max,HCO3}\left\{\left(\frac{[HCO_3^-]}{K_{HCO_3^-} + [HCO_3^-]}\right)\left(\frac{K_{CO_2}}{K_{CO_2} + [CO_2(aq)]}\right)\right\}$$

$$(14) \quad \mu_{CO3} = \mu_{max,HCO3}\left\{\left(\frac{[HCO_3^-]}{K_{HCO_3^-} + [HCO_3^-]}\right)\left(\frac{K_{CO_2}}{K_{CO_2} + [CO_2(aq)]}\right)\left(\frac{K_{HCO_3^-}}{K_{HCO_3^-} + [HCO_3^-]}\right)\right\}$$

The rate of biomass formation (r_X) is formulated by considering each equation for μ (equation 15), while the rate of biomass decay (r_D) is quantified using a decay constant, b (equation 16).

$$r_X = (\mu_{CO2} \cdot X_B) + (\mu_{HCO3} \cdot X_B) + (\mu_{CO3} \cdot X_B) \quad (15)$$

$$r_D = b \cdot X_B \quad (16)$$

Algal biomass molecular formula of $C_{106}H_{263}O_{110}N_{16}P$ (equation 1), can be alternatively represented as $(CH_2O)_{106}(NH_3)_{16}(H_3PO_4)$ based on work by Redfield et al. (1963). This stoichiometric equation can be generalized for algal cultures with C:N:P ratios (x:y:1) that vary from the Redfield proportions in equation 17 (Watson, 2009).

$$x \cdot CO_2 + y \cdot NO_3^- + HPO_4^{2-} + (-x - 3y + 2p) \cdot H_2O + (4x + 9y - 4p + 2) \cdot H^+ \leftrightarrow \{(CH_2O)_x(NH_3)_y(H_3PO_4)\} + p \cdot O_2 \quad (17)$$

Stoichiometric equations for algal growth on HCO_3^- were developed by re-balancing equation 16 with HCO_3^- (equation 18) and CO3 (equation 19) as inorganic carbon source (Watson, 2009).

$$x \cdot HCO_3^- + y \cdot NO_3^- + HPO_4^{2-} + (-2x - 3y + 2p) \cdot H_2O + (5x + 9y - 4p + 2) \cdot H^+ \leftrightarrow \{(CH_2O)_x(NH_3)_y(H_3PO_4)\} + p \cdot O_2 \quad (18)$$

$$x \cdot CO_3^{2-} + y \cdot NO_3^- + HPO_4^{2-} + (-2x - 3y + 2p) \cdot H_2O + (6x + 9y - 4p + 2) \cdot H^+ \leftrightarrow \{(CH_2O)_x(NH_3)_y(H_3PO_4)\} + p \cdot O_2 \quad (19)$$

The stoichiometric coefficient for photosynthetic oxygen production (p) can be experimentally determined or estimated. Redfield (1963) reports that 2 oxygen atoms are liberated during catabolic photosynthesis per carbon atom consumed in the anabolic phase, and an additional four oxygen atoms are produced for oxidation of each nitrate-nitrogen molecule. Thus, the Redfield (1963) prediction for photosynthetic oxygen production (p_r) is given by equation 20.

$$p_r = \frac{1}{2}(2x + 4y). \quad (20)$$

Rates of inorganic carbon species utilization (equation 21) are expressed based on inorganic carbon source and an appropriate stoichiometric algal growth equation (equations 17-19). In this expression, a "factor" is used to represent the molar ratio of species utilized per mol of biomass formed. Table 2.4 summarizes rates of species utilization and production for the inorganic carbon sources.

$$r_{S,C-source} = factor \cdot \mu_{c-source} \cdot X_B \quad (21)$$

Where, $r_{S,C\text{-source}}$ = rate of species (S) utilization for an inorganic carbon source (C-source), S = CO_2, HCO_3^-, NO_3^-, or H^+, and C_{source} = CO_2 HCO_3^- or CO_3

Table 2.4: Factors of Species Utilization

Rate Equation	Equation Number
$r_{C,CO_2} = x \cdot \mu_{CO_2} \cdot X$	(22)
$r_{H,CO_2} = (4x + 9y - 4p + 2) \cdot \mu_{CO_2} \cdot X$	(23)
$r_{NO_3^-,CO_2} = y \cdot \mu_{CO_2} \cdot X$	(24)
$r_{C,HCO_3} = x \cdot \mu_{HCO_3} \cdot X$	(25)
$r_{H,HCO_3} = (5x + 9y - 4p + 2) \cdot \mu_{HCO_3} \cdot X$	(26)
$r_{NO_3^-,HCO_3} = y \cdot \mu_{HCO_3} \cdot X$	(27)
$r_{C,CO_3} = x \cdot \mu_{CO_3} \cdot X$	(28)
$r_{H,CO_3} = (6x + 9y - 4p + 2) \cdot \mu_{HCO_3} \cdot X$	(29)
$r_{NO_3^-,CO_3} = y \cdot \mu_{CO_3} \cdot X$	(30)

Light Inhibition

Algal growth is significantly impacted by light availability, which is traditionally quantified using the Beer-Lambert Law for an unmixed water column. This law is applicable for relatively low total suspended solids concentrations, monochromatic light, and unidirectional path, displayed in equation 31 (Benson & Rusch, 2006).

$$I_z = I_0 e^{-K \cdot z} \quad (31)$$

Where, I_Z = scalar irradiance at depth z (μmol/m^2-s), I_0 = incident irradiance at the surface (μmol/m^2-s), K = extinction coefficient (m^{-1}), and z = depth (m).

The average scalar irradiance (I_{avg}) in a reactor is determined by integrating equation 31 over the reactor depth (d), which yields equation 32 (Benson & Rusch, 2006; Sánchez et al., 2008).

$$I_{avg} = \frac{I_0\left(1-e^{-K\cdot d}\right)}{K\cdot d}. \quad (32)$$

Some authors report the extinction coefficient as a constant factor of biomass concentration, such as in Sanchez (2008) a value of 0.08 m^2/g. However, this factor does not account for the attenuation of light by the growth media. The overall attenuation coefficient (K) is composed of factors for the media (K_M) and biomass (K_B) (equation 33) (Megard & Berman, 1989; Desmit et al., 2005; Benson & Rusch, 2006; Jayaraman & Rhinehart, 2015).

$$K = K_M + K_B X \quad (33)$$

Several researchers determined a linear relationship between TSS and the extinction coefficient (Table 2.5).

Table 2.5: Summary of algal biomass and water extinction coefficients

K_M (m^{-1})	K_B (m^2/g)	Species	Reference
1.97	0.0575	*Selenastrum capricornutum*	(Benson & Rusch, 2006)
1.4	0.0592	--	(Desmit et al., 2005)
--	0.038 – 0.041	*Porphyridium cruentum*	(Rebolloso Fuentes et al., 1999)
--	0.035	*Tetraselmis*	(Grima et al., 1994)
--	0.0382 – 0.1169[1]	*Isochrysis galbana*	(Grima et al., 1996)

[1]K_B calculated for various dilution rates and incident irradiances.

Some results suggest that a hyperbolic model is more appropriate for high biomass concentrations above 1300 mg/L (Fernández et. al, 1997). Photoinhibitory effects can occur at high photon flux densities and decrease the growth rate due to the

destruction of proteins in the photosynthetic process (Camacho Rubio et al., 2003; Huesemann et al., 2013). Several kinetic growth models have been proposed to account for the photo damages (Andrews, 1968; Camacho Rubio et al., 2003; Kurano & Miyachi, 2005; Sánchez et al., 2008; Béchet et al., 2013; Koller et al., 2017). The combination of Andrews (1968) proposed model with Beer-Lamberts Law and the Monod model has been found to produce the optimum lighting profile for high biomass concentrations and light intensities (Koller et al., 2017), equation 34 below.

$$\mu = \mu_{max} \left\{ \frac{I_{avg}}{K_{S,I} \cdot I_{avg} \cdot \frac{I_{avg}^2}{K_{I,I}}} \right\} \qquad (34)$$

Where $K_{S,I}$ is the half-saturation constant for light (μmol/m^{2}s), I_{avg} is the average scalar irradiance (μmol/m^2-s), and $K_{I,I}$ is the light inhibition coefficient (μmol/m^{2}s).

Reported values for $K_{S,I}$ vary from 39 – 237 μmol/m^{2}s and $K_{I,I}$ from 1152 – 4780 μmol/m^{2}s (Koller et al., 2017). These effects will vary based on species sensitivity to photo-inhibition. For example, *Scenedesmus almeriensis* is tolerant to high irradiances, showing no signs of photoinhibition up to 1625 μmol/m^2-s (Sánchez et al., 2008). In well mixed cultures additional growth can occur from the flashing-effect as cells are mixed from the bottom of the reactor with low light intensity to the top with higher intensity. This effect is amplified in dense cultures where the attenuation at the bottom of the culture can be significant (Béchet et al., 2013).

Given that the system modeled here has low light intensity and culture density (121 μmol/m^{2}s and under 100 mg TSS/L) equation 32 is used to estimate the average irradiance in the reactor. Light is considered as a complimentary nutrient to inorganic

carbon in the Monod growth model, completing equations 12-14 as follows in equations 35-37.

(35) $$\mu_{CO2} = \mu_{max,CO2}\left\{\left(\frac{[CO_2(aq)]}{K_{CO_2}+[CO_2(aq)]}\right)\left(\frac{I_{avg}}{K_{S,I}+I_{avg}}\right)\right\}$$

(36) $$\mu_{HCO3} = \mu_{max,HCO3}\left\{\left(\frac{[HCO_3^-]}{K_{HCO_3^-}+[HCO_3^-]}\right)\left(\frac{K_{CO_2}}{K_{CO_2}+[CO_2(aq)]}\right)\left(\frac{I_{avg}}{K_{S,I}+I_{avg}}\right)\right\}$$

(37) $$\mu_{CO3} = \mu_{max,HCO3}\left\{\left(\frac{[HCO_3^-]}{K_{HCO_3^-}+[HCO_3^-]}\right)\left(\frac{K_{CO_2}}{K_{CO_2}+[CO_2(aq)]}\right)\left(\frac{K_{HCO_3^-}}{K_{HCO_3^-}+[HCO_3^-]}\right)\left(\frac{I_{avg}}{K_{S,I}+I_{avg}}\right)\right\}$$

Completed Mass Balance Equations

To model a closed carbonate system in which the concentration of H_2CO_3 is assumed negligible, the CO_2 hydration summary reaction shown as equation 6 should be considered with remaining carbonate reactions (equations 4 and 7 through 9). Using kinetic rate laws for each of these reactions, mass balance equations (MBEs) for carbonate species, algal biomass, hydrogen, and hydroxide are formulated (equations 38 through 44).

$$\left(d\left[CO_2\right]/dt\right)_{closed} = \; - r_{C,CO2} + k_{-}\left[H^+\right]\left[HCO_3^-\right] - k_{+}\left[CO_2\right] + k_{-4}\left[HCO_3^-\right] - k_{+4}\left[CO_2\right]\left[OH^-\right]. \tag{38}$$

$$\left(d\left[HCO_3^-\right]/dt\right)_{closed} = \begin{array}{l} - r_{C,HCO3} + \\ k_{+}\left[CO_2\right] - k_{-}\left[H^+\right]\left[HCO_3^-\right] + k_{+4}\left[CO_2\right]\left[OH^-\right] - k_{-4}\left[HCO_3^-\right] \\ + k_{-5}\left[H^+\right]\left[CO_3^{2-}\right] - k_{+5}\left[HCO_3^-\right] - k_{+6}\left[HCO_3^-\right]\left[OH^-\right] + k_{-6}\left[CO_3^{2-}\right]. \end{array} \tag{39}$$

$$\left(d\left[CO_3^{2-}\right]/dt\right)_{closed} = \begin{array}{l} - r_{C,CO3} + \\ k_{+5}\left[HCO_3^-\right] - k_{-5}\left[H^+\right]\left[CO_3^{2-}\right] + k_{+6}\left[HCO_3^-\right]\left[OH^-\right] - k_{-6}\left[CO_3^{2-}\right]. \end{array} \tag{40}$$

$$\left(d\left[H^+\right]/dt\right)_{closed} = \begin{array}{l} -\left(r_{H,CO2} + r_{H,HCO3} + r_{H,CO3}\right) + \\ k_+\left[CO_2\right] - k_-\left[H^+\right]\left[HCO_3^-\right] + k_{+5}\left[HCO_3^-\right] - k_{-5}\left[H^+\right]\left[CO_3^{2-}\right] \\ +k_{+7} - k_{-7}\left[H^+\right]\left[OH^-\right]. \end{array} \quad (41)$$

$$\left(d\left[OH^-\right]/dt\right)_{closed} = \begin{array}{l} k_{-4}\left[HCO_3^-\right] - k_{+4}\left[CO_2\right]\left[OH^-\right] - k_{+6}\left[HCO_3^-\right]\left[OH^-\right] + k_{-6}\left[CO_3^{2-}\right] \\ +k_{+7} - k_{-7}\left[H^+\right]\left[OH^-\right]. \end{array} \quad (42)$$

$$d[TIC]/dt = \frac{d\left[CO_2\right]}{dt} + \frac{d\left[HCO_3^-\right]}{dt} + \frac{d\left[CO_3^{2-}\right]}{dt} \quad (43)$$

$$d[X]/dt = \left(\mu_{CO_2} \cdot X\right) + \left(\mu_{HCO_3} \cdot X\right) + \left(\mu_{CO_3} \cdot X\right) - (b \cdot X) \quad (44)$$

Alkalinity

Alkalinity defined as the acid-absorbing capacity of water is a critical parameter due to its use in calculating the total inorganic carbon. Alkalinity in natural freshwater is presented with the following equation 45.

$$ALK = [HCO_3^-] + 2[CO_3^{2-}] + [OH^-] - [H^+] \quad (45)$$

Roughly this refers to the number of weak bases in the solution that can be changed to uncharged species by an acid, where the moles of the base are multiplied by the charge of the ion. Some ions are not considered such as: Na^+, K^+, Ca^{2+}, Mg^{2+}, Cl^-, SO_4^{2-}, and NO_3^- because their concentrations are not changed with changes in pH (Drever, 1982). In-sea water, it expands to the following equation 46.

$$ALK = [HCO_3^-] + 2[CO_3^{2-}] + [B(OH)_4^-] + [OH^-] + 2[PO_4^{3-}] + [HPO_4^{2-}] + [SiO(OH)_3^-] - [H^+] - [HSO_4^-] - [HF] \quad (46)$$

In seawater, up to 5 percent of alkalinity can be due to borate, whereas HF, HSO_4^-, phosphates, and silica are typically negligible and at typical seawater pH values (Zeebe et al., 2001). Likewise, in algal culture systems, considerations must be made for the concentrations of these ions in the growth medium to ensure accurate calculation of total inorganic carbon concentrations. BG-11 growth medium used in this research, contains constituents that contribute to total alkalinity (Table 2.6). (Watson & Drapcho, 2016).

Table 2.6: Measured Alkalinity Contribution of BG-11 Media Components

Compound	Concentration in Modified BG-11 (g/L)	Measured ALK (mmol equiv/L)
$NaNO_3$	1.5	0.06 ± 0.01
K_2HPO_4	0.04	0.3 ± 0.01
$MgSO_4$ $7H_2O$	0.075	0.02
$CaCl_2$ $2H_2O$	0.036	0.02
Ferric ammonium citrate	0.006	0.003
EDTA	0.001	0.002
Na_2CO_3	0.2	3.72 ± 0.02
Trace Metal Mix A5	1.0 mL/1L	0.02 ± 0.004

Therefore, a correction factor was applied to account for the difference in initial measured alkalinity and known initial added sodium carbonate. This correction factor was determined using equations 47-49 below and the initial pH of 10.3.

$$[ALK\ Correction\ Factor] = \{[C_{T,error}] * (\propto_1 + 2 \propto_2)\} + [OH^-] - [H^+] \quad (47)$$

where:

$$\alpha_1 = \left(\frac{[H^+]}{K_1} + 1 + \frac{K_2}{[H^+]} \right)^{-1} \quad (48)$$

$$\alpha_2 = \left(\frac{[H^+]^2}{K_1 K_2} + \frac{[H^+]}{K_2} + 1 \right)^{-1} \quad (49)$$

and K_1 and K_2 are defined equilibrium constants in Table 2.2.

The resulting alkalinity correction factors for each reactor run can be seen in Table 2.7 below.

Table 2.7: Alkalinity Correction Factors

Reactor	Carbon Added (mmol C/L)	Carbon Calculated Error (mmol C/L)	ALK Correction Factor (meq/L)
25%	0.47	0.71	1.29
50%	0.94	0.75	1.35
75%	1.42	0.77	1.38
100%	1.89	0.83	1.47

TIC for experimental data was then calculated using the corrected alkalinity and the measured pH for every time point. The system of equations generated from closed mass balances by Stumm and Morgan (1996) were used to determine the TIC and concentration of H_2CO_3*, HCO_3, CO_3. The system of equations is shown in equations 50 – 54 below.

$$\alpha_o = \left(1 + \frac{K_1}{[H^+]} + \frac{K_1 K_2}{[H^+]^2}\right)^{-1} \quad (50)$$

$$\alpha_1 = \left(\frac{[H^+]}{K_1} + 1 + \frac{K_2}{[H^+]}\right)^{-1} \quad (48)$$

$$\alpha_2 = \left(\frac{[H^+]^2}{K_1 K_2} + \frac{[H^+]}{K_2} + 1\right)^{-1} \quad (49)$$

$$C_T = \frac{[ALK] - [OH^-] + [H^+]}{\alpha_1 + 2\alpha_2} \quad (51)$$

$$[H_2CO_3^*] = C_T * \alpha_o \quad (52)$$

$$[HCO_3^-] = C_T * \alpha_1 \quad (53)$$

$$[CO_3^{2-}] = C_T * \alpha_2 \qquad (54)$$

where: $[H^+]$ = hydrogen ion concentration, mol/L; [ALK] = Carbonate alkalinity, mol equivalence/L; $[OH^-]$ = hydroxyl ion concentration, mol/L; C_T = TIC concentration, mol/L; $[H_2CO_3]$, $[HCO_3^-]$, and $[CO_3^{2-}]$ expressed as mol/L. (Stumm & Morgan, 1996)

Model Construction

An algal growth model was developed using Matlab® R2018B software with MBEs displayed in equations 38-44. The systems of ordinary differential equations (ODEs) were solved for user-defined initial conditions using ODE23tb solvers provided by Matlab®. These solvers are used for "stiff" models which contain rapidly and slowly changing components using the trapezoidal rule and backward differentiation formula (Chapra, 2005). The developed algal growth model considers both rapid carbonate kinetics and relatively slow algal growth kinetics. The Matlab® code for the inputs and graphing file is in Appendix I, the closed system algal growth model with CO_2/HCO_3 substitutable is in Appendix II, and the closed system algal growth model with $CO_2/HCO_3/CO_3$ substitutable is in Appendix III.

Model Inputs

Culturing and characterization of freshwater algal growth as a function of media inorganic carbon content in closed and open batch reactors can be found in Watson and Drapcho (2016). Experiments were conducted by inoculating a freshwater algal inoculum containing primarily the Chlorophyta *Scenedesmus* into 4L reactors containing a modified BG-11 medium with various concentrations of Na_2CO_3. All reactors were exposed to 121 $\mu E/m^2$-s at 25°C in a controlled-environment room. Four levels of inorganic carbon treatment were used (6, 11, 17, or 23 mg C L^{-1}). Initial model inputs and

experimental data were corrected to be based solely on carbonate alkalinity (equation 47) instead of total measured alkalinity. A summary of all inputs can be found in Tables 2.8 and 2.9.

Table 2.8: Model Inputs

Variable	Value	Units	Reference
b	0.00285	hr^{-1}	(Watson & Drapcho, 2016)
$K_{S,CO2}$	5.36 x 10^{-4}	mg C/L	(Watson & Drapcho, 2016)
$K_{S,HCO3}$	6.84	mg C/L	(Watson & Drapcho, 2016)
$K_{S,CO3}$	10.44	mg C/L	(Watson & Drapcho, 2016)
$K_{S,L}$	45.9	$\mu E/m^2s$	(Watson & Drapcho, 2016)
Io	121	$\mu E/m^2s$	(Watson & Drapcho, 2016)
K	1.4+0.0592*TSS	$\mu E/m^2s$	(Desmit et al., 2005)
h	0.2032	m	(Watson & Drapcho, 2016)
$\mu_{max,CO2}$	0.079	hr^{-1}	(Watson, 2009)
$\mu_{max,HCO3}$	0.07935	hr^{-1}	(Watson, 2009)
$\mu_{max,CO3}$	0.0703	hr^{-1}	(Watson, 2009)

Due to the variations from Redfield's ratio based on media carbon content (Watson & Drapcho, 2016), Carbon (x), Nitrogen (y), and Phosphorous (z) factors were used to quantify the algae biomass.

Table 2.9: X, Y, and Z Factors based on Media Carbon

Parameter	Units	Closed Batch Reactors			
Initial TIC	mg C L^{-1}	6	11	17	23
Carbon (x)	mol C/mol X	6.16	6.18	7.67	10.16
Nitrogen (y)	mol N/mol X	1.01	0.947	1.25	1.52
Phosphorous (z)	mol P/mol X	1	1	1	1
Molecular Weight (MW)	g/mol	252.2	251.7	301.6	380.9

Model Results with CO_2/HCO_3 Substitutable

Model results for the carbon dioxide and bicarbonate substitutable model are shown in Figures 2.3 – 2.10 below. Carbon dioxide as the preferred substrate was quickly consumed during the exponential growth stage.

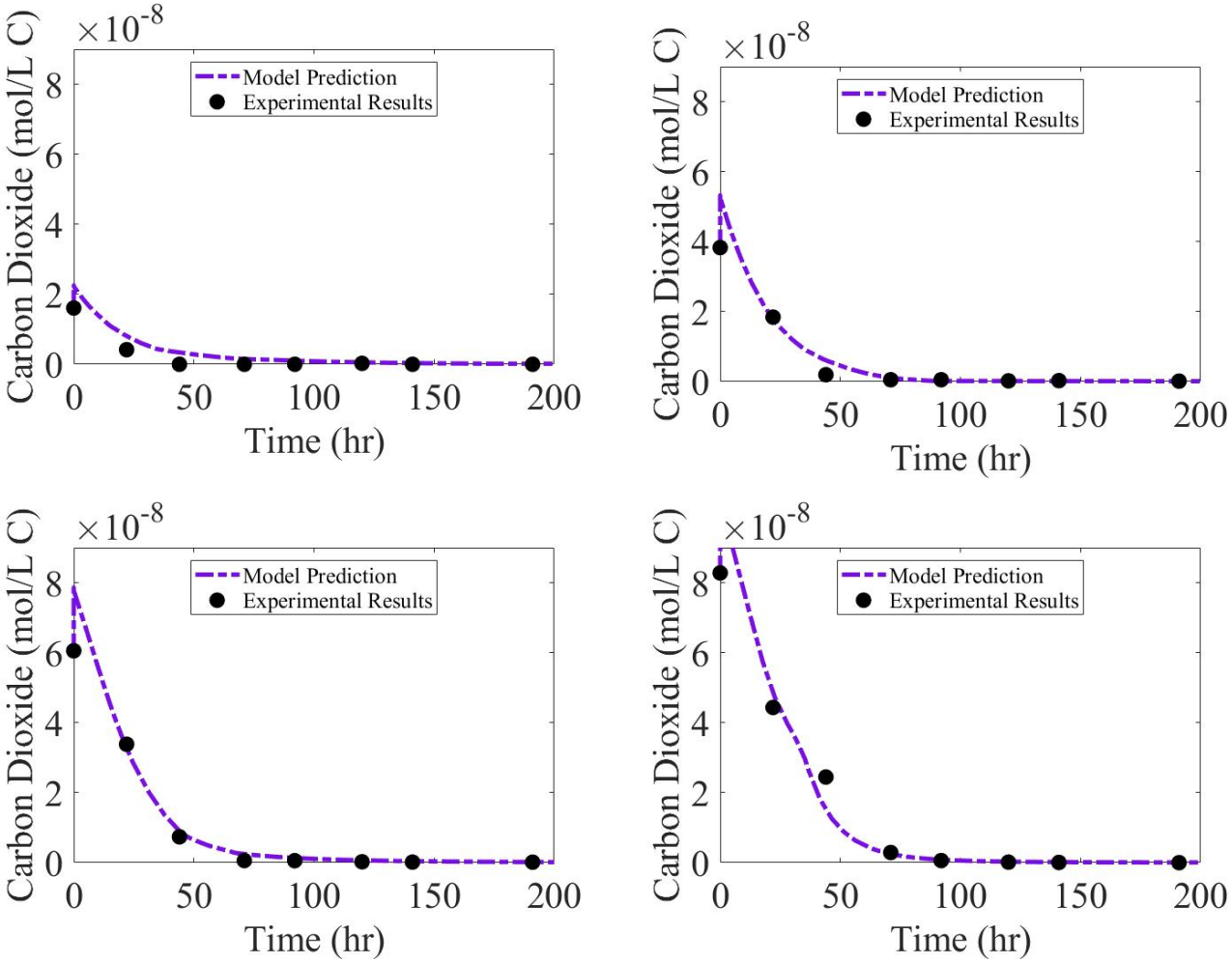

Figure 2.3: Carbon Dioxide Predictions for 6, 11 (Top, Left to Right) and 17, 23 (Bottom, Left to Right) mg C L^{-1} for CO_2/HCO_3 Substitutable Model

Bicarbonate was consumed secondarily as an alternate carbon source in the closed system and was depleted around 100 hours in all simulations, seen in Figure 2.4. Lastly carbonate was not modeled as a substrate, the changes in its concentration are due to the uptake of bicarbonate the subsequent equilibrizing of the carbonate system. Increases in carbonate are due to the rising pH of the system, seen in Figure 2.5.

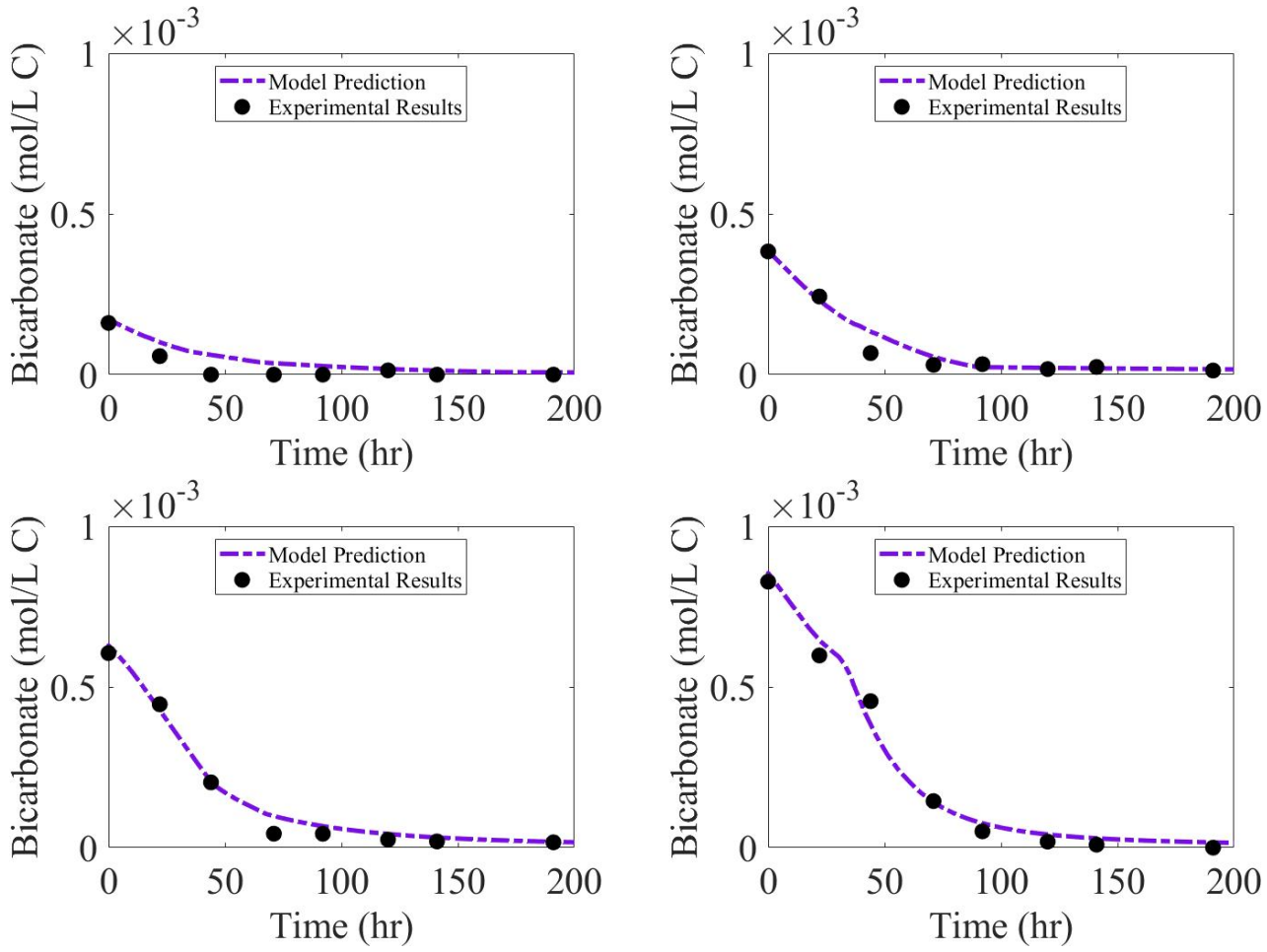

Figure 2.4: Bicarbonate Predictions for 6, 11 (Top, Left to Right) and 17, 23 (Bottom, Left to Right) mg C L^{-1} for CO_2/HCO_3 Substitutable Model

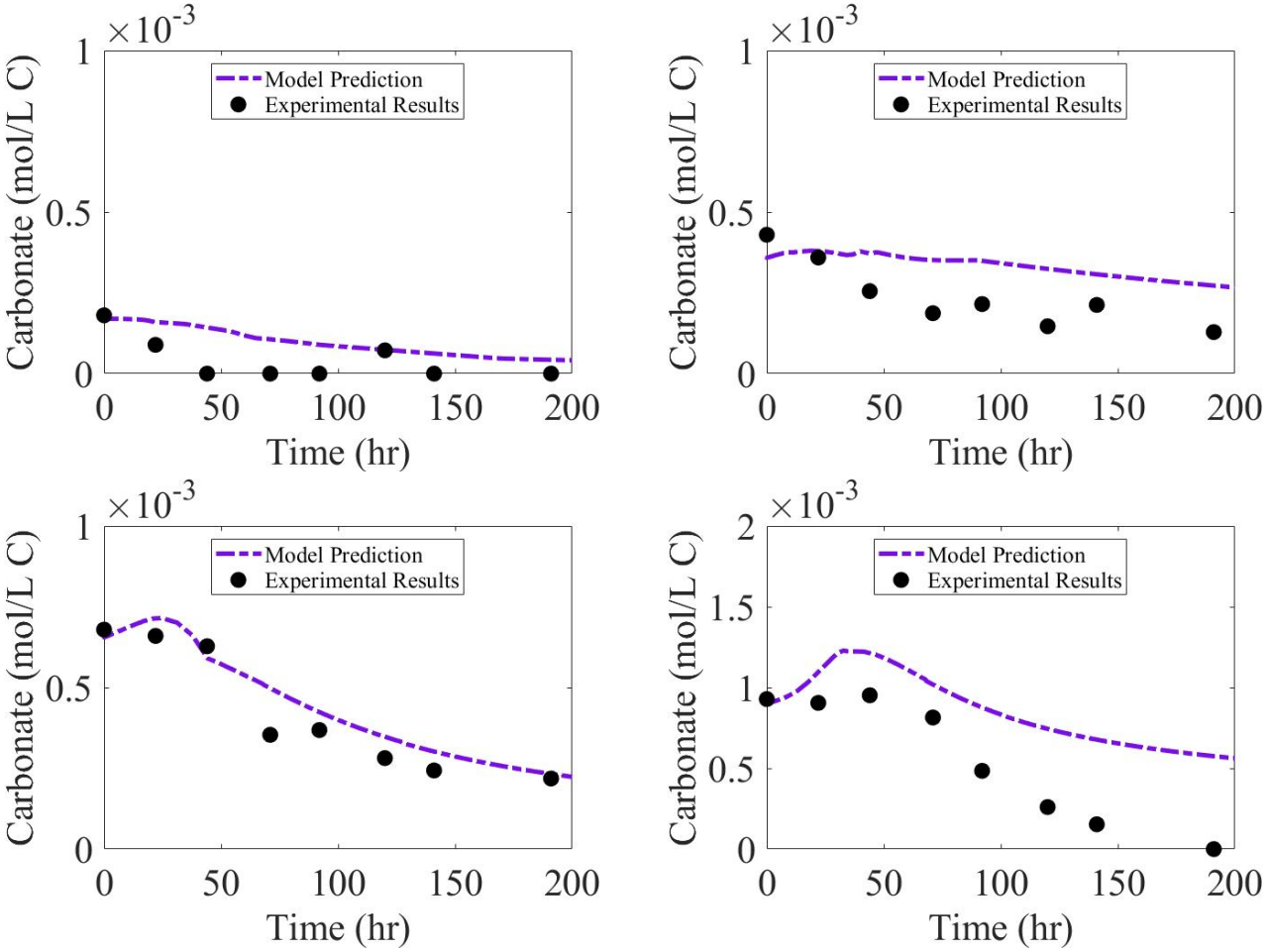

Figure 2.5: Carbonate Predictions for 6, 11 (Top, Left to Right) and 17, 23 (Bottom, Left to Right) mg C L^{-1} for CO_2/HCO_3 Substitutable Model

Total inorganic carbon is a sum of the previous three predictions leading to the trends seen in Figure 2.6 below. Alkalinity is calculated by the mass balance equations as the alkalinity that can be attributed to carbon alone, shown in Figure 2.7 below. The alkalinity correction factor could be added back in for a total alkalinity model.

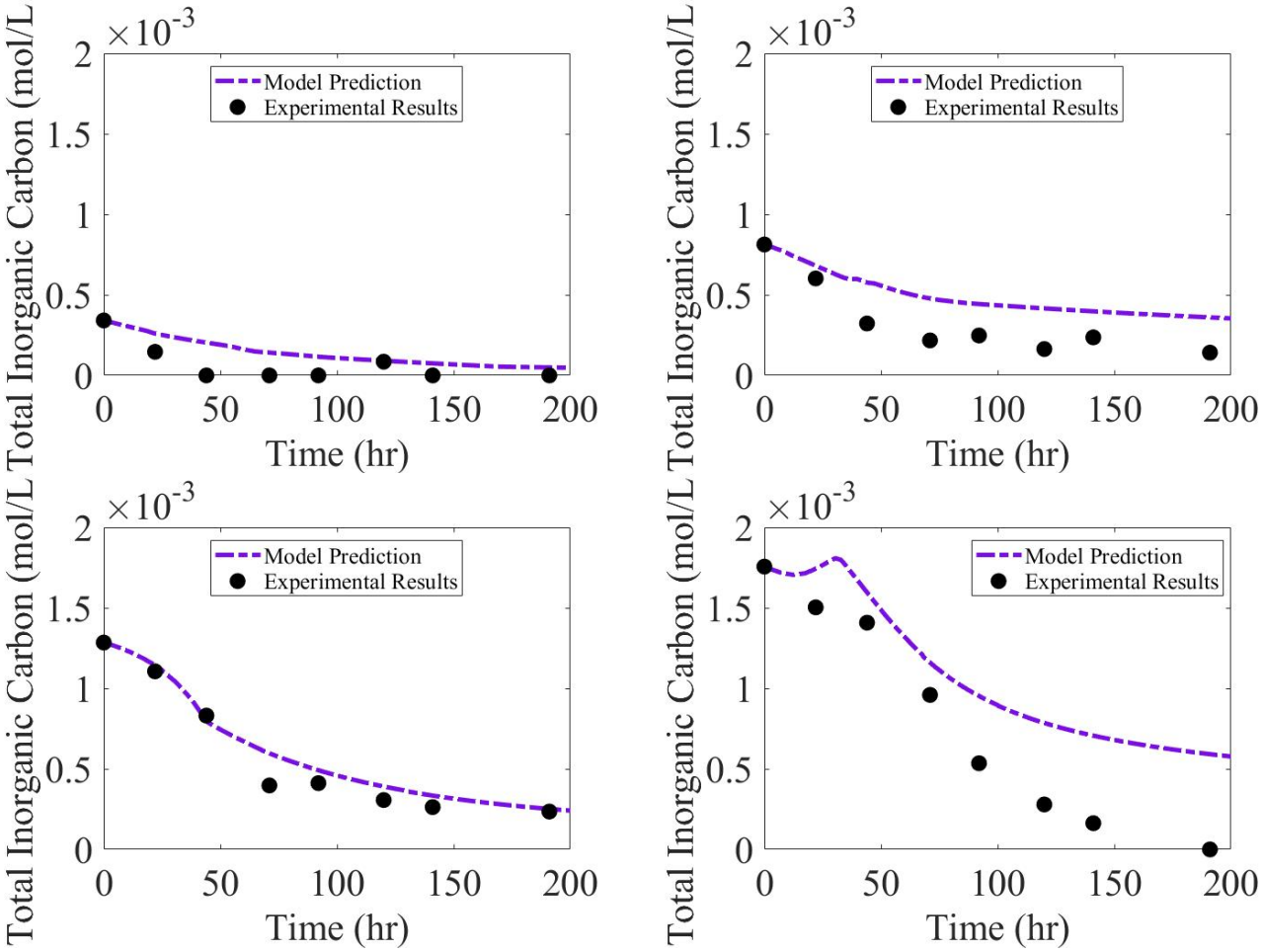

Figure 2.6: TIC Predictions for 6, 11 (Top, Left to Right) and 17, 23 (Bottom, Left to Right) mg C L^{-1} for CO_2/HCO_3 Substitutable Model

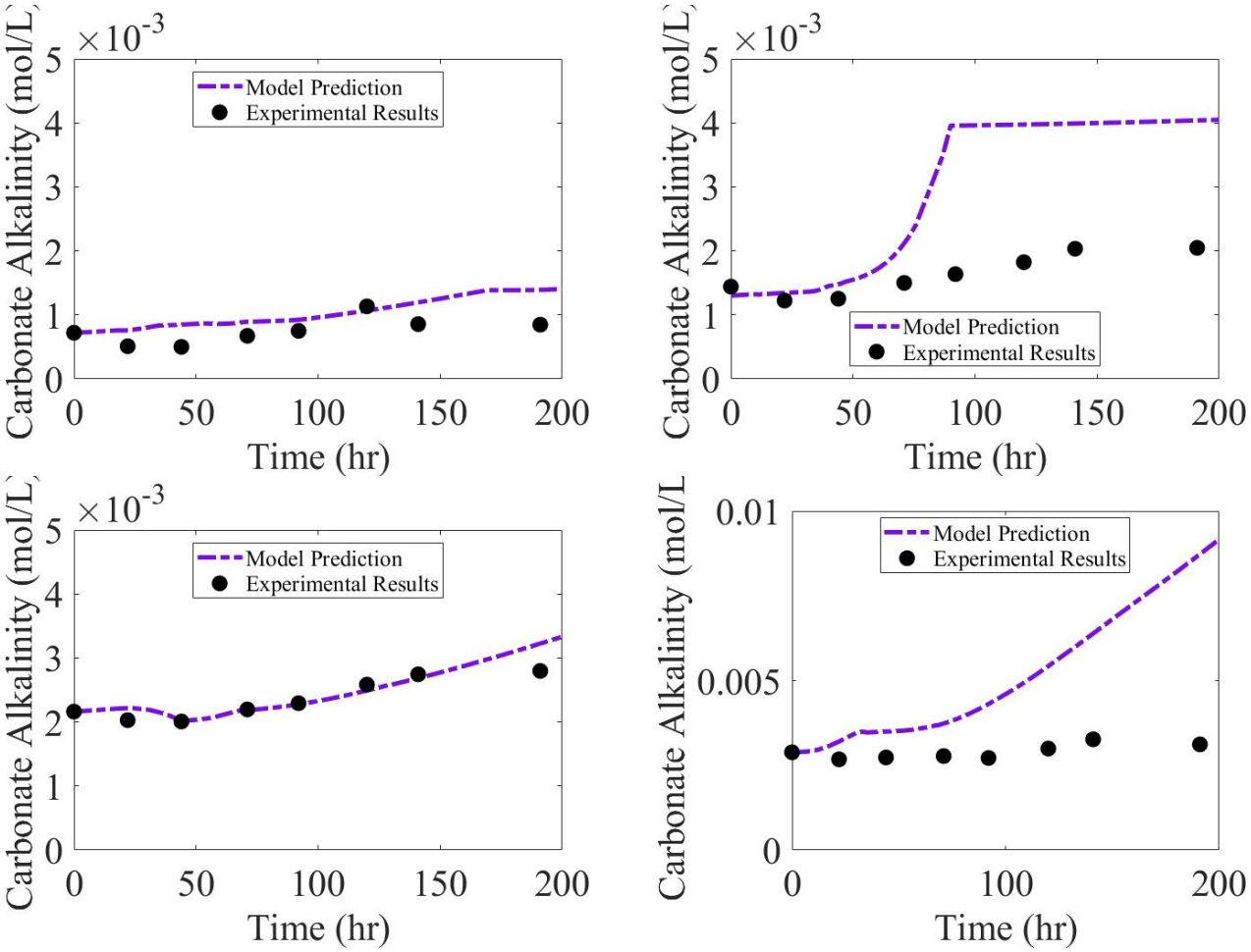

Figure 2.7: Carbonate Alkalinity Predictions for 6, 11 (Top, Left to Right) and 17, 23 (Bottom, Left to Right) mg C L^{-1} for CO_2/HCO_3 Substitutable Model

As discussed in Watson and Drapcho (2016), pH of the closed systems was allowed to rise naturally, and these high alkaline environments allow for increased CO_2 diffusion. The predictions of pH are below in Figure 2.8. The specific growth rates and decay rates are graphed and confirm that the rates are following the Monod trend and show preferential growth on carbon dioxide in Figure 2.9.

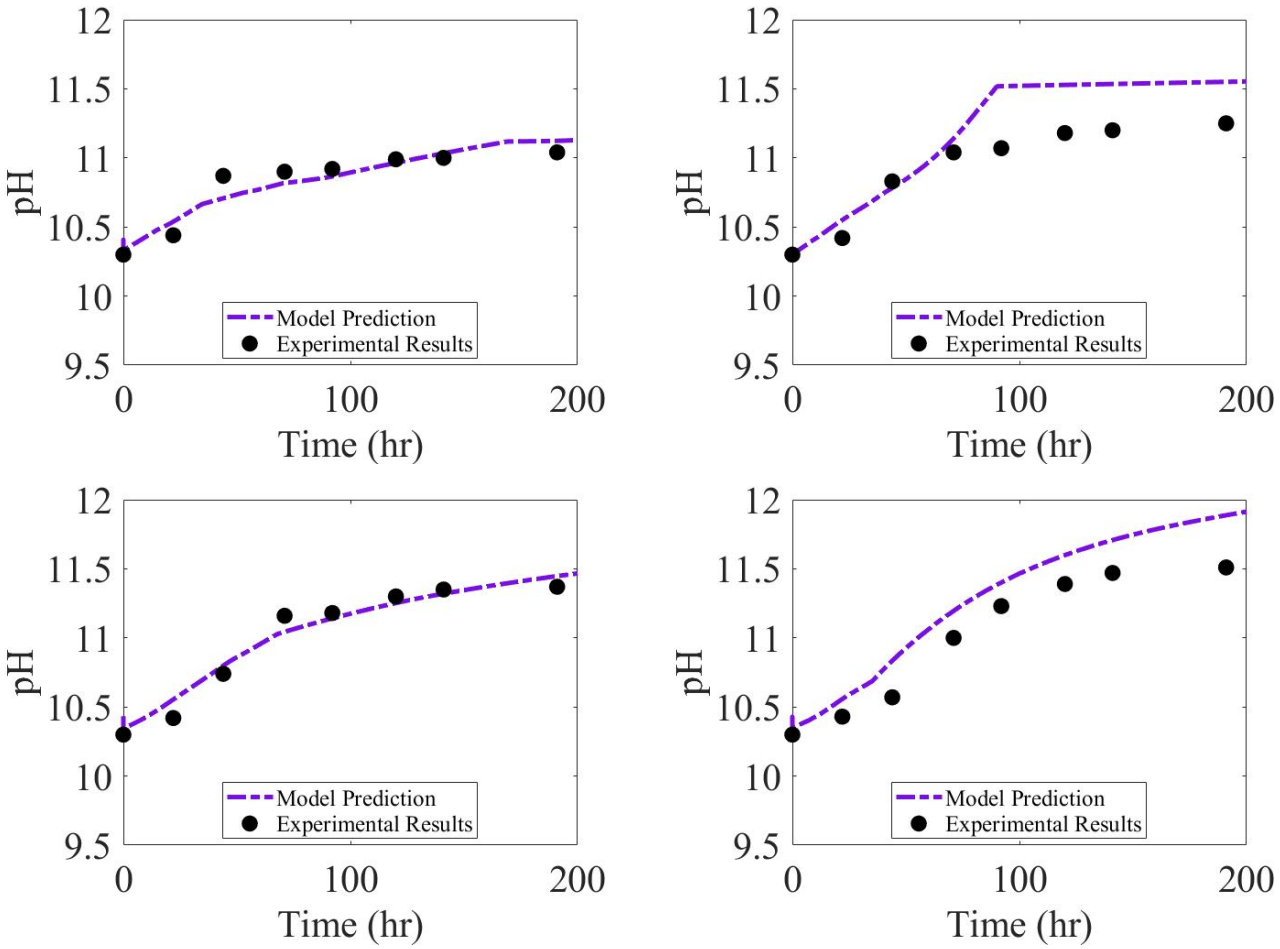

Figure 2.8: pH Predictions for 6, 11 (Top, Left to Right) and 17, 23 (Bottom, Left to Right) mg C L^{-1} for CO_2/HCO_3 Substitutable Model

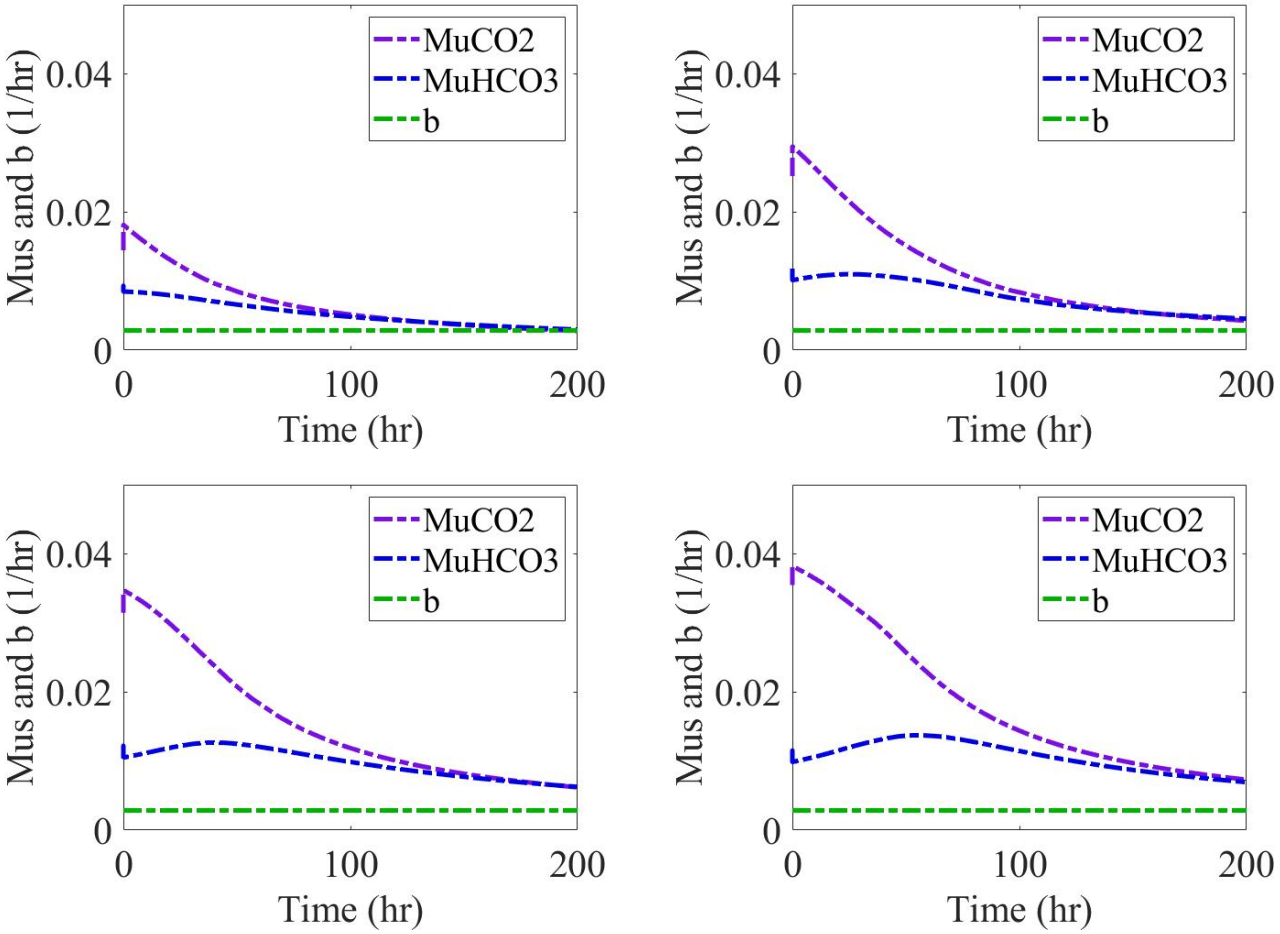

Figure 2.9: Specific Growth (Mu, equations 35 and 36) and Decay (b) Rates Predictions for 6, 11 (Top, Left to Right) and 17, 23 (Bottom, Left to Right) mg C L^{-1} for CO_2/HCO_3 Substitutable Model

Lastly, algal biomass measured as total suspended solids (TSS) is predicted based on the mass balance presented in equation 44 in Figure 2.10. For the CO_2/HCO_3 substitutable model, biomass TSS is largely underpredicted after 25 hours. The RMSE of all predicted variables are summarized in Table 2.10 below. Residual plots for all predicted variables can be found in Appendix IV.

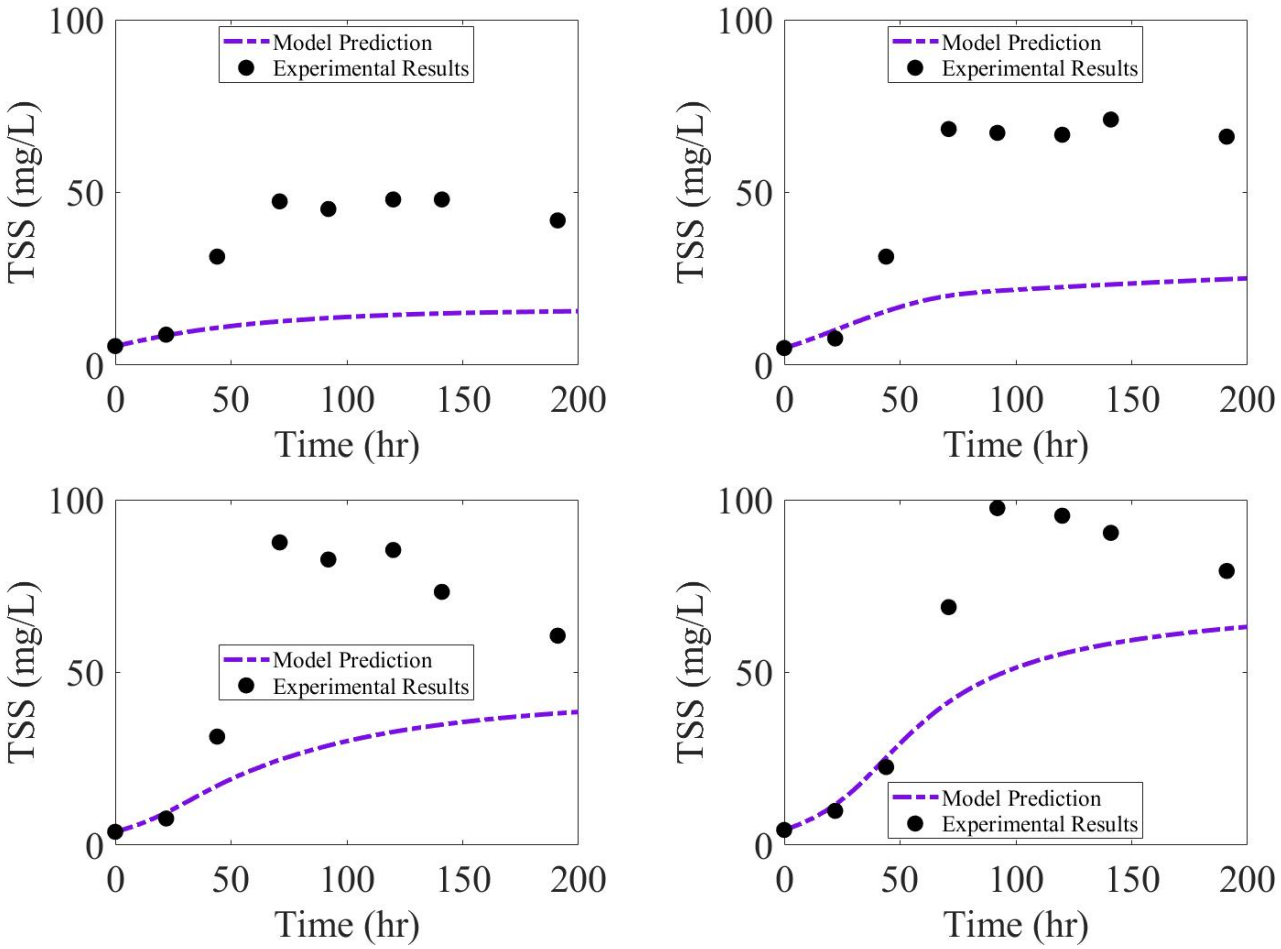

Figure 2.10: Biomass TSS Predictions for 6, 11 (Top, Left to Right) and 17, 23 (Bottom, Left to Right) mg C L^{-1} for CO_2/HCO_3 Substitutable Model

Table 2.10: RMSE of All Predicted Variables for CO_2/HCO_3 Substitutable Model

Media Carbon Content (mg C/L)	Biomass (mg/L)	TIC (mol/L)	CO_2 (mol/L)	HCO_3 (mol/L)	CO_3 (mol/L)	Alkalinity (mol eq/L)	pH
23	56.2103	9.45E-04	3.05E-09	8.47E-06	9.37E-04	5.30E-03	0.5681
17	86.0737	1.65E-04	2.00E-09	3.71E-05	1.27E-04	1.57E-04	0.0086
11	84.8943	4.99E-04	5.69E-10	2.22E-05	2.77E-04	3.20E-03	0.5736
6	63.5747	2.47E-04	3.81E-09	6.75E-05	1.80E-04	6.75E-04	0.0231
Average	72.68825	4.64E-04	2.36E-09	3.38E-05	3.80E-04	2.33E-03	0.2934
Sum	290.753	1.86E-03	9.43E-09	1.35E-04	1.52E-03	9.33E-03	1.1734

Model Results with $CO_2/HCO_3/CO_3$ Substitutable

Model results for the carbon dioxide and bicarbonate substitutable model are shown in Figures 2.11 – 2.18 below. Carbon dioxide is still the preferred substrate and was quickly consumed during the exponential growth stage shown in Figure 2.11. In this model bicarbonate was consumed secondarily as an alternate carbon source in the closed system and was depleted around 75 hours in all simulations as shown in Figure 2.12.

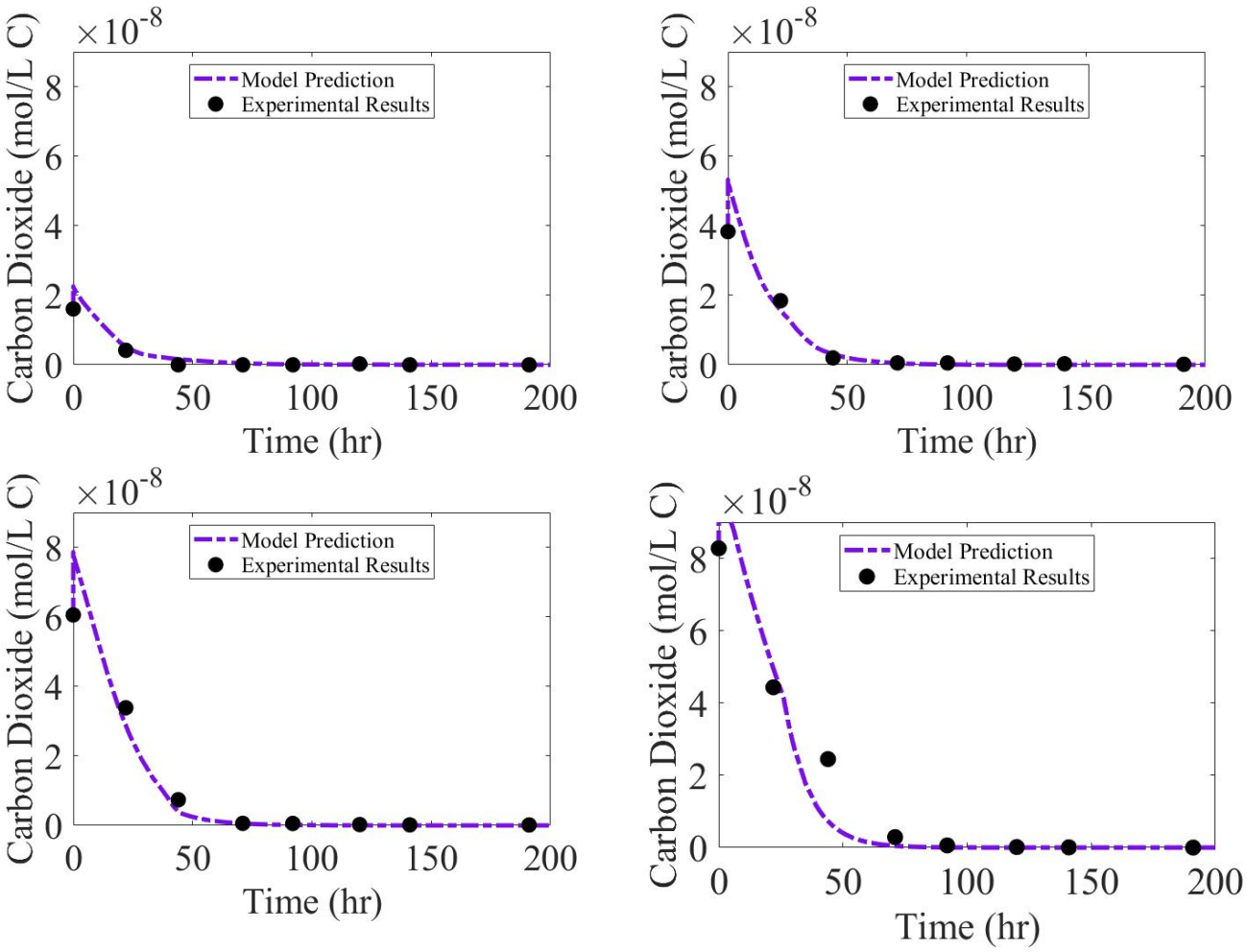

Figure 2.11: Carbon Dioxide Predictions for 6, 11 (Top, Left to Right) and 17, 23 (Bottom, Left to Right) mg C L^{-1} for $CO_2/HCO_3/CO_3$ Substitutable Model

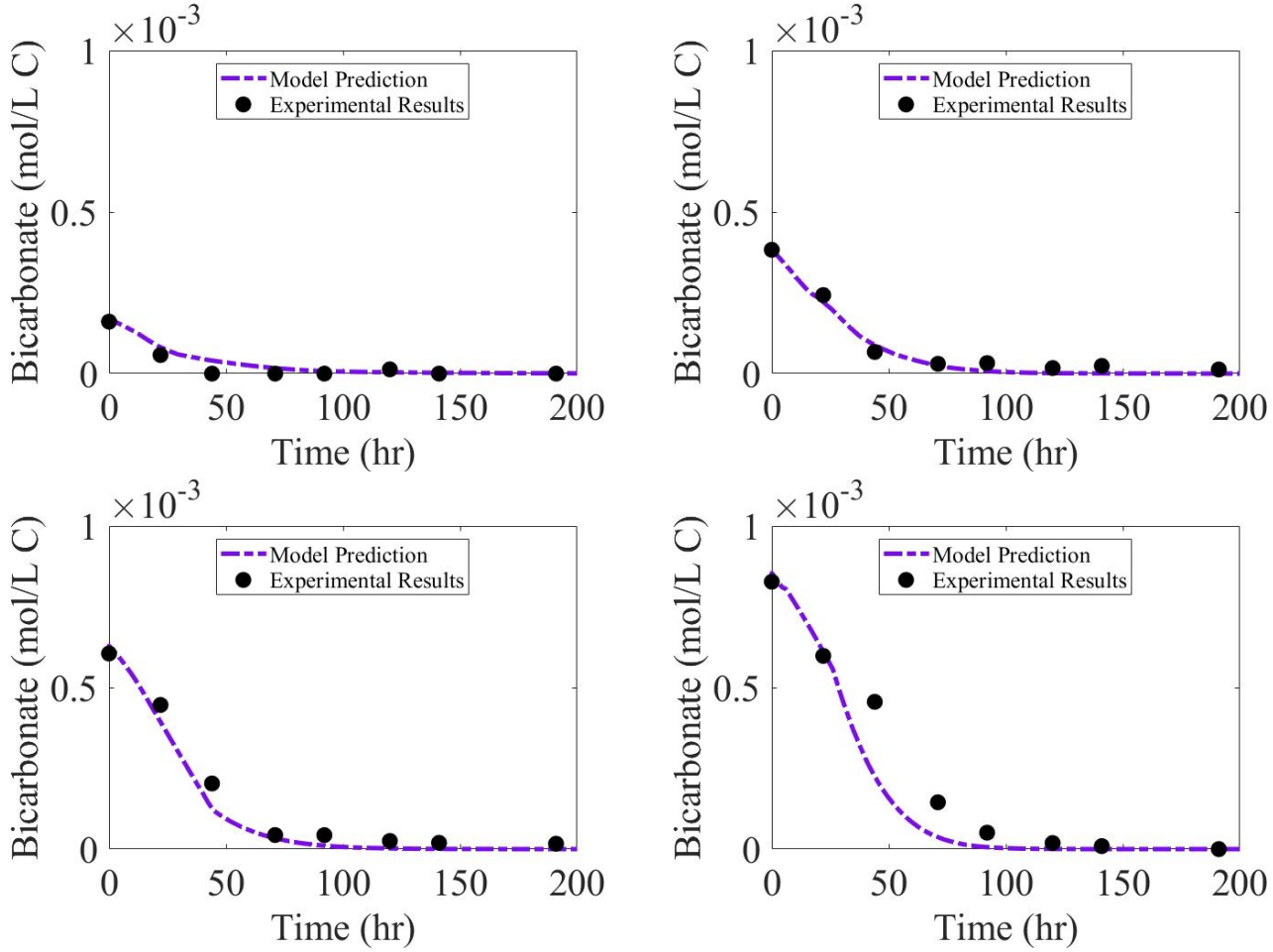

Figure 2.12: Bicarbonate Predictions for 6, 11 (Top, Left to Right) and 17, 23 (Bottom, Left to Right) mg C L^{-1} for $CO_2/HCO_3/CO_3$ Substitutable Model

Lastly carbonate was modeled as a substrate in this model, so it is modeled based on consumption of carbonate by algae and equilibrizing of the carbonate system. Increases in carbonate are due to the rising pH of the system. Total inorganic carbon is a sum of the previous 3 predictions leading to the trends seen in Figure 2.14 below.

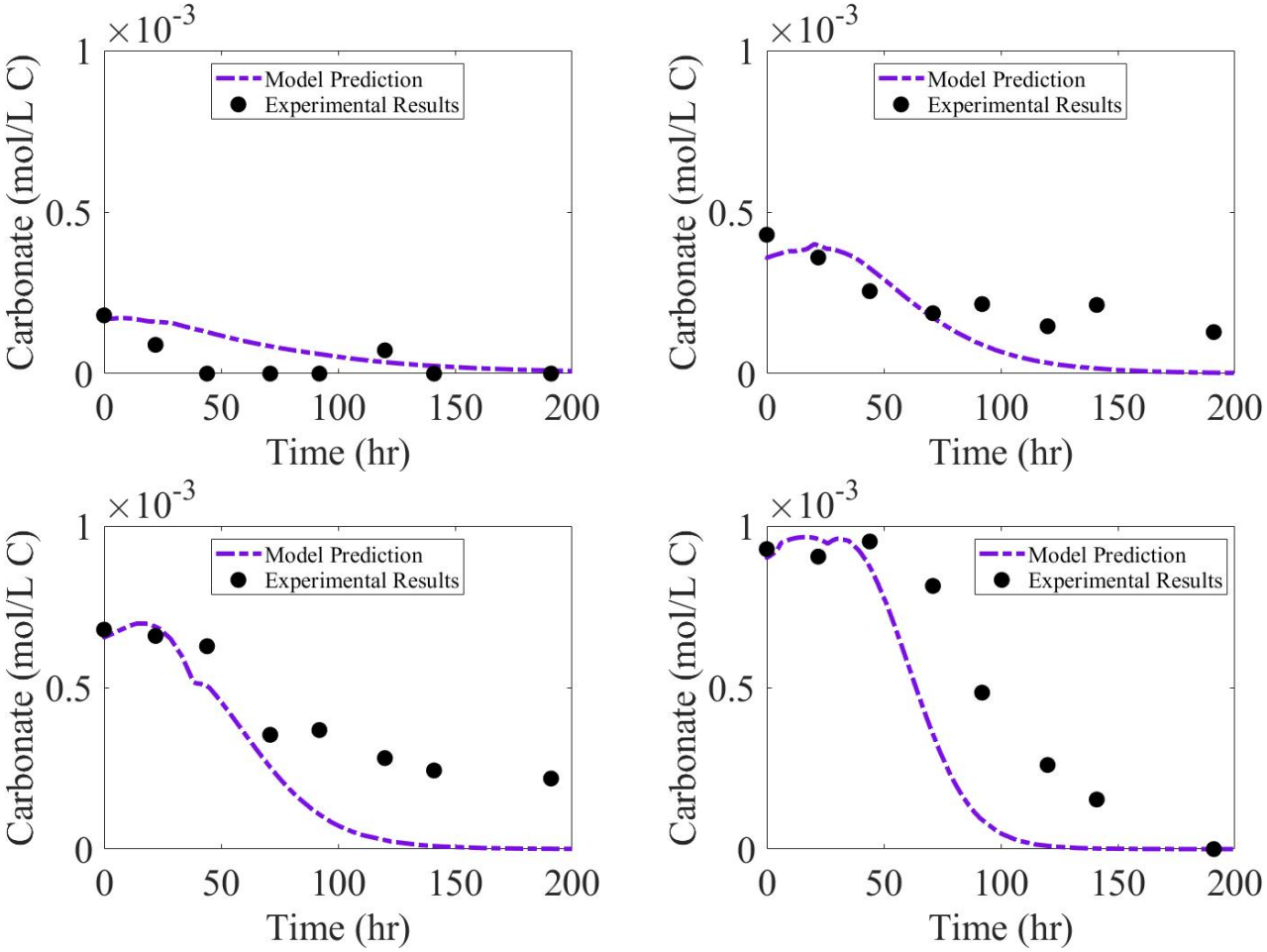

Figure 2.13: Carbonate Predictions for 6, 11 (Top, Left to Right) and 17, 23 (Bottom, Left to Right) mg C L^{-1} for $CO_2/HCO_3/CO_3$ Substitutable Model

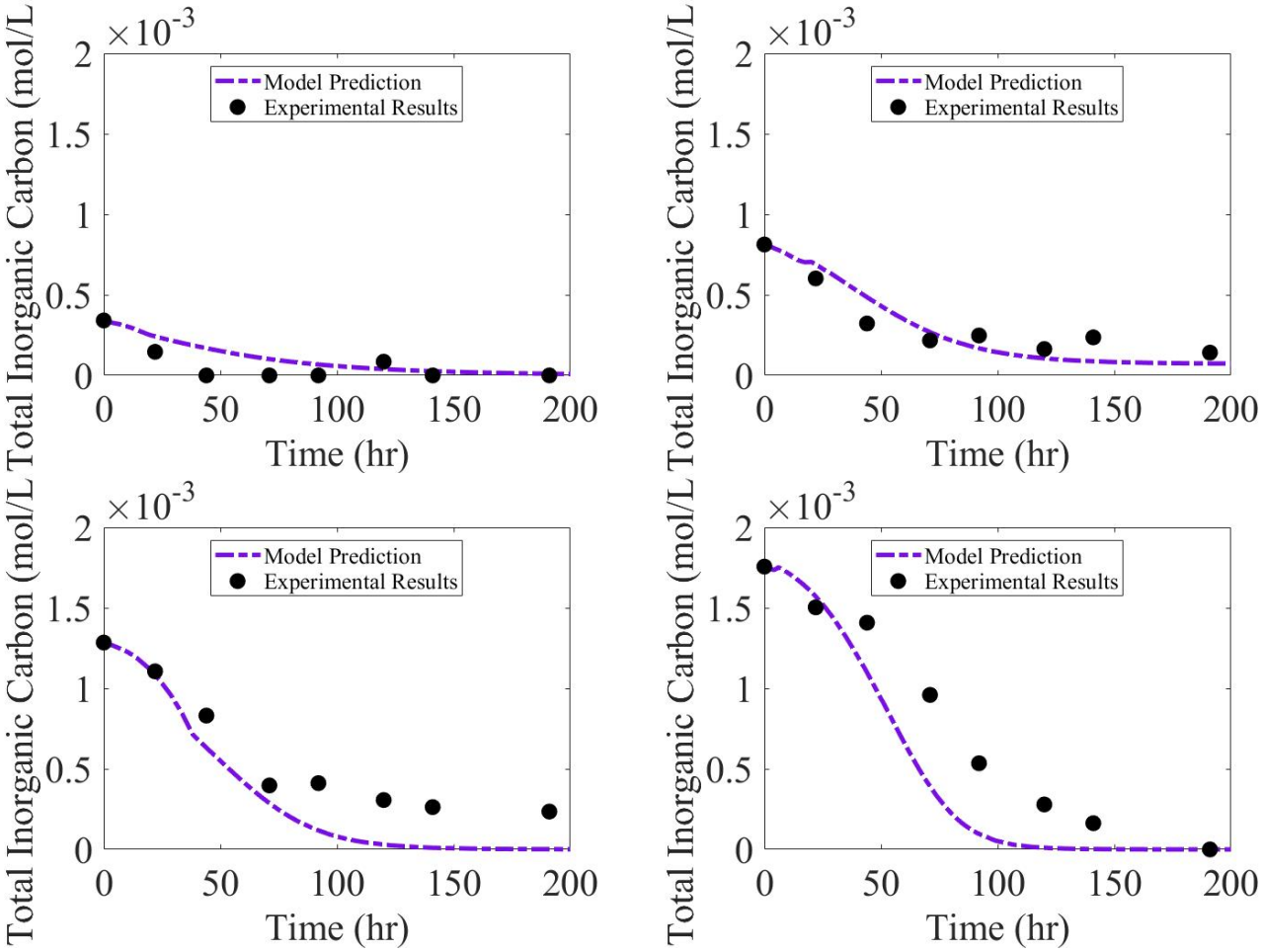

Figure 2.14: TIC Predictions for 6, 11 (Top, Left to Right) and 17, 23 (Bottom, Left to Right) mg C L^{-1} for $CO_2/HCO_3/CO_3$ Substitutable Model

Alkalinity is calculated by the same mass balance equations as the alkalinity that can be attributed to carbon alone, shown in Figure 2.15 below. As discussed in Watson and Drapcho (2016), pH of the closed systems was allowed to rise naturally, and these high alkaline environments allow for increased CO_2 diffusion. The predictions of pH are below in Figure 2.16.

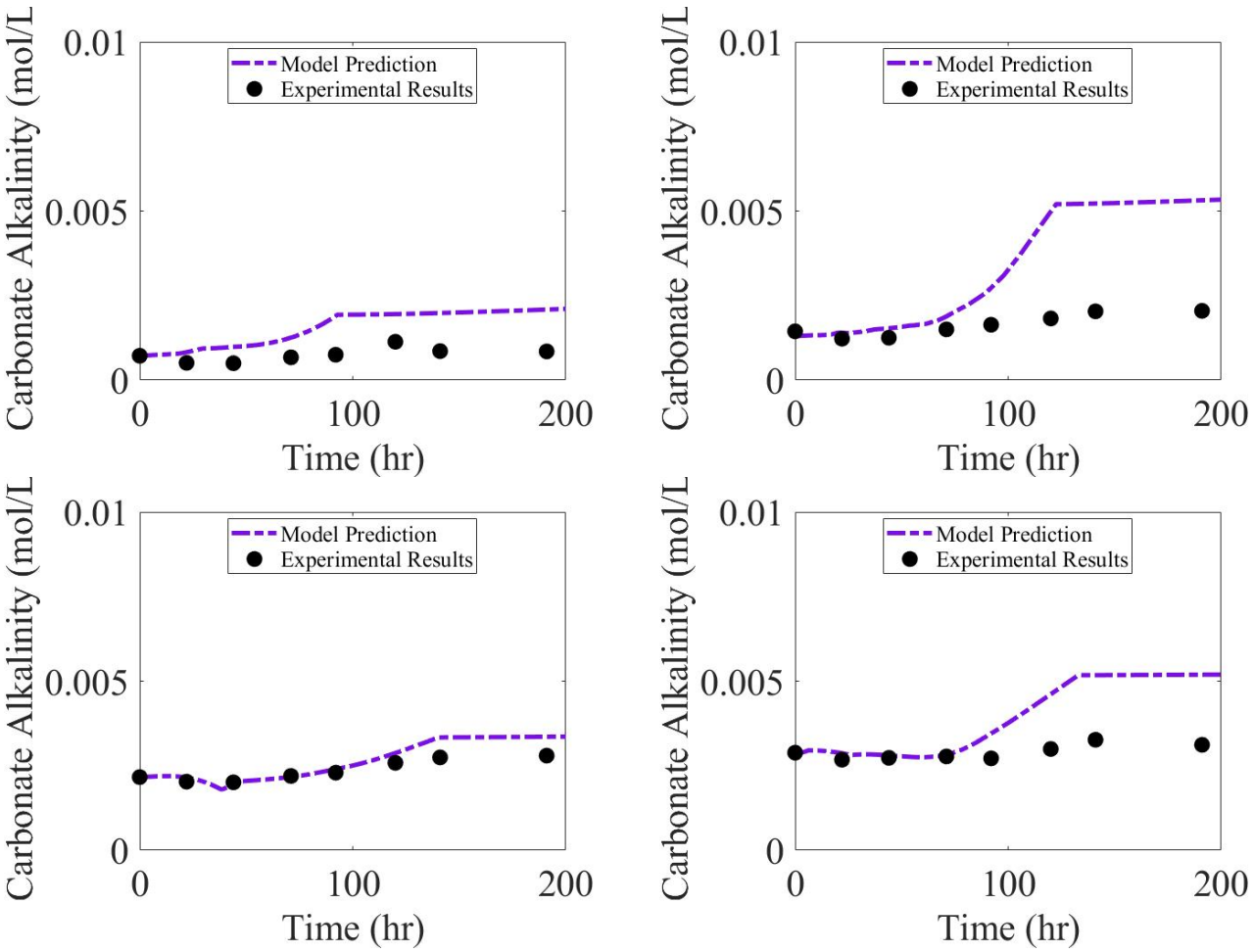

Figure 2.15: Carbonate Alkalinity Predictions for 6, 11 (Top, Left to Right) and 17, 23 (Bottom, Left to Right) mg C L^{-1} for $CO_2/HCO_3/CO_3$ Substitutable Model

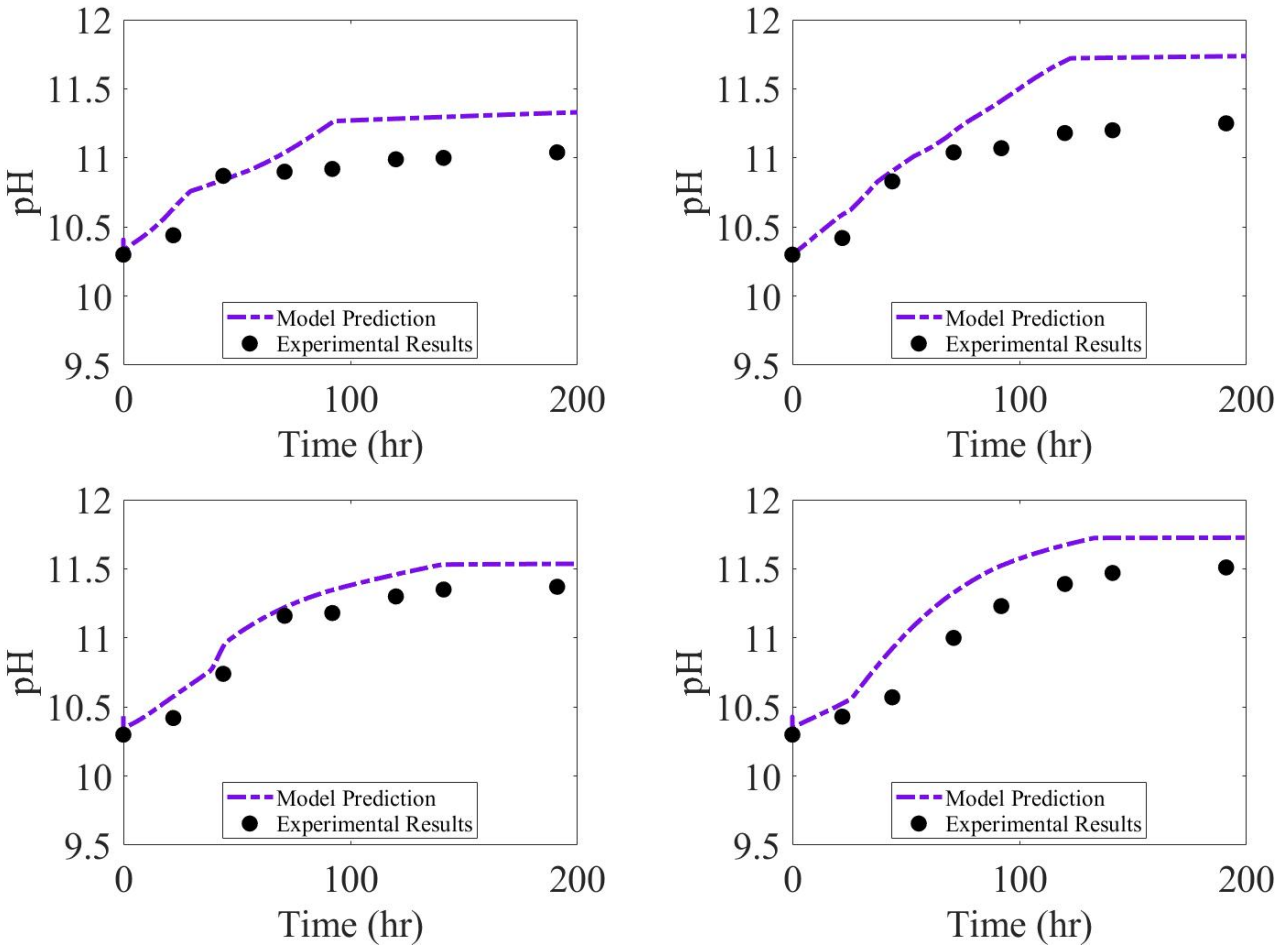

Figure 2.16: pH Predictions for 6, 11 (Top, Left to Right) and 17, 23 (Bottom, Left to Right) mg C L^{-1} for $CO_2/HCO_3/CO_3$ Substitutable Model

The specific growth rates and decay rates are graphed and confirm that the rates are following the Monod trend and show preferential growth on carbon dioxide, followed by bicarbonate, and then carbonate as seen in Figure 2.17. Lastly, algal biomass measured as total suspended solids (TSS) is predicted based on the mass balance presented in equation 44 as seen in Figure 2.18.

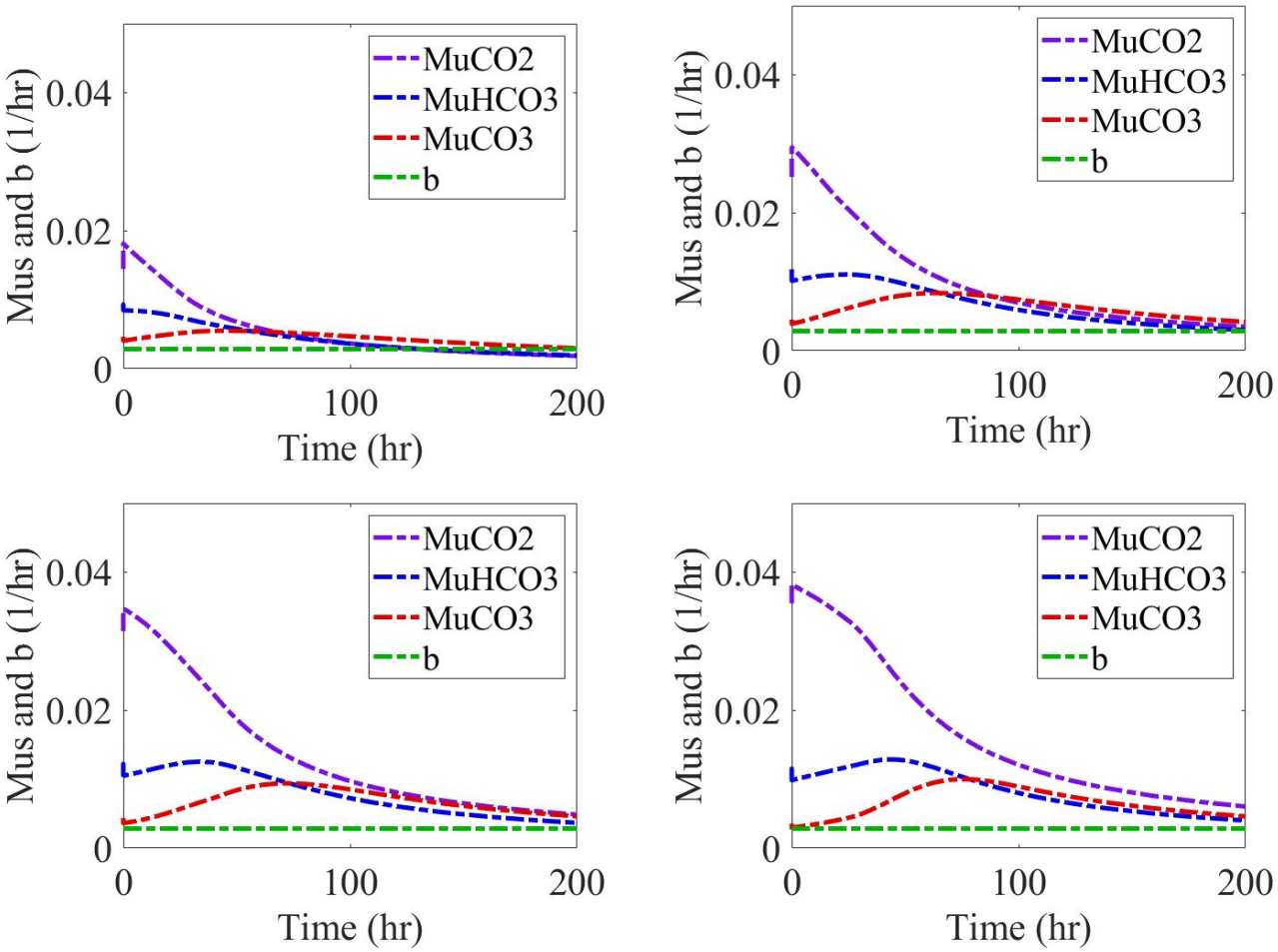

Figure 2.17: Specific Growth (Mu, equations 35-37) and Decay (b) Rate Predictions for 6, 11 (Top, Left to Right) and 17, 23 (Bottom, Left to Right) mg C L^{-1} for $CO_2/HCO_3/CO_3$ Substitutable Model

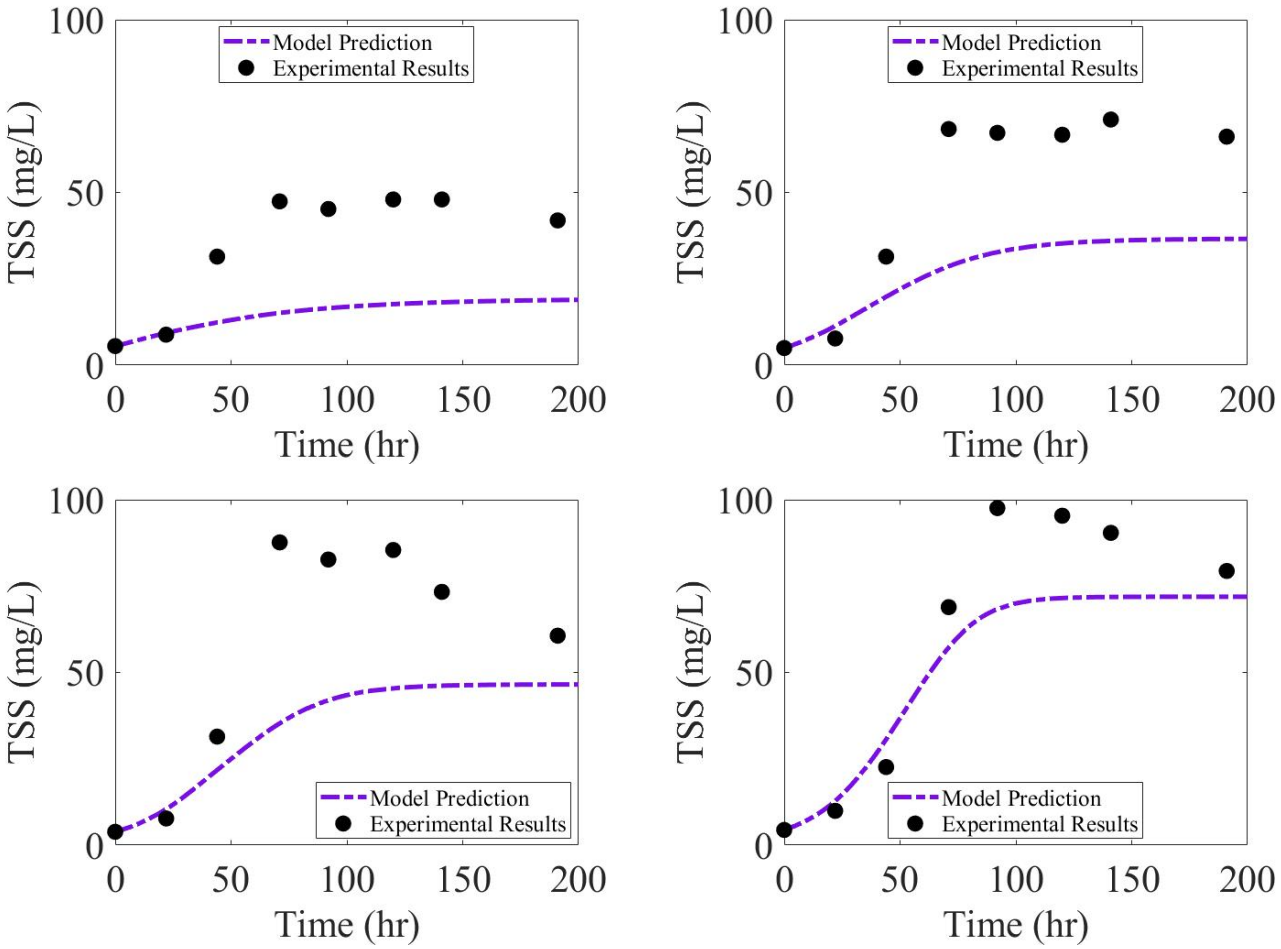

Figure 2.18: Algal Biomass TSS Predictions for 6, 11 (Top, Left to Right) and 17, 23 (Bottom, Left to Right) mg C L^{-1} for $CO_2/HCO_3/CO_3$ Substitutable Model

For the $CO_2/HCO_3/CO_3$ substitutable model, biomass TSS predictions are improved. The RMSE of all predicted variables are summarized in Table 2.11 below.

Table 2.11: RMSE of All Predicted Variables for $CO_2/HCO_3/CO_3$ Substitutable Model

Media Carbon Content (mg C/L)	Biomass (mg/L)	TIC (mol/L)	CO_2 (mol/L)	HCO_3 (mol/L)	CO_3 (mol/L)	Alkalinity (mol eq/L)	pH
23	28.7248	5.81E-04	5.18E-09	1.38E-04	4.42E-04	2.40E-03	0.6399
17	63.9485	4.99E-04	4.29E-09	8.78E-05	4.12E-04	5.78E-04	0.3903
11	63.4828	9.59E-06	5.84E-10	2.42E-05	1.86E-04	4.10E-03	0.7888
6	57.5426	1.50E-04	1.19E-09	3.01E-05	1.21E-04	2.00E-03	0.5407
Average	53.4247	3.10E-04	2.81E-09	7.01E-05	2.90E-04	2.27E-03	0.5899
Sum	213.6987	1.24E-03	1.12E-08	2.80E-04	1.16E-03	9.08E-03	2.3597

Residual plots for all predicted variables can be found in Appendix V.

Results Comparisons between Models

Comparison in the difference of RMSE between the two models indicates that the CO_2/HCO_3 substitutable model (2-sub model) is only better at predicting CO_2, HCO_3, and pH. The difference in CO_2 and HCO_3 predictions is very small, and the only difference of interest is those in the predictions of pH. The $CO_2/HCO_3/CO_3$ substitutable model (3-sub model) has better predictions for biomass, TIC, CO_3, and alkalinity. The comparison of these results can be seen in Table 2.12 below.

Table 2.12: Change in RMSE from All 3 Substitutable Model to 2 Substitutable Model (Negative indicates better predictions by all 3)

Media Carbon Content (mg C/L)	Biomass (mg/L)	TIC (mol/L)	CO_2 (mol/L)	HCO_3 (mol/L)	CO_3 (mol/L)	Alkalinity (mol eq/L)	pH
23	-27.48550	-3.65E-04	2.13E-09	1.30E-04	-4.95E-04	-2.90E-03	0.0718
17	-22.12520	3.34E-04	2.29E-09	5.07E-05	2.85E-04	4.21E-04	0.3817
11	-21.41150	-4.90E-04	1.54E-11	1.97E-06	-9.13E-05	9.00E-04	0.2152
6	-6.03210	-9.65E-05	-2.62E-09	-3.74E-05	-5.92E-05	1.32E-03	0.5176
Average	-19.26358	-1.54E-04	4.53E-10	3.62E-05	-9.01E-05	-6.36E-05	0.2966
Sum	-77.05430	-6.17E-04	1.81E-09	1.45E-04	-3.61E-04	-2.54E-04	1.1863

Overall carbon species, TIC, alkalinity, and pH measurements showed good agreement. Biomass however is largely underpredicted past 50 hours in both models, discussed later. Model fit of carbon dioxide and bicarbonate exceeds fit for carbonate.

Implications and Future Work

The $CO_2/HCO_3^-/CO_3^{2-}$ substitutable substrates model best predicts both the length of exponential growth and peak biomass concentration in closed batch algal reactors, furthering indicating the ability of algae to use all three species as substrate as discussed in Watson and Drapcho (2016). This may indicate that there is an unknown mechanism of carbonate transport into algal cells.

Inaccuracy in carbonate predictions may also be due to discrepancy of sources for reaction rate constants of equation 8 (Table 2.3). Modeled here is the geometric mean of these two rate constants, but this rapid reaction may require more quantification to determine a more accurate rate constant and might improve the carbonate species predictions.

The $CO_2/HCO_3^-/CO_3^{2-}$ substitutable substrates model while fits best for most predictions still underpredicts algal biomass (TSS). This may be due to the C-factor used in the model. Carbon concentrating mechanisms of algae are complex systems and using a singular value for carbon concentration inside the cell may not be appropriate. Further experimentation is necessary to determine how the C-factor varies with varying TIC conditions. Some exploration was done on this term as can be seen in Table 2.13 below.

Table 2.13: Effects of Varying C-factor on RMSE for 17 mg C/L Run

C factor (mol C/mol X)	Biomass (mg/L)	TIC (mol/L)	Alkalinity (mol eq/L)	pH
2	61.24	3.63E-4	0.0028	0.11
3	27.17	1.47E-6	4.98E-4	0.23
4	24.25	9.50E-4	0.0032	0.41
5	37.00	3.72E-6	0.0014	0.15
6	45.81	7.44E-5	0.0057	0.54
7	62.99	5.69E-5	0.0045	0.59
7.67 (original)	62.26	2.68E-4	2.30E-3	0.46
8	46.54	2.25E-4	0.0015	0.32
9	25.63	6.77E-4	9.63E-4	0.04
10	61.64	7.17E-4	4.61E-4	0.36
11	45.73	4.59E-4	0.0051	0.74

As seen in Table 2.13, changing C-factor greatly effects model results and should be explored further. Lastly, the modifications of alkalinity that led to modifications of inorganic carbon concentrations could have implications for the biological kinetics described in Table 2.8 that should be explored.

Conclusions

Here dynamic algal growth models intended to predict algal biomass and carbonate species concentrations in closed batch reactors were developed and evaluated. Total inorganic carbon, CO_2, HCO_3^-, CO_3^{2-}, pH, and alkalinity were well-predicted, while algal biomass concentrations were under-predicted. This model improves upon those reviewed by incorporating kinetic rates of carbon species interconversion instead of the equilibrium assumption. Discrepancies in rate constants of the bicarbonate hydroxylation reaction indicate more exploration of these parameters is needed. Underprediction of algal biomass and improved response of $CO_2/HCO_3^-/CO_3^{2-}$ substitutable model over a

CO_2/HCO_3^- substitutable alone may indicate an unknown biological pathway for the use of carbonate for growth.

As atmospheric CO_2 concentrations and global temperatures continue to escalate, researchers must develop creative methods to offset these trends. Cultivation of algal biomass in large outdoor ponds is an appealing strategy because biomass can be harvested and converted to biofuels to reduce use of traditional carbon-intensive fuels. Once further work is completed to improve the presented algal growth model, it can be used to aid in design and optimization of systems to produce algae for carbon mitigation and other bioproducts.

CHAPTER III: AIRLIFT PUMP DESIGN, IMPLEMENTATION, AND MODELING

Introduction

The Partitioned Aquaculture System (PAS), Figure 3.1 below, at Clemson University was originally designed to optimize oxygen dynamics in aquaculture systems through management of photosynthetic oxygen production by freshwater algae (Drapcho & Brune, 2000). The original design incorporated raceway ponds for algae cultivation for nutrient removal and oxygen production. Adjacent tanks were used for fish production. The system is now being revitalized through a variety of projects, including this one, to become an Algal Carbon Capture System (ACCS).

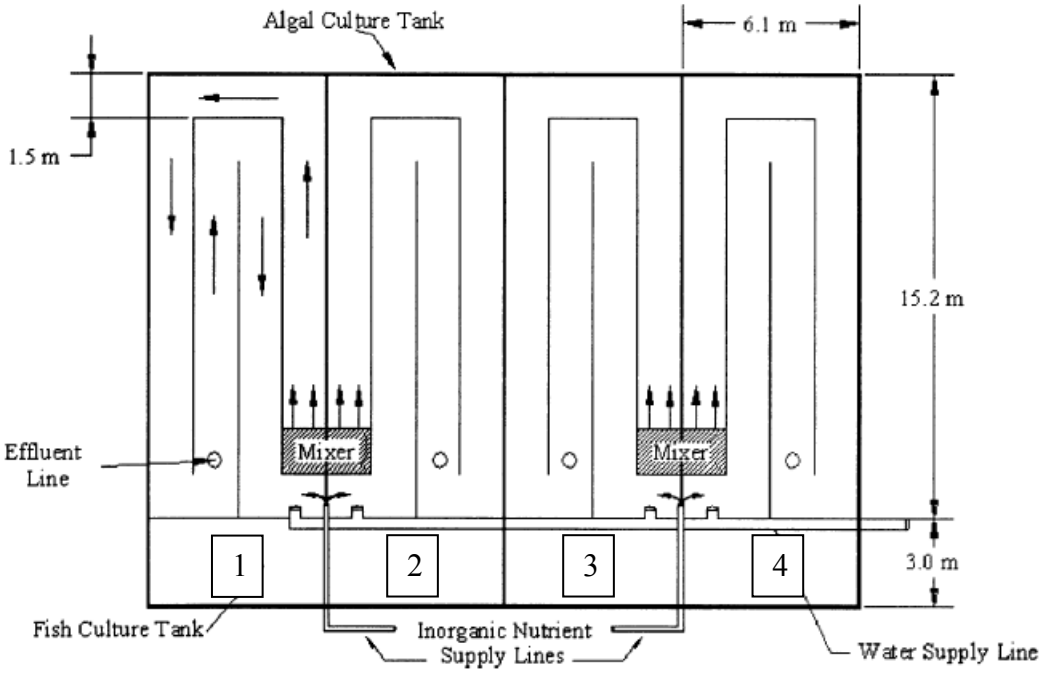

Figure 3.1: Partitioned Aquaculture System Schematic (Drapcho & Brune, 2000)

A key component of the system is the movement of water, depicted in Figure 3.1 as the

"Mixer." Mixing in the ponds allows for the algae on the bottom to be moved to the top where the cells can receive sunlight. This reduces the light inhibition of growth and increases productivity. Increasing water velocity was found to increase algal productivity up to a water velocity of 12.5 cm/s (Drapcho & Brune, 2000). In the past, mixing has been accomplished with the use of paddle wheels powered by AC electrical motors. These systems of creating water movement have ultimately failed due to the harsh conditions and exposure to the elements at the ACCS.

Air lift pumps provide an alternative method for mixing water that has high reliability and low maintenance (Clark & Dabolt, 1986). The simplicity and low cost of air lift pump systems makes them suitable to provide water flow and mixing in the ACCS (Parker, 1991). Airlift pumps provide the added benefit of facilitating gas transfer and creating water flow simultaneously. This may be beneficial in the conversion to an Algal Carbon Capture System as compressed CO_2 or flue gas could be used as the feed gas. Flue gas from a municipal waste incinerator has been shown to increase biomass productivity by 30% compared to compressed CO_2 due to the presence of supplemental nutrients like sulfur and nitrate that are present in flue gas (Douskova et al., 2009; Sayre, 2010) and compressed CO_2 elevates biomass yields up to three times (Jeong et al., 2003; Lage et al., 2018). While these methods are costly when carbon prices are low (Bayer & Aklin, 2020), with the predicted increased cost of carbon on the Emissions Trading System they may become more financially appealing (Reuters, 2021) in some countries.

Design

Airlift pumps use compressed gas to generate lift of liquid surrounding the gas. Airlift pumps were first designed for use in separating corrosive or harmful materials in mixtures in applications like dewatering mines and oil removal from wells. Airlift pumps are useful in these applications because they incorporate no moving parts that would erode or wear. They also can function with any liquid and gas combination (Clark & Dabolt, 1986). They generally lift liquids over large distances and operate in the slug flow regime, also described as the bubbly stable slug, bubble unstable slug, and slug churn (Catrawedarma, 2021). In this flow regime large slugs of liquid are moved through the pipe on top of large air bubbles, shown in Figure 3.2 below

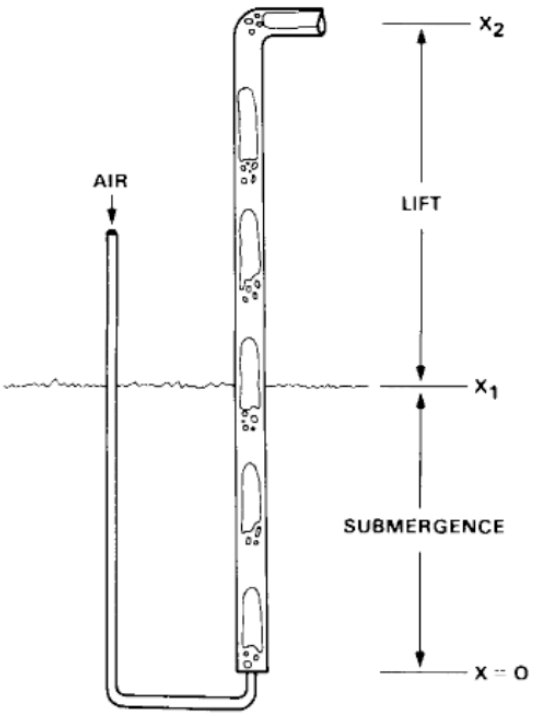

Figure 3.2: Airlift pump in Slug Flow Regime (Clark & Dabolt, 1986)

In aquaculture and hydroponics another form of airlift is gaining attraction: the rectangular airlift. In these applications, the required lift elevations are not as high as those in the oil and gas industry. Therefore, low static air pressure can be used and with the combination of a rectangular airlift to create a larger volume of water flow than can be achieved in a cylindrical airlift (Wurts, 2012).

The geometry of the rectangular airlift allows for a lower surface area to volume ratio than what can be achieved in an assembly of multiple cylindrical airlifts. Decreasing the surface area of the airlift allows for decreased friction and therefore decreased fluid resistance within the pump. Grids systems of pipes are typically deployed in rectangular airlift pumps to deliver air, however large grid systems with the incorporation of many 90º bends increase resistance and turbulence within the air distribution lines. A single row of holes in the top of each air injection cylinder is unlikely to be able to handle the total air volume delivery (Wurts, 2012). An example of a rectangular airlift design in shown in Figure 3.3 below.

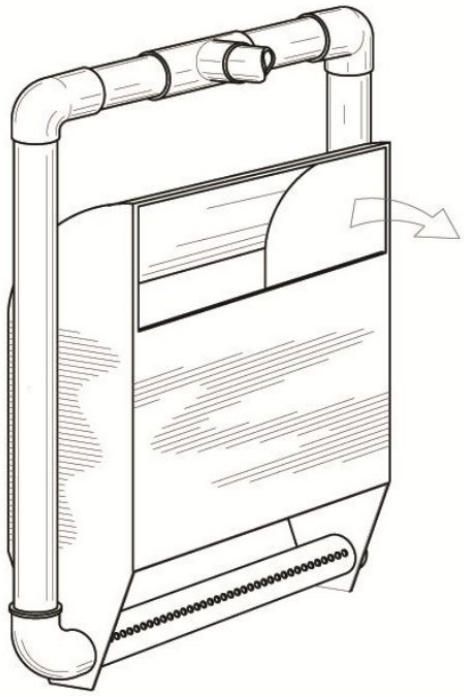

Figure 3.3: Rectangular Airlift Design from Wurts (2012)

In the design for the ACCS, a rectangular air lift pump was chosen given the small lift that is required at a maximum depth of 18 inches (45.72 cm) and the greater volumetric flow required in the raceway lanes. The airlift was constructed to match the depth of the raceway ponds and incorporated two air outlets cylinders with two rows of holes per a cylinder to maximize air flow rate.

The rectangular airlift and its dimensions are shown in Figure 3.6 below. Each channel in the algal raceways measures 1.5 m wide with water depth of 15 to 60 cm. The airlift was designed to span 42 inches (106.68 cm) across the ACCS lane to allow water flow around the sides of the pump. The design depth was 18 inches (45.72 cm), minimum depth required is 12 inches (30.48 cm) and the maximum is 20 inches (50.8 cm).

The system was designed to run off a DC powered air compressor so that the system could be connected to the existing solar power present at the ACCS. The air compressor chosen was the Puma 3.4 HP 1.5 gallon 12-volt continuous duty air compressor pictured in Figure 3.4 below.

Figure 3.4: Puma DC Air Compressor (a) Stock Image (Air Compressors Direct) (b) Attached to PVC for Connection

This air compressor attaches directly to 12-Volt deep cycle marine batteries and its oil-less design allows for it to be mounted in any direction necessary. It has a deep cooling fin that improves the cooling capacity of the air compressor to allow it to run longer before it needs to cool. It has a 100% continuous duty cycle that allows for continual operation of the air compressor in this high demand application. Its maximum output pressure is 135 PSI (Air Compressors Direct). The system is powered by the ACCS Photovoltaic (PV) system shown in Figure 3.5 below.

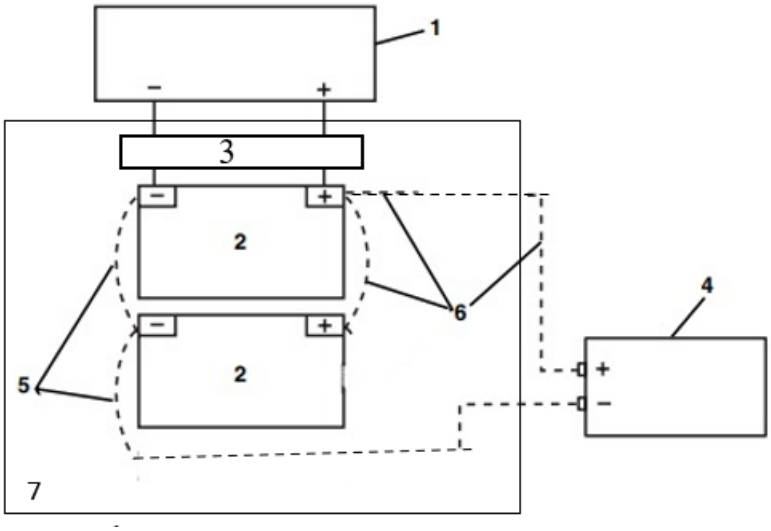

Figure 3.5: Algal Carbon Capture PV System Schematic Legend: 1) PV panel 2) 12 Volt Deep Cycle Marine Batteries Connected in Parallel 3) Solar Pro Charge Controller CC20 4) Peak 400-Watt Inverter 5) Negative Cables 6) Positive Cables 7) Protective cover

The PV system has a maximum output of 12 volts, 160 amp-hours, 20 amps, and 240 watts. The alligator clamps of the air compressor are connected directly to a marine battery (part 2 of Figure 3.5) when the airlift is in use. The air compressor is in the work shed at the ACCS. Compressed air is conveyed from the compressor to the airlift pump via 1/2” (1.27cm) Sch 40 PVC pipe. Raceway 3 of the ACCS was used to evaluate the airlift pump performance.

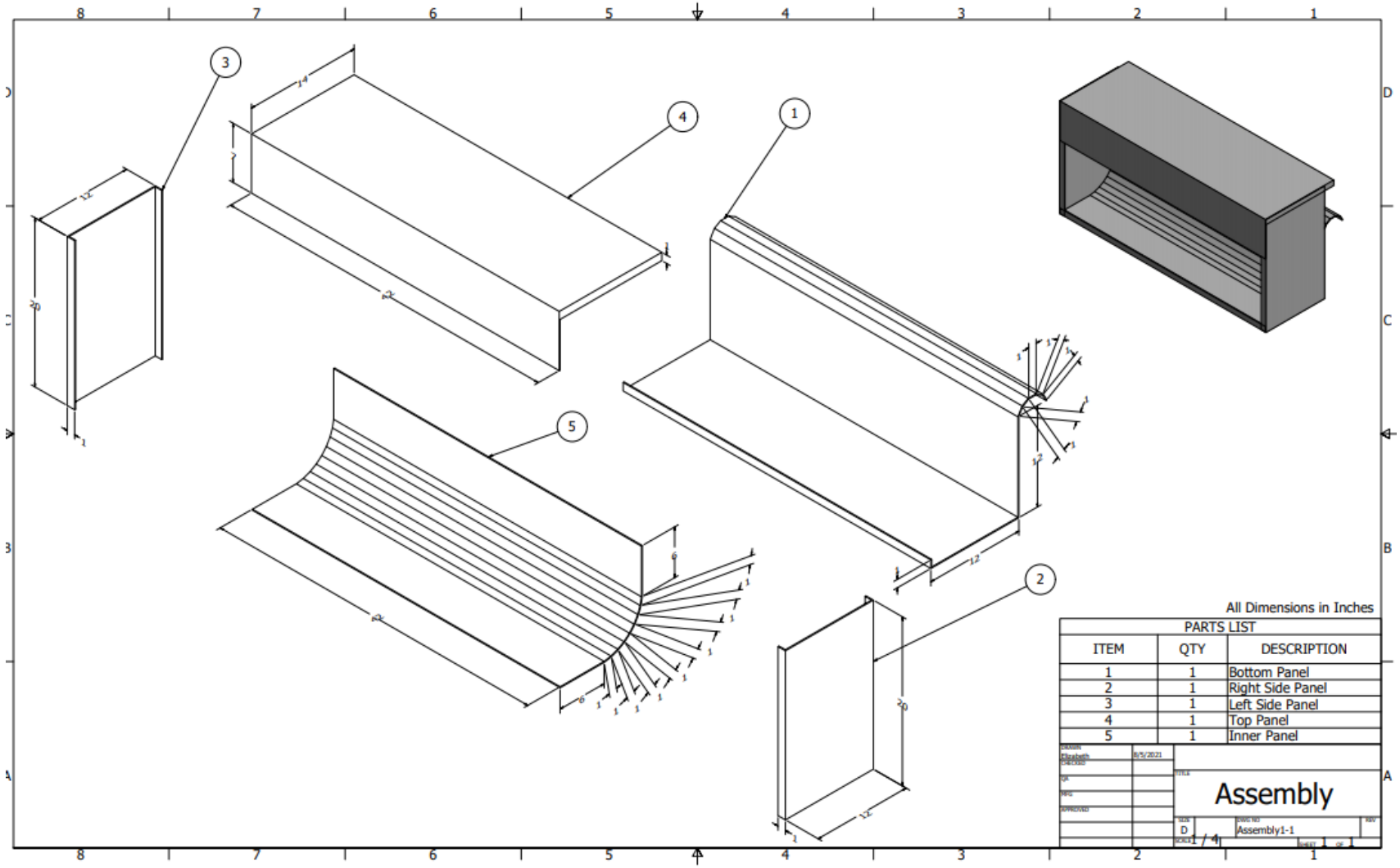

Figure 3.6: Inventor Airlift Pump Design Drawings

Fabrication

Fabrication began with the prototype of the design by Rodney Morgan pictured below in Figure 3.7.

Figure 3.7: Rectangular Airlift Pump Design Prototype by Rodney Morgan

After this was discussed and reviewed full fabrication began. One piece (4’ by 8’) of 16-gauge galvanized sheet metal is required per rectangular air lift pump. Stainless steel could be used for increased durability if funds are available. To minimize waste, cuts were laid out and traced on the metal and can be repeated as follows.

1) Cut 33” by 42” (83.82 x 106.68 cm) out of bottom corner, this piece will become the bottom piece, piece 1
2) Cut 14” by 40” (35.56 x 101.6 cm) next up, cut this piece in half to create two 14” by 20” pieces for the sides, pieces 2 and 3

3) Cut 21” by 44” (53.34 x 111.76 cm) for the top, piece 4, cut 1” by 7” (2.54 x 17.78 cm) out of the corners of this piece
4) Cut 19” by 42” (48.26 x 106.68 cm) for the interior bend piece, piece 5

Once these are cut, they were bent with a 10-foot metal break as follows:

1) Piece one is bent at 1”, 13”, 25” (2.54, 33.02, 63.5 cm) and then every 1” after that into a downward curve

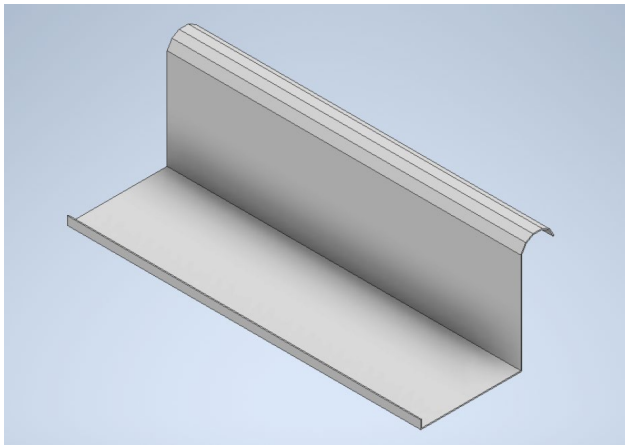

2) Pieces two and three are bent 1” of each side with 20” (50.8 cm) being the height of the piece

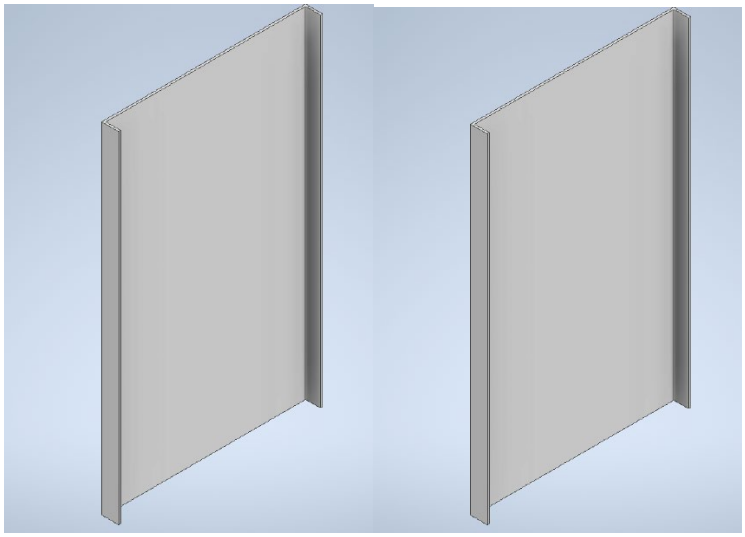

3) Piece four is bent so that the 14” (35.56 cm) section has 1” coming up each side and there are an additional 7” (17.78 cm)

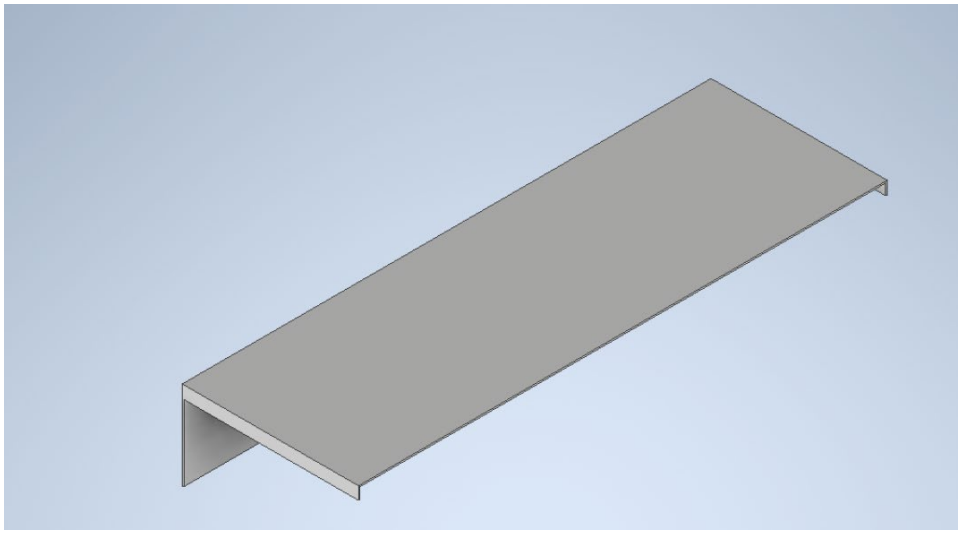

4) Piece five is bent starting at 6” (15.24) then every 1” for 9 bends leaving an additional 6” flat

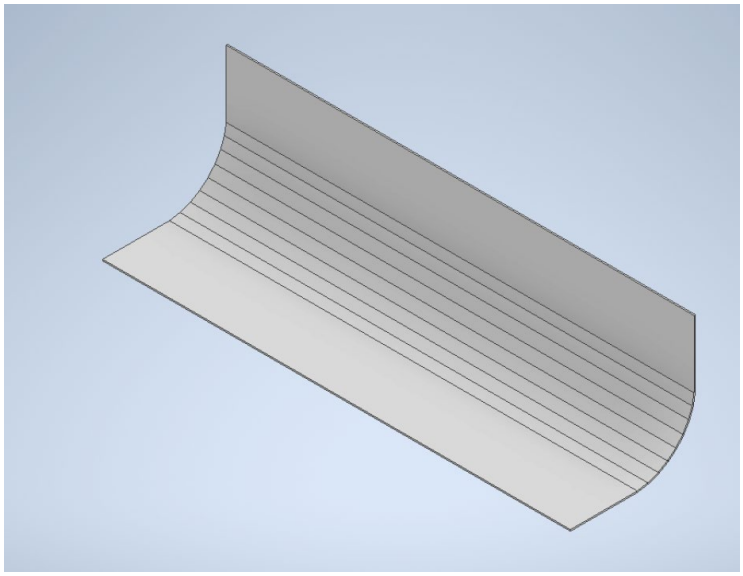

These pieces are displayed in Figure 3.8 below.

Figure 3.8: Rectangular Airlift Pump Metal Pieces for Fabrication

After the pieces are cut and bent, they can be slid together and attached with 1” metal screws at points of overlap. Completed metal portion of the rectangular airlift is shown in Figure 3.9 below.

Figure 3.9: Completed Metal Assembly of Rectangular Airlift Pump

After the completion of the metal assembly 3/4" (1.905 cm) holes were drilled in each side 6” (15.24 cm) back and 2” (5.08 cm) up from the base of the airlift. The next component to add was the PVC air distribution line. In each corner 90º 1/2” (1.27 cm) PVC enters through the holes. This was immediately attached to a 1/2" x 1-1/2” (3.81 cm) t slip coupling. This t coupling was then immediately attached to two 90º 1-1/2” corners with two lines of 1-1/2” piping running through. Two rows of holes were drilled into the top of each pipe to create the air distribution system which can be seen in Figure 3.10 below.

Figure 3.10: Air Distribution System within the Rectangular Air Lift

Lastly the exterior 1/2" t-fittings were connected to the main air distribution line via 2 more 90º 1/2"corners and 2 more 1/2” t-fittings as shown in Figure 3.11 below. Total cost of the system was $791.38, additional lifts could be added for ~$450 since another air compressor would not need to be purchased.

Figure 3.11: (Left) Airlift with 1/2" connection pieces before install into ACCS (Right) with full connection to 70’ Long Air Distribution Line

Testing

Testing of the airlift pump was achieved using multiple devices to measure water velocity in the channel. First was the use of a pygmy meter (Figure 3.12).

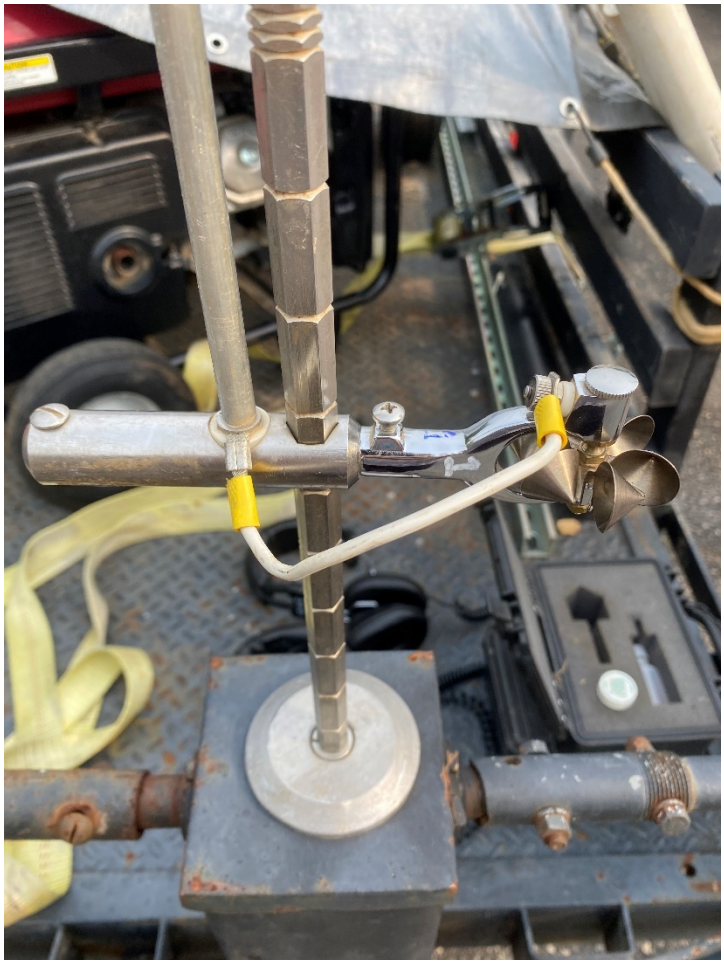

Figure 3.12: Pygmy Meter

Pygmy meters are a tool used by the United States Geological Survey (USGS) to measure the velocity of water in streams and rivers. There are varying sizes of pygmy meters for various applications. The one used here is scaled to be two-fifths as large as the standard Type AA current meter and has a range of operation of 0.03 to 1.5 m/s (Hubbard et al., 1988). The six cups should be positioned in the direction of water flow.

The revolutions of the cups are equated to water velocity through a standardized equation, equation 1 below.

$$V = (0.9604 R + 0.0312) * 0.3048 \quad (1)$$

Where R = revolutions per second and V = velocity (m/s) (Rickly Hydrological Co, n.d.)

Revolutions of the meter can be counted through the audio connection established through the wading rod. Revolutions were counted for 60 seconds and repeated in at least duplicate. In hydrogeological applications the counts should be within one to two revolutions of each other. Given the nature of the cycling of the air compressor there is more variability in measured flow of the airlift pump than this standard. Measurements were taken at distances from airlift pump outlet of 1 inch, 33 inches (83.82 cm), and 5 feet (1.52 m) at depths up to 8 inches (20.32 cm). Results can be seen in Table 3.1 below.

Five feet away from the airlift pump the flow decreased below detectable limits for the pygmy meter, so a different testing mechanism was used. Drogue are used to monitor the oceans currents and to locate areas of the ocean that are collecting pollution and oil (Klemas et al., 1977). They operate with a weighted net below the surface attached to a detectable float with satellite communication. Three miniature drogues were fabricated to operate at depths experienced in the ACCS, pictured in Figure 3.13 below.

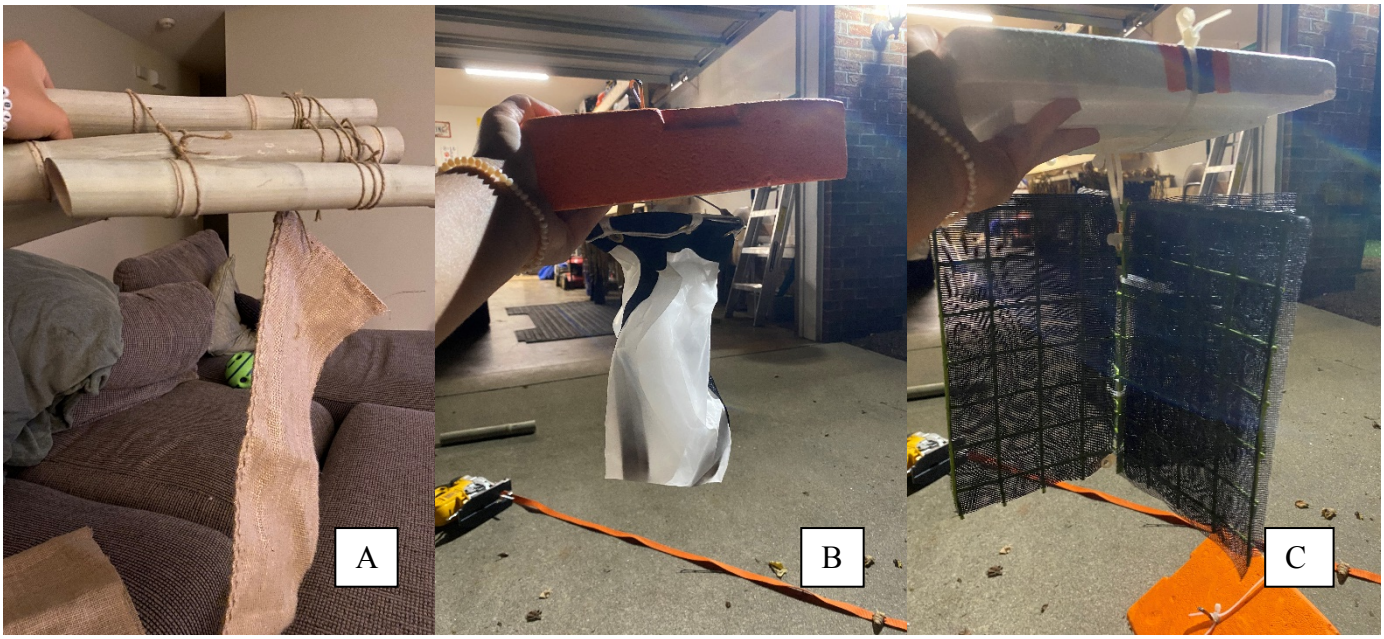

Figure 3.13: Experimental Drogues A, B, and C Left to Right

After use in the ACCS, experimental drogue C had the best floating capabilities compared to drogues A and B. Drogue C was used in testing of the airlift pump. It was placed directly in front of the airlift pump and its travel over 30 feet (9.144 m) was timed. The drogue was then placed in the far lane of the raceway from the airlift for travel in the opposite direction. Both tests were repeated in duplicate.

Results

Visual confirmation indicated that the water was flowing in all lanes of the raceway pond in the correct directions of flow. This can be seen in Figure 3.14 below.

Figure 3.14: Algae movement around the channels of the raceway

Pygmy meter operation was also successful and clear audio was detected through the headphones. Libby Flanagan, author, can be seen in Figure 3.15 below operating the pygmy meter at the first testing location in front of the airlift pump.

Figure 3.15: Libby Flanagan operates pygmy meter in front of airlift pump

Water bubbles and ripples can be clearly seen at airlift exit and drogue device has moved approximately 2 feet from airlift in Figure 3.16a. In Figure 3.16b it has continued to move down lane 1 in its first test run.

Figure 3.16: (a) Start of Drogue Test Run with visual water movement at Airlift opening (b) Middle of Drogue Test Run in Lane 1 of Raceway 3

These visual indicators demonstrated that the airlift was indeed working to move water around the entirety of ACCS raceway 3. The pygmy meter measurements are summarized in Table 3.1 below.

Table 3.1: Pygmy Meter Measurements

Distance from Airlift	Depth (in)	R (count/min)	R (count/s)	Velocity (m/s)	Average Velocity (m/s)	Average Velocity (cm/s)	Standard Deviation (cm/s)
1 in	2	24	0.400	0.1266	0.129	12.86	0.024
		16	0.267	0.0876			
		28	0.467	0.1461			
		28	0.467	0.1461			
		26	0.433	0.1364			
	Deeper	Undetectable	-	-	-	-	-
33 in	4	2	0.033	0.0193	0.014	1.44	0.007
		0	0.000	0.0095			
	0	11	0.183	0.0632	0.048	4.76	0.012
		6	0.100	0.0388			
		10	0.167	0.0583			
		6	0.100	0.0388			
		6	0.100	0.0388			
5 feet	8	1.5	0.025	0.0168	0.013	1.32	0.005
		0	0.000	0.0095			

As can be seen in Table 3.1 above, water velocity at airlift exit is over the design goal of 12.5 cm/s but this velocity quickly decreases with increasing distance from the airlift pump. Right at the airlift exit there is no measurable flow at deeper depths, due to the design of the pump the flow at the exit is at the surface. As distance is increased away from the pump the velocity can be measured at greater depths. At 5 feet of distance water flow in column was homogeneous so USGS standard 40% depth was used.

The drogue measurements of water velocity can be seen in Table 3.2 below.

Table 3.2: Surface Water Velocity Measured with Drogue over 30 feet (9.144 meters)

Lane	Time (seconds)	Velocity (m/s)	Velocity (cm/s)	Average Velocity (cm/s)	Standard Deviation (cm/s)
In Front of Airlift – Red	942	0.0097	0.971	0.904	0.095
	1093	0.0084	0.837		
Furthest from Airlift - Green	1010	0.0091	0.905	0.834	0.101
	1199	0.0076	0.763		

These drogue water velocity measurements were taken in channels in opposing directions indicating the drogue was not largely affected by wind. The locations can be seen in Figure 3.17 below.

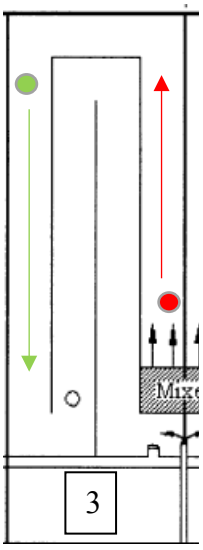

Figure 3.17: Drogue Testing Lanes

The velocity that the drogue achieved through the raceway was similar to those measured by the pygmy meter at a distance of 5 feet away from the airlift. The agreement between the two forms of measurement indicates that this was the likely velocity of water throughout the ACCS lanes. Table 3.3 below shows average velocities measured across lanes using the drogue and the pygmy meter.

Table 3.3: Average Water Surface Velocity Measurements Across Methods

Method	Location	Depth	Average Measured Velocity (cm/s)	Average Velocity (cm/s)	Standard Deviation (cm/s)
Drogue	Channel in front of Airlift – Red	Surface	0.904		
Drogue	Furthest Channel from Airlift - Green	Surface	0.834	1.02	0.26
Pygmy Meter	5’ from Airlift	8”	1.32		

Given these results the water velocity generated by this airlift is 1.02 ± 0.15 cm/s through the ACCS raceway. This is considerably less than the design goal, but linear velocities as low as 1 cm/s have been used in open raceway systems (Abeliovich, 1986; Oswald, 1988; Drapcho & Brune, 2000). Some recommendations are provided as potential methods to improve this prototype.

Recommendations

To improve the airlift pump design the following recommendations are provided:

1) Increase the pressure at the bubble outlet by decreasing the exit pipe diameter to match that of the rest of the system (1/2” Sch 40 PVC)
2) Increase pressure at bubble outlet by including one outlet pipe per pump
3) Add additional airlifts into each ACCS lane to increase volumetric flow produced
4) Increase the width of the airlift to cover the whole width of the ACCS lane to decrease the reliance on the airlift sitting level to avoid eddies in flow
5) Lastly, an air blower could be tested over the air compressor for increased air flow rates at lower pressures as some commercial systems employ.

Cost and Power Comparison

The air compressor for the airlift pump requires a 12-volt battery and has a 46 amp draw for the 0.75 horsepower engine. If the airlift runs for 15 minutes every hour it will consume 3312 watt-hours per day or 1209 kWh per year. Using a cost of 13 cents/kWh, the total yearly operational cost is $57/year if the system was powered by the power grid. If two of these airlifts were installed in every raceway of the ACCS for a total of 8 airlift pumps, the total yearly power use would be 9672 kWh/year operational cost would be $1257/year. Using the EPA's greenhouse gas equivalencies calculator (EPA, 2021) this power use is equivalent to 6.9 metric tons of CO_2. These costs and emissions were avoided by use of the already available PV system (Figure 3.5) but will be used for comparison to paddlewheel.

Paddlewheels require between 0.22 – 0.73 W/m^2 (Rogers et al., 2014), for an average of 0.475 W/m^2. The overall area of all four ACCS raceways shown in Figure 3.1 is 370.88m^2. Using paddlewheels with continuous operation would require 1543 kWh/yr and an operational cost of $200/yr. This is equivalent to 1.1 metric tons of CO_2 (EPA, 2021). Given this calculation, airlift pumps may not be a suitable alternative unless additional benefits of gas transfer are considered.

REFERENCES

Abeliovich, A, (1986). Algae in wastewater oxidation ponds. *CRC Handbook of Microalgal Mass Culture* 331–338.

Acién Fernández, F. G., García Camacho, F., Sánchez Pérez, J. A., Fernández Sevilla, J. M., & Molina Grima, E. (1997). A model for light distribution and average solar irradiance inside outdoor tubular photobioreactors for the microalgal mass culture. *Biotechnology and Bioengineering*, *55*(5), 701–714. https://doi.org/10.1002/(SICI)1097-0290(19970905)55:5<701::AID-BIT1>3.0.CO;2-F

Air Compressors Direct. (n.d.). Puma 3.4-HP 1.5-Gallon 12-Volt Continuous Duty DC Air Compressor. Retrieved August 5, 2021, from https://www.aircompressorsdirect.com/Puma-PD1006-Air-Compressor/p13972.html?gclid=CjwKCAjwmK6IBhBqEiwAocMc8oNwOzOZ80xf3pG2gLTbuD5NHZdTddcxBH4debOJMYWMLCCyxPRcFhoCA8oQAvD_BwE

Amoroso, G., Sültemeyer, D., Thyssen, C., & Fock, H. P. (1998). Uptake of HCO3- and CO2 in cells and chloroplasts from the microalgae Chlamydomonas reinhardtii and Dunaliella tertiolecta. *Plant Physiology*, *116*(1), 193–201. https://doi.org/10.1104/pp.116.1.193

Andrews, J. F. (1968). A mathematical model for the continuous culture of microorganisms utilizing inhibitory substrates. *Biotechnology and Bioengineering*, *10*(6), 707–723. https://doi.org/https://doi.org/10.1002/bit.260100602

Banks, H. T., Collins, E., Flores, K., Pershad, P., Stemkovski, M., & Stephenson, L. (2017). Statistical error model comparison for logistic growth of green algae (Raphidocelis subcapitata). *Applied Mathematics Letters*, *64*, 213–222. https://doi.org/10.1016/j.aml.2016.09.006

Bayer, P., & Aklin, M. (2020). The European Union Emissions Trading System reduced CO2 emissions despite low prices. *Proceedings of the National Academy of Sciences of the United States of America*, *117*(16), 8804–8812. https://doi.org/10.1073/pnas.1918128117

Beardall, J., & Morris, I. (1976). The Concept of Light Intensity Adaptation in Marine Phytoplankton: Some Experiments with Phaeodactylum tricomutum. *Marine Biology*, *37*, 377–387.

Béchet, Q., Shilton, A., & Guieysse, B. (2013). Modeling the effects of light and temperature on algae growth : State of the art and critical assessment for productivity prediction during outdoor cultivation. *Biotechnology Advances*, *31*(8), 1648–1663. https://doi.org/10.1016/j.biotechadv.2013.08.014

Benson, B. C., & Rusch, K. A. (2006). Investigation of the light dynamics and their impact on algal growth rate in a hydraulically integrated serial turbidostat algal reactor (HISTAR). *Aquacultural Engineering*, *35*(2), 122–134. https://doi.org/10.1016/j.aquaeng.2005.09.005

Buxton, G. V., & Elliot, A. J. (1986). Rate constant for reaction of hydroxyl radicals with bicarbonate ions. *International Journal of Radiation Applications and Instrumentation. Part*, *27*(3), 241–243. https://doi.org/10.1016/1359-0197(86)90059-7

Camacho Rubio, F., García Camacho, F., Fernández Sevilla, J. M., Chisti, Y., & Molina Grima, E. (2003). A mechanistic model of photosynthesis in microalgae. *Biotechnology and Bioengineering*, *81*(4), 459–473. https://doi.org/10.1002/bit.10492

Caperon, J. (1968). Population Growth Response of Isochrysis Galbana to Nitrate Variation at Limiting Concentrations. *Ecological Society of America*, *49*(5), 866–872.

Casagli, F., Zuccaro, G., Bernard, O., Steyer, J. P., & Ficara, E. (2021). ALBA: A comprehensive growth model to optimize algae-bacteria wastewater treatment in raceway ponds. *Water Research*, *190*, 116734. https://doi.org/10.1016/j.watres.2020.116734

Catrawedarma, I. (2021). International Journal of Multiphase Flow Statistical Characterization of Flow Structure of Air – water Two-phase Flow in Airlift Pump – Bubble Generator System. *International Journal of Multiphase Flow*, *138*, 103596. https://doi.org/10.1016/j.ijmultiphaseflow.2021.103596

Chapra, S. C., (2005). *Applied Numerical Methods with MATLAB for Engineers and Scientists*, 1st ed., McGraw Hill, New York, NY.

Chrachri, A., Hopkinson, B. M., Flynn, K., Brownlee, C., & Wheeler, G. L. (2018). Dynamic changes in carbonate chemistry in the microenvironment around single marine phytoplankton cells. *Nature Communications*, *9*(1), 1–12. https://doi.org/10.1038/s41467-017-02426-y

Clark, N., & Dabolt, R. (1986). A General Design Equation for Air Lift Pumps Operating in Slug Flow. *AlChE*, *32*(1), 56–64.

Crill, P. A. (1977). *The Photosynthesis-Light Curve : A Simple Analog Model*. 503–516.

Desmit, X., Vanderborght, J. P., Regnier, P., & Wollast, R. (2005). Control of phytoplankton production by physical forcing in a strongly tidal, well-mixed estuary. *Biogeosciences*, *2*(2), 205–218. https://doi.org/10.5194/bg-2-205-2005

Douskova, I., Doucha, J., Livansky, K., MacHat, J., Novak, P., Umysova, D., … Vitova, M. (2009). Simultaneous flue gas bioremediation and reduction of microalgal biomass production costs. *Applied Microbiology and Biotechnology*, *82*(1), 179–185. https://doi.org/10.1007/s00253-008-1811-9

Drapcho, C. M., & Brune, D. E. (2000). The partitioned aquaculture system: Impact of design and environmental parameters on algal productivity and photosynthetic oxygen production. *Aquacultural Engineering*, *21*(3), 151–168. https://doi.org/10.1016/S0144-8609(99)00028-X

Drever, J. I. (1982). The Carbonate System and pH Control. In *The Geochemistry of Natural Waters* (pp. 35–75).

Edsall, J. T. (1969). Carbon Dioxide, Carbonic Acid and Bicarbonate Ion: Physical Properties and Kinetics of Interconversion. In *NASA Special Publication* (Vol. 188, p. 15).

Eigen, M. (1964). Proton Transfer, Acid-Base Catalysis, and Enzymatic Hydrolysis. Part I: Elementary Processes. *Angewandte Chemie International Edition in English*, *3*(1), 1–19. https://doi.org/https://doi.org/10.1002/anie.196400011

Eigen, Manfred, & Hammes, G. G. (1963, January 1). Elementary Steps in Enzyme Reactions (as Studied by Relaxation Spectrometry). *Advances in Enzymology and Related Areas of Molecular Biology*, pp. 1–38. https://doi.org/https://doi.org/10.1002/9780470122709.ch1

EPA. (2021, March). *Greenhouse Gas Equivalencies Calculator*. EPA. https://www.epa.gov/energy/greenhouse-gas-equivalencies-calculator.

Feng, F., Li, Y., Latimer, B., Zhang, C., Nair, S. S., & Hu, Z. (2021). Prediction of maximum algal productivity in membrane bioreactors with a light-dependent growth model. *Science of the Total Environment*, *753*, 141922. https://doi.org/10.1016/j.scitotenv.2020.141922

Gao, S., Waller, P., Khawam, G., Attalah, S., Huesemann, M., & Ogden, K. (2018). Incorporation of salinity, nitrogen, and shading stress factors into the Huesemann Algae Biomass Growth model. *Algal Research*, *35*(November 2017), 462–470. https://doi.org/10.1016/j.algal.2018.09.021

Goldman, J. C., Jenkins, D., & Oswald, W. J. (1974). The kinetics of inorganic carbon limited algal growth. *Journal of the Water Pollution Control Federation*, *46*(12), 2785–2787.

Goldman, J. C., & Stanley, H. I. (1974). Relative growth of different species of marine algae in wasterwater-seawater mixtures. *Marine Biology*, *28*(1), 17–25. https://doi.org/10.1007/BF00389113

Greenwood, Norman N. Earnshaw, A. (1997). Oxides and Carbonates. In *Chemistry of the Elements (2nd ed.)*. (Vol. 5, p. 310).

Grima, M. E., Fernández Sevilla, J. M., Sánchez Pérez, J. A., & García Camacho, F. (1996). A study on simultaneous photolimitation and photoinhibition in dense microalgal cultures taking into account incident and averaged irradiances. *Journal of Biotechnology*, *45*(1), 59–69. https://doi.org/10.1016/0168-1656(95)00144-1

Grobbelaarl, J. U., Nedbal, L., & Tichy, V. (1996). *Influence of high frequency light / dark fluctuations on photosynthetic characteristics of microalgae photoacclimated to different light intensities and implications for mass algal cultivation*. 335–343.

Harned, H. S., & Davis, R. (1943). The Ionization Constant of Carbonic Acid in Water and the Solubility of Carbon Dioxide in Water and Aqueous Salt Solutions from 0 to 50°. *Journal of the American Chemical Society*, *65*(10), 2030–2037. https://doi.org/10.1021/ja01250a059

Hikita, H., Asai, S., & Takatsuka, T. (1976). Absorption of carbon dioxide into aqueous sodium hydroxide and sodium carbonate-bicarbonate solutions. *The Chemical Engineering Journal*, *11*(2), 131–141. https://doi.org/10.1016/S0300-9467(76)80035-4

Ho, C., & Strurtevant, J. M. (1963). the Kinetics of the Hydration of Carbon Dioxide At 25 Degrees. *The Journal of Biological Chemistry*, *238*(10), 3499–3501.

Hsueh, H. T., Li, W. J., Chen, H. H., & Chu, H. (2009). Carbon bio-fixation by photosynthesis of Thermosynechococcus sp. CL-1 and Nannochloropsis oculta. *Journal of Photochemistry and Photobiology B: Biology*, *95*(1), 33–39. https://doi.org/10.1016/j.jphotobiol.2008.11.010

Hubbard, E. F., Thibodeaux, K. G., & Duong, M. N. (1988). *Quality Assurance of U.S. Geological Survey Stream Current Meters*.

Huesemann, M. H., Van Wagenen, J., Miller, T., Chavis, A., Hobbs, S., & Crowe, B. (2013). A screening model to predict microalgae biomass growth in photobioreactors and raceway ponds. *Biotechnology and Bioengineering*, *110*(6), 1583–1594. https://doi.org/10.1002/bit.24814

IPCC. (2019). *Special Report: The Ocean and Cryosphere in a Changing Climate*. (September), in preparation. https://doi.org/https://www.ipcc.ch/report/srocc/

James, S. C., & Boriah, V. (2010). Modeling algae growth in an open-channel raceway. *Journal of Computational Biology*, *17*(7), 895–906. https://doi.org/10.1089/cmb.2009.0078

Jayaraman, S. K., & Rhinehart, R. R. (2015). *Modeling and Optimization of Algae Growth*. (August). https://doi.org/10.1021/acs.iecr.5b01635

Jeong, M. L., Gillis, J. M., & Hwang, J. Y. (2003). Carbon Dioxide Mitigation by Microalgal Photosynthesis. *Bulletin of the Korean Chemical Society*, *24*(12), 1763–1766. https://doi.org/10.5012/bkcs.2003.24.12.1763

Johnson, K. S. (1982). Carbon dioxide hydration and dehydration kinetics in seawater. *Limnology and Oceanography*, *27*(5), 849–855. https://doi.org/10.4319/lo.1982.27.5.0849

Johnson, S. (1982). *Carbon dioxide hydration kinetics in seawateri and dehydration + Vs) l. 27*(5), 849–855.

Kern, D. M. (1960). The hydration of carbon dioxide. *Journal of Chemical Education*, *37*(1), 14–23. https://doi.org/10.1021/ed037p14

King, D. L. (1970). The Role of Carbon in Eutrophication. *Journal (Water Pollution Control Federation)*, *42*(12), 2035–2051. Retrieved from http://www.jstor.org/stable/25036835

Klemas, V., Davis, G. R., Henry, R. D., Journal, S., Pollution, W., Federation, C., … Henry, R. D. (1977). *Satellite and current of ocean-disposed waste drift drogue studies*. *49*(5), 757–763.

Knoche, W. (1980). Chemical Reactions of CO2 in Water. *Biophysics and Physiology of Carbon Dioxide.* (pp. 3-11). Springer-Veriag Berlin Heidelberg.

Koller, A. P., Hannes, L., Schmid, V., Mundt, S., & Weuster-botz, D. (2017). *Model-Supported Phototrophic Growth Studies With Scenedesmus obtusiusculus in a Flat-Plate Photobioreactor*. *114*(2), 308–320. https://doi.org/10.1002/bit.26072

Kurano, N., & Miyachi, S. (2005). Selection of microalgal growth model for describing specific growth rate-light response using extended information criterion. *Journal of Bioscience and Bioengineering*, *100*(4), 403–408. https://doi.org/10.1263/jbb.100.403

Lage, S., Gojkovic, Z., Funk, C., & Gentili, F.. (2018). Algal Biomass from Wastewater and Flue Gases as a Source of Bioenergy. *Energies*, *11*(3), 664. https://doi.org/10.3390/en11030664

Lee, E., Jalalizadeh, M., & Zhang, Q. (2015). Growth kinetic models for microalgae cultivation: A review. *Algal Research*, *12*, 497–512. https://doi.org/10.1016/j.algal.2015.10.004

Lemesle, V., & Mailleret, L. (2008). A mechanistic investigation of the algae growth "droop" model. *Acta Biotheoretica*, *56*(1–2), 87–102. https://doi.org/10.1007/s10441-008-9031-3

Ludden, E., Admiraal, W., & Colijn, F. (1985). Cycling of carbon and oxygen in layers of marine microphytes; a simulation model and its eco-physiological implications. *Oecologia*, *66*(1), 50–59. https://doi.org/10.1007/BF00378551

Megard, R. O., & Berman, T. (1989). Effects of algae on the Secchi transparency of the southeastern Mediterranean Sea. *Limnology and Oceanography*, *34*(8), 1640–1655. https://doi.org/10.4319/lo.1989.34.8.1640

Molina, G. E., Camacho, F. G., Sanchez Perez, J. A., Gomez, A. C., & Sanz, F. V. (1994). Outdoor turbidostat culture of the marine microalga Tetraselmis sp. *Aquaculture Research*, *25*(5), 547–555. https://doi.org/https://doi.org/10.1111/j.1365-2109.1994.tb00718.x

Monod, J. (1949). The Growth of Bacterial Cultures. *Annual Review of Microbiology*, *3*(1), 371–394.

Moroney, J. V, & Somanchi, A. (1999). *How Do Algae Concentrate CO_2 to Increase the Efficiency of Photosynthetic Carbon Fixation? 119*(1), 9–16.

Novak, J. T., & Brune, D. E. (1985). Inorganic carbon limited growth kinetics of some freshwater algae. *Water Research*, *19*(2), 215–225. https://doi.org/10.1016/0043-1354(85)90203-9

Nyholm, N. (1977). Kinetics Of Nitrogen-Limited Algal Growth. In S. H. B. T.-P. of the C. on N. A. a W. P. Jenkins (Ed.), *J of Intl Association of Water Pollution Research* (pp. 347–358). https://doi.org/https://doi.org/10.1016/B978-1-4832-1344-6.50028-9

Ono, E., & Cuello, J. (2003). Selection of Optimal Microalgae Species for CO2 Sequestration. *Proceedings of the 2nd Annual Conference on Carbon Sequestration, Alexandria*, *1*.

Oswald, W.J. (1988). Large-scale algal culture systems (engineering aspects), *Micro-algal Biotechnology.* Cambridge University Press, Cambridge, 357–394.

Park, S., & Li, Y. (2015). Integration of biological kinetics and computational fluid dynamics to model the growth of Nannochloropsis salina in an open channel raceway. *Biotechnology and Bioengineering*, *112*(5), 923–933. https://doi.org/10.1002/bit.25509

Parker, N. C. (1991). *L. Swann (Ed.) 1991. Second Annual Workshop on Commercial Aquaculture Using Water Recirculating Systems. (IL-IN-SG-E-91-8). Illinois-lndiana Sea Grant, Illinois State University, Normal, Illinois*. (Parker 1983), 2–6.

Patel, R. C., Boe, R. J., & Atkinson, G. (1973). The CO2-water system. I. Study of the slower hydration-dehydration step. *Journal of Solution Chemistry*. https://doi.org/10.1007/BF00713250

Pinsent, B. R. W., Pearson, L., Roughto, F. J. W. (1956). The Kinetics of Combination of Carbon Dioxide with Hydroxide Ions. *Journal of Chemical Information and Modeling*, 1512–1520.

Portielje, R., & LiJklema, L. (1995). Carbon dioxide fluxes across the air-water interface and its impact on carbon availability in aquatic systems. *Limnology and Oceanography*, *40*(4), 690–699. https://doi.org/10.4319/lo.1995.40.4.0690

Quinn, J., de Winter, L., & Bradley, T. (2011). Microalgae bulk growth model with application to industrial scale systems. *Bioresource Technology*, *102*(8), 5083–5092. https://doi.org/10.1016/j.biortech.2011.01.019

Rebolloso Fuentes, M. M., García Sánchez, J. L., Fernández Sevilla, J. M., Acién Fernández, F. G., Sánchez Pérez, J. A., & Molina Grima, E. (1999). Outdoor continuous culture of Porphyridium cruentum in a tubular photobioreactor: Quantitative analysis of the daily cyclic variation of culture parameters. *Journal of Biotechnology*, *70*(1–3), 271–288. https://doi.org/10.1016/S0168-1656(99)00080-2

Redfield, A. C., Ketchum, B. H., & Richards, F. A. (1963). The influence of organisms on the composition of sea-water. *The sea, volume 2: The composition of seawater: Comparative and descriptive oceanography*, (pp. 26-77). Cambridge, MA: Harvard University Press.

Reichle, D., Houghton, J., Kane, B., Ekmann, J., & et al. (1999). Carbon sequestration research and development. In *Other Information: PBD: 31 Dec 1999*. Retrieved from http://www.osti.gov/bridge/servlets/purl/810722/

Reuters. (2021). Europe carbon prices expected to rise to 2030-industry survey.

Rickly Hydrological Co. (n.d.). *Open Channel Flow Measurement Instrument USGS Pygmy Current Meter*. Retrieved from https://www.tttenviro.com/wp-content/uploads/Manual-Pygmy-Meter.pdf

Rogers, J. N., Rosenberg, J. N., Guzman, B. J., Oh, V. H., Mimbela, L. E., Ghassemi, A., Donohue, M. D. (2014). A critical analysis of paddlewheel-driven raceway ponds for algal biofuel production at commercial scales. *Algal Research, 4(1),* 76–88. https://doi.org/10.1016/j.algal.2013.11.007

Ruiz, J., Arbib, Z., Álvarez-Díaz, P. D., Garrido-Pérez, C., Barragán, J., & Perales, J. A. (2013). Photobiotreatment model (PhBT): A kinetic model for microalgae biomass growth and nutrient removal in wastewater. *Environmental Technology (United Kingdom)*, *34*(8), 979–991. https://doi.org/10.1080/09593330.2012.724451

Sánchez, J. F., Fernández-Sevilla, J. M., Acién, F. G., Cerón, M. C., Pérez-Parra, J., & Molina-Grima, E. (2008). Biomass and lutein productivity of Scenedesmus almeriensis: Influence of irradiance, dilution rate and temperature. *Applied Microbiology and Biotechnology*, *79*(5), 719–729. https://doi.org/10.1007/s00253-008-1494-2

Sayre, R. (2010). Microalgae: The potential for carbon capture. *BioScience*, *60*(9), 722–727. https://doi.org/10.1525/bio.2010.60.9.9

Schulz, K. G., Riebesell, U., Rost, B., Thoms, S., & Zeebe, R. E. (2006). Determination of the rate constants for the carbon dioxide to bicarbonate inter-conversion in pH-buffered seawater systems. *Marine Chemistry*, *100*(1–2), 53–65. https://doi.org/10.1016/j.marchem.2005.11.001

Sightlines Report. (2019). *Clemson Sightlines Report*. (December).

Sirs, B. Y. J. A. (1957). *Electrometric Stopped Flow Measurements*.

Sommer, U. (1991). A Comparison of the Droop and the Monod Models of Nutrient Limited Growth Applied to Natural Populations of Phytoplankton. *Functional Ecology*, *5*(4), 535. https://doi.org/10.2307/2389636

Spijkerman, E., de Castro, F., & Gaedke, U. (2011). Independent colimitation for carbon dioxide and inorganic phosphorus. *PLoS ONE*, *6*(12). https://doi.org/10.1371/journal.pone.0028219

Stumm, W., & Morgan, J. J. (1996). *Aquatic chemistry: chemical equilibria and rates in natural waters*. https://doi.org/10.5860/choice.33-6312

Watson, M. K. (2009). *Growth and Modeling of Freshwater Algae as a Function of Media Inorganic Carbon Content*.

Watson, M. K., & Drapcho, C. M. (2016). Kinetics of inorganic carbon-limited freshwater algal growth at high ph. *Transactions of the ASABE*, *59*(6), 1633–1643. https://doi.org/10.13031/trans.59.11520

Wijanarko, A., Dianursanti, Sendjaya, A. Y., Hermansyah, H., Witarto, A. B., Gozan, M., … Song, S. K. (2008). Enhanced Chlorella vulgaris Buitenzorg growth by photon flux density alteration in serial photobioreactors. *Biotechnology and Bioprocess Engineering*, *13*(4), 476–482. https://doi.org/10.1007/s12257-008-0149-6

Wissbrun, K. F., French, D. M., & Patterson, A. (1954). The true ionization constant of carbonic acid in aqueous solution from 5 to 45°. *Journal of Physical Chemistry*, *58*(9), 693–695. https://doi.org/10.1021/j150519a004

Wurts, W. A. (2012). Rectangular Airlift Pump Design Outperforms Cylindrical Units. *Global Aquaculture Advocate*, (December), 77–78.

Zeebe, Richard E. and Wolf-Gladrow, D. (2001). Chapter 2 Kinetics. In *CO2 in Seawater: Equilibrium, Kinetics, Isotopes* (pp. 85–140).

Zeebe, R. E., Sanyal, A., Ortiz, J. D., & Wolf-Gladrow, D. A. (2001). A theoretical study of the kinetics of the boric acid-borate equilibrium in seawater. *Marine Chemistry*, *73*(2), 113–124. https://doi.org/10.1016/S0304-4203(00)00100-6

APPENDICES

APPENDIX I: MATLAB INPUT FILE

```
clear
clc
close all

%original code by Dr. Mary Katherine Watson and updated
by Libby Flanagan

type LZalgalModelCarbonateClosedFinal;
%NOTE: THIS FILE SOLVES THE SET OF DIFFERENTIAL
EQUATIONS USING
%USER-DEFINIED INITIAL CONDITIONS. OUTPUT PLOTS INCLUDE
CARBONATE
%SPECIES,BIOMASS CONCENTRATION (mg/L), pH, and
ALKALINITY.

%% Define Initial Conditions

% Note: Choose initial value vector or input a new one.
t0 = 0;
tfinal = 200;
%initial conditions = [CO2, CO3, H, HCO3, OH, H2O,
Biomass, TIC, N, Biomass(for TSS), MuMaxCO2, MuMaxHCO3,
MuMaxCO3, b];

%ALK changes for total error by MKW 8/15/2021
y0 = [1.60771e-8 0.0001804 5.01187e-11 0.00016077
0.0002 55.5 2.18584e-5 0.000341 0.0176 2.18584e-5
0.079, 0.07935, 0.0703, 0.00285]; %25C with alk error
%y0 = [3.83048e-8 0.0003593 5.01187e-11 0.00038305
0.0002 55.5 1.97116E-5 0.000813 0.0176 1.97116E-5
0.079, 0.07935, 0.0703, 0.00285]; %50C with alk error
%y0 = [6.05325e-8 0.0006792 5.01187e-11 0.00060533
0.0002 55.5 1.27947e-5 0.001285 0.0176 1.27937e-5
0.079, 0.07935, 0.0703, 0.00285]; %75C with alk error
%y0 = [8.27602e-8 0.0009286 5.01187e-11 0.00082760
0.0002 55.5 1.15782E-5 0.001756 0.0176 1.15782E-5
0.079, 0.07935, 0.0703, 0.00285]; %100C with alk error

%% Simulate the System of Differential Equations
%change based on model running
```

```
[t,y] = ode23tb(@LZalgalModelCarbonateClosedFinal,[t0
tfinal],y0); %use for 3 sub model
%[t,y] =
ode23tb(@LZalgalModelCarbonateClosedFinal2sub,[t0
tfinal],y0); %use for 2 sub model

%% Values for Graphing

%use for 25%
Nfactor = 1.01; % (mol N/mol X)
Pfactor = 1; % (mol P/mol X)
Cfactor = 6.16; % (mol C/mol X)

%use these for 50% C
% Nfactor = 0.947; % (mol N/mol X)
% Pfactor = 1; % (mol P/mol X)
% Cfactor = 6.18; % (mol C/mol X)

% %use for 75%
% Nfactor = 1.25; % (mol N/mol X)
% Pfactor = 1; % (mol P/mol X)
% Cfactor = 7.67; % (mol C/mol X)

% %use for 100%
% Nfactor = 1.52; % (mol N/mol X)
% Pfactor = 1; % (mol P/mol X)
% Cfactor = 10.16; % (mol C/mol X)

CH2O = Cfactor*(12.0107+(2*1.00794)+15.9994);
NH3 = Nfactor*(14.0067+(3*1.00794));
H3PO4 = Pfactor*(3*1.00794)+30.9738+15.9994;
MWalgae = CH2O + NH3 + H3PO4; % (g/mol X)
carbalk = (y(:,4))+(2*y(:,2)) + y(:,5) - y(:,3);
pH = -log10(y(:,3));
totalcarbon = (y(:,1)) + (y(:,2)) + (y(:,4));

%% Get experimental results from excel

[ExpData, Text] = xlsread('Data for
MATLAB.xlsx','MKW25');
 Time = ExpData(:,1);
 Time = Time(isfinite(Time));
```

```
 Biomass_mgperL = ExpData(:,2);
 Biomass_mgperL =
Biomass_mgperL(isfinite(Biomass_mgperL));
 TIC_molperL = ExpData(:,3);
 TIC_molperL = TIC_molperL(isfinite(TIC_molperL));
 CarbonDioxide = ExpData(:,4);
 CarbonDioxide =
CarbonDioxide(isfinite(CarbonDioxide));
 Bicarbonate = ExpData(:,5);
 Bicarbonate = Bicarbonate(isfinite(Bicarbonate));
 Carbonate = ExpData(:,6);
 Carbonate = Carbonate(isfinite(Carbonate));
 Alk_molperL = ExpData(:,7);
 Alk_molperL = Alk_molperL(isfinite(Alk_molperL));
 pHexperimental = ExpData(:,8);
 pHexperimental =
pHexperimental(isfinite(pHexperimental));

%% Create Formatted Output Plots
grid on
% Format Chart Axes
set (0, 'defaultaxesfontsize',25);
set (0, 'defaultaxesfontname','Times');

%graphing active biomass
predictBiomass = y(:,10)*MWalgae*1000; %change to y(7)
if
% not wanting to use TSS
% figure(1);
% plot(t, predictBiomass,
'-.','Color',[0.48,0.06,0.89],'LineWidth',3)
% % hold on
% % plot(Time, Biomass_mgperL, 'ko','MarkerSize', 10,
'MarkerFaceColor','k')
% ylim ([0.0,100]);
% xlim ([0,tfinal]);
% xlabel('Time (hr)', 'FontSize', 25, 'FontName',
'Times');
% ylabel('Algal Biomass (mg/L)', 'FontSize', 25,
'FontName', 'Times');
```

```
% h_legend=legend('Model Prediction', 'Experimental
Results','Location','best');
% set(h_legend, 'FontName', 'Times', 'FontSize', 15);

%graphing TIC
figure(2);
predictTIC = y(:,8);
plot(t,
predictTIC,'-.','Color',[0.48,0.06,0.89],'LineWidth',3)
hold on
plot(Time, TIC_molperL,'ko','MarkerSize', 10,
'MarkerFaceColor', 'k')
ylim ([0,0.002]);
xlim ([0,tfinal]);
xlabel('Time (hr)', 'FontSize', 25, 'FontName',
'Times');
ylabel('Total Inorganic Carbon (mol/L C)', 'FontSize',
25, 'FontName','Times');
h_legend=legend('Model Prediction', 'Experimental
Results','Location','best');
set(h_legend, 'FontName', 'Times', 'FontSize', 15);

%graphing Carbon Dioxide
figure(3);
predictCO2 = y(:,1);
plot(t, predictCO2,
'-.','Color',[0.48,0.06,0.89],'LineWidth',3)
hold on
plot(Time, CarbonDioxide, 'ko','MarkerSize', 10,
'MarkerFaceColor','k')
ylim ([0.0,9e-8]);
xlim ([0,tfinal]);
xlabel('Time (hr)', 'FontSize', 25, 'FontName',
'Times');
ylabel('Carbon Dioxide (mol/L C)', 'FontSize', 25,
'FontName','Times');
h_legend=legend('Model Prediction', 'Experimental
Results','Location','best');
set(h_legend, 'FontName', 'Times', 'FontSize', 15);

%graphing Bicarbonate
```

```
figure(4);
predictHCO3 = y(:,4);
plot(t,
predictHCO3,'-.','Color',[0.48,0.06,0.89],'LineWidth',3
)
hold on
plot(Time, Bicarbonate, 'ko','MarkerSize', 10,
'MarkerFaceColor', 'k')
ylim ([0.0,0.001]);
xlim ([0,tfinal]);
xlabel('Time (hr)', 'FontSize', 25, 'FontName',
'Times');
ylabel('Bicarbonate (mol/L C)', 'FontSize', 25,
'FontName', 'Times');
h_legend=legend('Model Prediction', 'Experimental
Results','Location','best');
set(h_legend, 'FontName', 'Times', 'FontSize', 15);

%graphing Carbonate
figure(5);
predictCO3 = y(:,2);
plot(t,
predictCO3,'-.','Color',[0.48,0.06,0.89],'LineWidth',3)
hold on
plot(Time, Carbonate, 'ko','MarkerSize', 10,
'MarkerFaceColor', 'k')
ylim ([0.0,0.001]);
xlim ([0,tfinal]);
xlabel('Time (hr)', 'FontSize', 25, 'FontName',
'Times');
ylabel('Carbonate (mol/L C)', 'FontSize', 25,
'FontName', 'Times');
h_legend=legend('Model Prediction', 'Experimental
Results','Location','best');
set(h_legend, 'FontName', 'Times', 'FontSize', 15);

%graphing ALK
figure(6);
plot(t, carbalk,
'-.','Color',[0.48,0.06,0.89],'LineWidth',3)
hold on
```

```
plot(Time, Alk_molperL, 'ko','MarkerSize', 10,
'MarkerFaceColor', 'k')
ylim ([0,0.01]);
xlim ([0,tfinal]);
xlabel('Time (hr)', 'FontSize', 25, 'FontName',
'Times');
ylabel('Carbonate Alkalinity (mol/L)', 'FontSize', 25,
'FontName', 'Times');
h_legend=legend('Model Prediction', 'Experimental
Results','Location','best');
set(h_legend, 'FontName', 'Times', 'FontSize', 15);

%graphing pH
figure(7);
plot(t, pH,
'-.','Color',[0.48,0.06,0.89],'LineWidth',3)
ylim ([9.5,12]);
xlim ([0,tfinal]);
hold on
plot(Time, pHexperimental, 'ko','MarkerSize', 10,
'MarkerFaceColor','k')
xlabel('Time (hr)', 'FontSize', 25, 'FontName',
'Times');
ylabel('pH', 'FontSize', 25, 'FontName', 'Times');
h_legend=legend('Model Prediction', 'Experimental
Results','Location','best');
set(h_legend, 'FontName', 'Times', 'FontSize', 15);


%graphing TSS
figure(8);
plot(t, y(:,10)*MWalgae*1000,
'-.','Color',[0.48,0.06,0.89],'LineWidth',3)
ylim ([0.0,100]);
xlim ([0,tfinal]);
hold on
plot(Time, Biomass_mgperL, 'ko','MarkerSize', 10,
'MarkerFaceColor','k')
xlabel('Time (hr)', 'FontSize', 25, 'FontName',
'Times');
```

```
ylabel('TSS (mg/L)', 'FontSize', 25, 'FontName',
'Times');
h_legend=legend('Model Prediction', 'Experimental
Results','Location','best');
set(h_legend, 'FontName', 'Times', 'FontSize', 15);


%graph specific growth rates an decay rate - change
based on model (2sub/3sub) running
MuCO2 = (y(:,11)-y0(11))./t;
MuHCO3 = (y(:,12)-y0(12))./t;
MuCO3 = (y(:,13)-y0(13))./t;
b = (y(:,14)-y0(14))./t;
figure(9);
plot(t, MuCO2,
'-.','Color',[0.48,0.06,0.89],'LineWidth',3)
hold on
plot(t, MuHCO3, '-.','Color',[0,0,0.89],'LineWidth',3)
plot(t, MuCO3, '-.','Color',[0.89,0,0],'LineWidth',3)
plot(t, b, '-.','Color',[0,0.7,0],'LineWidth',3)
%legend('MuCO2', 'MuHCO3','b')
legend('MuCO2', 'MuHCO3', 'MuCO3','b')
ylim ([0,0.05]);
xlim ([0,tfinal]);
xlabel('Time (hr)', 'FontSize', 25, 'FontName',
'Times');
ylabel('Mus and b (1/hr)', 'FontSize', 25, 'FontName',
'Times');
hold off

%% Residuals Calculations and Plotting

%index data points
[minValue, closestIndex] = min(abs(t - Time.'));

residualBiomass = Biomass_mgperL -
predictBiomass(closestIndex);
residualTIC = TIC_molperL - predictTIC(closestIndex);
residualCO2 = CarbonDioxide - predictCO2(closestIndex);
residualHCO3 = Bicarbonate - predictHCO3(closestIndex);
residualCO3 = Carbonate - predictCO3(closestIndex);
```

```
residualALK = Alk_molperL - carbalk(closestIndex);
residualpH =  pHexperimental - pH(closestIndex);

% plot residual biomass
figure(10);
plot(Time, residualBiomass, 'ko','MarkerSize', 10,
'MarkerFaceColor','k')
yline(0);
ylim ([-60 ,66]);
xlim ([0,tfinal]);
xlabel('Time (hr)', 'FontSize', 25, 'FontName',
'Times');
ylabel('Algal Biomass Residuals (mg/L)', 'FontSize',
25, 'FontName', 'Times');

% plot residual carbonate
figure(11);
plot(Time, residualCO3, 'ko','MarkerSize', 10,
'MarkerFaceColor','k')
yline(0);
ylim ([-6e-4 , 6e-4]);
xlim ([0,tfinal]);
xlabel('Time (hr)', 'FontSize', 25, 'FontName',
'Times');
ylabel('Carbonate Residuals (mol/L)', 'FontSize', 25,
'FontName', 'Times');

% plot residual bicarbonate
figure(12);
plot(Time, residualHCO3, 'ko','MarkerSize', 10,
'MarkerFaceColor','k')
yline(0);
ylim ([-4e-4 , 4e-4]);
xlim ([0,tfinal]);
xlabel('Time (hr)', 'FontSize', 25, 'FontName',
'Times');
ylabel('Bicarbonate Residuals (mol/L)', 'FontSize', 25,
'FontName', 'Times');

% plot residual carbon dioxide
figure(13);
```

```
plot(Time, residualCO2, 'ko','MarkerSize', 10,
'MarkerFaceColor','k')
yline(0);
ylim ([-4e-4 , 4e-4]);
xlim ([0,tfinal]);
xlabel('Time (hr)', 'FontSize', 25, 'FontName',
'Times');
ylabel('Carbon Dioxide Residuals (mol/L)', 'FontSize',
25, 'FontName', 'Times');

% plot residual TIC
figure(14);
plot(Time, residualTIC, 'ko','MarkerSize', 10,
'MarkerFaceColor','k')
yline(0);
ylim ([-7e-4 , 7e-4]);
xlim ([0,tfinal]);
xlabel('Time (hr)', 'FontSize', 25, 'FontName',
'Times');
ylabel('TIC Residuals (mol/L)', 'FontSize', 25,
'FontName', 'Times');

% plot residual ALK
figure(15);
plot(Time, residualALK, 'ko','MarkerSize', 10,
'MarkerFaceColor','k')
yline(0);
ylim ([-4e-3 , 4e-3]);
xlim ([0,tfinal]);
xlabel('Time (hr)', 'FontSize', 25, 'FontName',
'Times');
ylabel('Alkalinity Residuals (mol/L)', 'FontSize', 25,
'FontName', 'Times');

% plot residual pH
figure(16);
plot(Time, residualpH, 'ko','MarkerSize', 10,
'MarkerFaceColor','k')
yline(0);
ylim ([-0.6, 0.6]);
xlim ([0,tfinal]);
```

```
xlabel('Time (hr)', 'FontSize', 25, 'FontName',
'Times');
ylabel('pH Residuals', 'FontSize', 25, 'FontName',
'Times');

%calculating Root Mean Square Error
N = length(closestIndex);

SumResBiomass = sum(residualBiomass, 'all');
RMSEBiomass = sqrt((SumResBiomass^2)/N)

SumResTIC = sum(residualTIC, 'all');
RMSETIC = sqrt((SumResTIC^2)/N)

SumResCO2 = sum(residualCO2, 'all');
RMSECO2 = sqrt((SumResCO2^2)/N)

SumResHCO3 = sum(residualHCO3, 'all');
RMSEHCO3 = sqrt((SumResHCO3^2)/N)

SumResCO3 = sum(residualCO3, 'all');
RMSECO3 = sqrt((SumResCO3^2)/N)

SumResALK = sum(residualALK, 'all');
RMSEALK = sqrt((SumResALK^2)/N)

SumRespH = sum(residualpH, 'all');
RMSEpH = sqrt((SumRespH^2)/N)
```

APPENDIX II: MATLAB FUNCTION FILE CO_2/HCO_3 SUBSITUTABLE

```
function yp =
LZalgalModelCarbonateClosedFinal2sub(t,y);
%y(1)=carbon dioxide
%y(2)=carbonate
%y(3)=hydrogen ion
%y(4)=bicarb
%y(5)=hydroxide ion
%y(6)=water
%y(7)=active biomass
%y(8)= TIC
%y(9)= Nitrogen
%y(10)= TSS
%y(11-13) = muco2, muhco3, muco3, b respectively

%% Equilibrium Constants

%Note: Temperatures in Kelvin. K1, K2, K3, and KW are
specified for
%25C, but temperature-dependent relationships may also
be used.
T = 25+273.15;

%LF Values
KH2CO3 = 2.5e-4;
KW = 10^(-14.01);
K1 = 4.45e-7;
K2 = 4.84e-11;
K3 = 4645.3;

%Temp dependent relationships
% K1 = exp(290.9097-(14554.21/T)-(45.0575*log(T)));
% K2 = exp(207.6548-(11843.79/T)-(33.6485*log(T)));
% K3 = 10^((1568.94/T)+0.4134-(0.006737*T));

%% Carbonate Kinetic Constants

%Note: Temperatures in Kelvin.
kplus = 10^(10.685-(3618/T))*3600; % (1/hr)
kH2CO3 = 10^(13.770-(3699/T))*3600; % (1/hr)
kminus = kplus/K1; % (1/M-hr)
```

```
kplus4 = 10^(13.589-(2887/T))*3600; % (1/M-hr)
kminus4 = 10^(14.88-(5524/T))*3600; % (1/hr)
kminus5 = 5e10 * 3600; % (1/hr)
kplus5 = kminus5 * K2; % (1/M-hr)
kplus6 = 2.25e8 * 3600; %geo mean
kminus6 = kplus6/K3; %(1/hr)
kplus7 = 1.4e-3 *3600; % (M*hr)
kminus7 = kplus7/KW; %(1/M *hr)

%% Carbonate Rate Definitions

rf1 = kplus*y(1);%equation 6
rr1 = kminus*y(3)*y(4); %equation 6

rf2 = kplus4*y(1)*y(5); %equation 7
rr2 = kminus4*y(4); %equation 7

rf3 = kplus7;% equation 9
rr3 = kminus7*y(3)*y(5); %equation 9

rf4 = kplus5*y(4); % equation 4
rr4 = kminus5*y(2)*y(3); %equation 4

rf5 = kplus6*y(4)*y(5); %equation 8
rr5 = kminus6*y(2); %equation 8

%% TIC-limited Algal Growth Kinetic Constants
b = 0.00285; % (1/hr)
%KsCO2 = 4.47e-8; % (mol/L C)
KsCO2 = 5.36e-4 *(1/1000)*(1/12.0107); %uses conversion
factor and number from paper LZF 6/22/20
%KsHCO3 = 5.7e-4; % (mol/L C)
KsHCO3 = 6.84 *(1/1000)*(1/12.0107);
%KsCO3 = 8.7e-4; % (mol/L C)
KsCO3 = 10.4 *(1/1000)*(1/12.0107);
MuMax = 0.0726; % (hr^-1) TIC

%Note: Choose Nfactor, Pfactor, Cfactor based on TIC
treatment. Be
%sure C:N:P ratios are also specified correctly in the
demo file.
```

```
%use for 25%
%Nfactor = 1.01; % (mol N/mol X)
%Pfactor = 1; % (mol P/mol X)
%Cfactor = 6.16; % (mol C/mol X)

%use these for 50% C
% Nfactor = 0.947; % (mol N/mol X)
% Pfactor = 1; % (mol P/mol X)
% Cfactor = 6.18; % (mol C/mol X)

%use for 75%
Nfactor = 1.25; % (mol N/mol X)
Pfactor = 1; % (mol P/mol X)
Cfactor = 7.67; % (mol C/mol X)

%use for 100%
% Nfactor = 1.52; % (mol N/mol X)
% Pfactor = 1; % (mol P/mol X)
% Cfactor = 10.16; % (mol C/mol X)

%Note: Molecular weight of algae calculated based on
C:N:P ratios and
%general stoichiometric equation for algal growth
CH2O = Cfactor*(12.0107+(2*1.00794)+15.9994);
NH3 = Nfactor*(14.0067+(3*1.00794));
H3PO4 = Pfactor*(3*1.00794)+30.9738+15.9994;
MWalgae = CH2O + NH3 + H3PO4; % (g/mol X)

%% Light-Limited Algal Growth Kinetic Constants
Ksl = 45.9; % (micro-E/m^2*s) orginal
Io = 121; % (micro-E/m^2*s)
TSS = y(10)*MWalgae*1000; % (g/m^3) or (mg/L)
K = 1.4+0.0592*TSS; % (1/m)
h = 0.2032; %/3; %(m)--8 in.
I = (Io*(1-exp(-K*(h))))/(K*(h)); %original

%% TIC-Limited Algal Growth Stoichiometric Constants

%photosynthetic oxygen production
p = (0.5* ((212/106*Cfactor)+(4*Nfactor)));
```

```
%Note: H2Ofactors (mol H2O/mol X) and Hfactors (mol
H/mol X)
%are calculated based on C:N:P ratios and general
stoichiometric
%%equation for algal growth.
H2OfactorCO2 = -Cfactor-(3*Nfactor)+(2*p);
HfactorCO2 = (2*Cfactor)+(3*Nfactor)+2-
(2*H2OfactorCO2);
H2OfactorHCO3 = (-Cfactor*2)-(3*Nfactor)+(2*p);
HfactorHCO3 = Cfactor+(3*Nfactor)+3-1-
(2*H2OfactorHCO3);
% H2OfactorCO3= (-2*Cfactor)-(3*Nfactor)+(2*p);
% HfactorCO3 = (2*Cfactor)+(3*Nfactor)+2-
(2*H2OfactorCO3);

%% TIC and Light-Limited Algal Specific Growth Rates

% MuMax = 0.0726; % (hr^-1) TIC
% Ks = 1.46E-3; % (mol/L C) TIC

% MuMaxCO2 = 0.0728; %(hr-1) SAS avg only
% MuMaxHCO3 = 0.0743; %(hr-1) SAS avg only
% MuMaxCO3 = 0.071;   %(hr-1) SAS avg only

MuMaxCO2 = 0.079; %(hr-1) all averaged together
MuMaxHCO3 = 0.07935; %(hr-1)all averaged together
MuMaxCO3 = 0.0703;   %(hr-1) all averaged together

MuCO2 = MuMaxCO2 *(y(1)/(KsCO2+y(1)))*(I/(Ksl+I));
MuHCO3 = MuMaxHCO3
*(y(4)/(KsHCO3+y(4)))*(KsCO2/(KsCO2+y(1)))*(I/(Ksl+I));
MuCO3 = MuMaxCO3
*(y(2)/(KsCO3+y(2)))*(KsCO2/(KsCO2+y(1)))*(KsHCO3/(KsHC
O3+y(4)))*(I/(Ksl+I));

%% Nutrient Utilization Rates

CutilizationCO2 = Cfactor*MuCO2*y(7);
CutilizationHCO3 = Cfactor*MuHCO3*y(7);

HutilizationCO2 = HfactorCO2*MuCO2*y(7);
HutilizationHCO3 = HfactorHCO3*MuHCO3*y(7);
```

```
H2OutilizationCO2 = H2OfactorCO2*MuCO2*y(7);
H2OutilizationHCO3 = H2OfactorHCO3*MuHCO3*y(7);

Nutilization = Nfactor*(MuCO2*y(7)+MuHCO3*y(7));%

%% Differential Mass Balance Equations

%CO2 -- y(1)
CO2_balance = -rf1 +rr1 -rf2 +rr2 -CutilizationCO2;

%CO3 -- y(2)
CO3_balance = -rr4 +rf4 +rf5 -rr5;

%H -- y(3)
H_balance = rf1 -rr1 +rf3 -rr3 -rr4 +rf4 -
HutilizationCO2 -HutilizationHCO3;

%HCO3 -- y(4)
HCO3_balance = rf1 -rr1 +rf2 -rr2 +rr4 -rf4 -rf5 +rr5 -
CutilizationHCO3;

%OH -- y(5)
OH_balance = -rf2 +rr2 +rf3 -rr3 -rf5 +rr5  ;%

%H2O -- y(6)
H2O_balance = -rf1 +rr1 -rf3 +rr3 +rf5 -rr5 -
H2OutilizationCO2 -H2OutilizationHCO3;

%Biomass -- y(7)
XformCO2 = MuCO2*y(7);
XformHCO3 = MuHCO3*y(7);
%XformCO3 = MuCO3*y(7);
Xdecay = b*y(7);
Xbalance = XformCO2  + XformHCO3  - Xdecay ;%+XformCO3

% TIC -- y(8)
CarbonBalance = (CO2_balance + CO3_balance +
HCO3_balance);

% Nitrogen -- y(9)
N_balance = - Nutilization;
```

```
% Biomass, TSS -- y(10)
XT = XformCO2 + XformHCO3; %+XformCO3

%% System of Differential Equations Output
yp = [CO2_balance
CO3_balance
H_balance
HCO3_balance
OH_balance
H2O_balance
Xbalance
CarbonBalance
N_balance
XT
MuCO2
MuHCO3
MuCO3
b];
```

APPENDIX III: MATLAB FUNCTION FILE $CO_2/HCO_3/CO_3$ SUBSITUTABLE

```
function yp = LZalgalModelCarbonateClosedFinal(t,y);
%y(1)=carbon dioxide
%y(2)=carbonate
%y(3)=hydrogen ion
%y(4)=bicarb
%y(5)=hydroxide ion
%y(6)=water
%y(7)=active biomass
%y(8)= TIC
%y(9)= Nitrogen
%y(10)= TSS
%y(11-13) = muco2, muhco3, muco3, b respectively

%% Equilibrium Constants

%Note: Temperatures in Kelvin. K1, K2, K3, and KW are
specified for
%25C, but temperature-dependent relationships may also
be used.
T = 25+273.15;

%LF Values
KH2CO3 = 2.5e-4;
KW = 10^(-14.01);
K1 = 4.45e-7;
K2 = 4.84e-11;
K3 = 4645.3;

%Temp dependent relationships
% K1 = exp(290.9097-(14554.21/T)-(45.0575*log(T)));
% K2 = exp(207.6548-(11843.79/T)-(33.6485*log(T)));
% K3 = 10^((1568.94/T)+0.4134-(0.006737*T));

%% Carbonate Kinetic Constants

%Note: Temperatures in Kelvin.
kplus = 10^(10.685-(3618/T))*3600; % (1/hr)
kH2CO3 = 10^(13.770-(3699/T))*3600; % (1/hr)
kminus = kplus/K1; % (1/M-hr)
kplus4 = 10^(13.589-(2887/T))*3600; % (1/M-hr)
```

```
kminus4 = 10^(14.88-(5524/T))*3600; % (1/hr)
kminus5 = 5e10 * 3600; % (1/hr)
kplus5 = kminus5 * K2; % (1/M-hr)
kplus6 = 2.25e8 * 3600; %geo mean
kminus6 = kplus6/K3; %(1/hr)
kplus7 = 1.4e-3 *3600; % (M*hr)
kminus7 = kplus7/KW; %(1/M *hr)

%% Carbonate Rate Definitions

rf1 = kplus*y(1);%equation 6
rr1 = kminus*y(3)*y(4); %equation 6

rf2 = kplus4*y(1)*y(5); %equation 7
rr2 = kminus4*y(4); %equation 7

rf3 = kplus7;% equation 9
rr3 = kminus7*y(3)*y(5); %equation 9

rf4 = kplus5*y(4); % equation 4
rr4 = kminus5*y(2)*y(3); %equation 4

rf5 = kplus6*y(4)*y(5); %equation 8
rr5 = kminus6*y(2); %equation 8

%% TIC-limited Algal Growth Kinetic Constants
% if t < 92
%     b = 0;
% else
%     b = 0.00285; % (1/hr)
% end
b = 0.00285; % (1/hr)
%KsCO2 = 4.47e-8; % (mol/L C)
KsCO2 = 5.36e-4 *(1/1000)*(1/12.0107); %uses conversion
factor and number from paper LZF 6/22/20
%KsHCO3 = 5.7e-4; % (mol/L C)
KsHCO3 = 6.84 *(1/1000)*(1/12.0107);
%KsCO3 = 8.7e-4; % (mol/L C)
KsCO3 = 10.4 *(1/1000)*(1/12.0107);
MuMax = 0.0726; % (hr^-1) TIC
```

```
%Note: Choose Nfactor, Pfactor, Cfactor based on TIC
treatment. Be
%sure C:N:P ratios are also specified correctly in the
demo file.

%use for 25%
Nfactor = 1.01; % (mol N/mol X)
Pfactor = 1; % (mol P/mol X)
Cfactor = 6.16; % (mol C/mol X)

%use these for 50% C
% Nfactor = 0.947; % (mol N/mol X)
% Pfactor = 1; % (mol P/mol X)
% Cfactor = 6.18; % (mol C/mol X)

%use for 75%
% Nfactor = 1.25; % (mol N/mol X)
% Pfactor = 1; % (mol P/mol X)
% Cfactor = 7.67; % (mol C/mol X)

%use for 100%
% Nfactor = 1.52; % (mol N/mol X)
% Pfactor = 1; % (mol P/mol X)
% Cfactor = 10.16; % (mol C/mol X)

%Cfactor = (-7e9 * y(1))+10.898; %trail value

%Note: Molecular weight of algae calculated based on
C:N:P ratios and
%general stoichiometric equation for algal growth
CH2O = Cfactor*(12.0107+(2*1.00794)+15.9994);
NH3 = Nfactor*(14.0067+(3*1.00794));
H3PO4 = Pfactor*(3*1.00794)+30.9738+15.9994;
MWalgae = CH2O + NH3 + H3PO4; % (g/mol X)

%% Light-Limited Algal Growth Kinetic Constants
Ksl = 45.9; % (micro-E/m^2*s) orginal
Io = 121; % (micro-E/m^2*s)
TSS = y(10)*MWalgae*1000; % (g/m^3) or (mg/L)
K = 1.4+0.0592*TSS; % (1/m)
h = 0.2032; %/3; %(m)--8 in.
I = (Io*(1-exp(-K*(h))))/(K*(h)); %original
```

```
%% TIC-Limited Algal Growth Stoichiometric Constants

%photosynthetic oxygen production
p = (0.5* ((212/106*Cfactor)+(4*Nfactor)));

%Note: H2Ofactors (mol H2O/mol X) and Hfactors (mol
H/mol X)
%are calculated based on C:N:P ratios and general
stoichiometric
%%equation for algal growth.
H2OfactorCO2 = -Cfactor-(3*Nfactor)+(2*p);
HfactorCO2 = (2*Cfactor)+(3*Nfactor)+2-
(2*H2OfactorCO2);
H2OfactorHCO3 = (-Cfactor*2)-(3*Nfactor)+(2*p);
HfactorHCO3 = Cfactor+(3*Nfactor)+3-1-
(2*H2OfactorHCO3);
H2OfactorCO3= (-2*Cfactor)-(3*Nfactor)+(2*p);
HfactorCO3 = (2*Cfactor)+(3*Nfactor)+2-
(2*H2OfactorCO3);

%% TIC and Light-Limited Algal Specific Growth Rates

% MuMax = 0.0726; % (hr^-1) TIC
% Ks = 1.46E-3; % (mol/L C) TIC

% MuMaxCO2 = 0.0728; %(hr-1) SAS avg only
% MuMaxHCO3 = 0.0743; %(hr-1) SAS avg only
% MuMaxCO3 = 0.071;   %(hr-1) SAS avg only

MuMaxCO2 = 0.079; %(hr-1) all averaged together
MuMaxHCO3 = 0.07935; %(hr-1)all averaged together
MuMaxCO3 = 0.0703;   %(hr-1) all averaged together

MuCO2 = MuMaxCO2 *(y(1)/(KsCO2+y(1)))*(I/(Ksl+I));
MuHCO3 = MuMaxHCO3
*(y(4)/(KsHCO3+y(4)))*(KsCO2/(KsCO2+y(1)))*(I/(Ksl+I));
MuCO3 = MuMaxCO3
*(y(2)/(KsCO3+y(2)))*(KsCO2/(KsCO2+y(1)))*(KsHCO3/(KsHC
O3+y(4)))*(I/(Ksl+I));

%% Nutrient Utilization Rates
```

```
CutilizationCO2 = Cfactor*MuCO2*y(7);
CutilizationHCO3 = Cfactor*MuHCO3*y(7);
CutilizationCO3 = Cfactor*MuCO3*y(7);

HutilizationCO2 = HfactorCO2*MuCO2*y(7);
HutilizationHCO3 = HfactorHCO3*MuHCO3*y(7);
HutilizationCO3 = HfactorCO3*MuCO3*y(7);

H2OutilizationCO2 = H2OfactorCO2*MuCO2*y(7);
H2OutilizationHCO3 = H2OfactorHCO3*MuHCO3*y(7);
H2OutilizationCO3 = H2OfactorCO3*MuCO3*y(7);

Nutilization = Nfactor*(MuCO2*y(7)+MuHCO3*y(7));%

%% Differential Mass Balance Equations

%CO2 -- y(1)
CO2_balance = -rf1 +rr1 -rf2 +rr2 -CutilizationCO2;

%CO3 -- y(2)
CO3_balance = -rr4 +rf4 +rf5 -rr5 -CutilizationCO3;

%H -- y(3)
H_balance = rf1 -rr1 +rf3 -rr3 -rr4 +rf4 -
HutilizationCO2 -HutilizationHCO3-HutilizationCO3;

%HCO3 -- y(4)
HCO3_balance = rf1 -rr1 +rf2 -rr2 +rr4 -rf4 -rf5 +rr5 -
CutilizationHCO3;

%OH -- y(5)
OH_balance = -rf2 +rr2 +rf3 -rr3 -rf5 +rr5  ;%

%H2O -- y(6)
H2O_balance = -rf1 +rr1 -rf3 +rr3 +rf5 -rr5 -
H2OutilizationCO2 -H2OutilizationHCO3 -
H2OutilizationCO3 ;

%Biomass -- y(7)
XformCO2 = MuCO2*y(7);
XformHCO3 = MuHCO3*y(7);
```

```
XformCO3 = MuCO3*y(7);
Xdecay = b*y(7);
Xbalance = XformCO2  + XformHCO3  - Xdecay +XformCO3 ;%

% TIC -- y(8)
CarbonBalance = (CO2_balance + CO3_balance +
HCO3_balance);

% Nitrogen -- y(9)
N_balance = - Nutilization;

% Biomass, TSS -- y(10)
XT = XformCO2 + XformHCO3 +XformCO3; %

%% System of Differential Equations Output
yp = [CO2_balance
CO3_balance
H_balance
HCO3_balance
OH_balance
H2O_balance
Xbalance
CarbonBalance
N_balance
XT
MuCO2
MuHCO3
MuCO3
b];
```

APPENDIX IV: RESIDUAL PLOTS OF CO_2/HCO_3 SUBSTITUTABLE MODEL

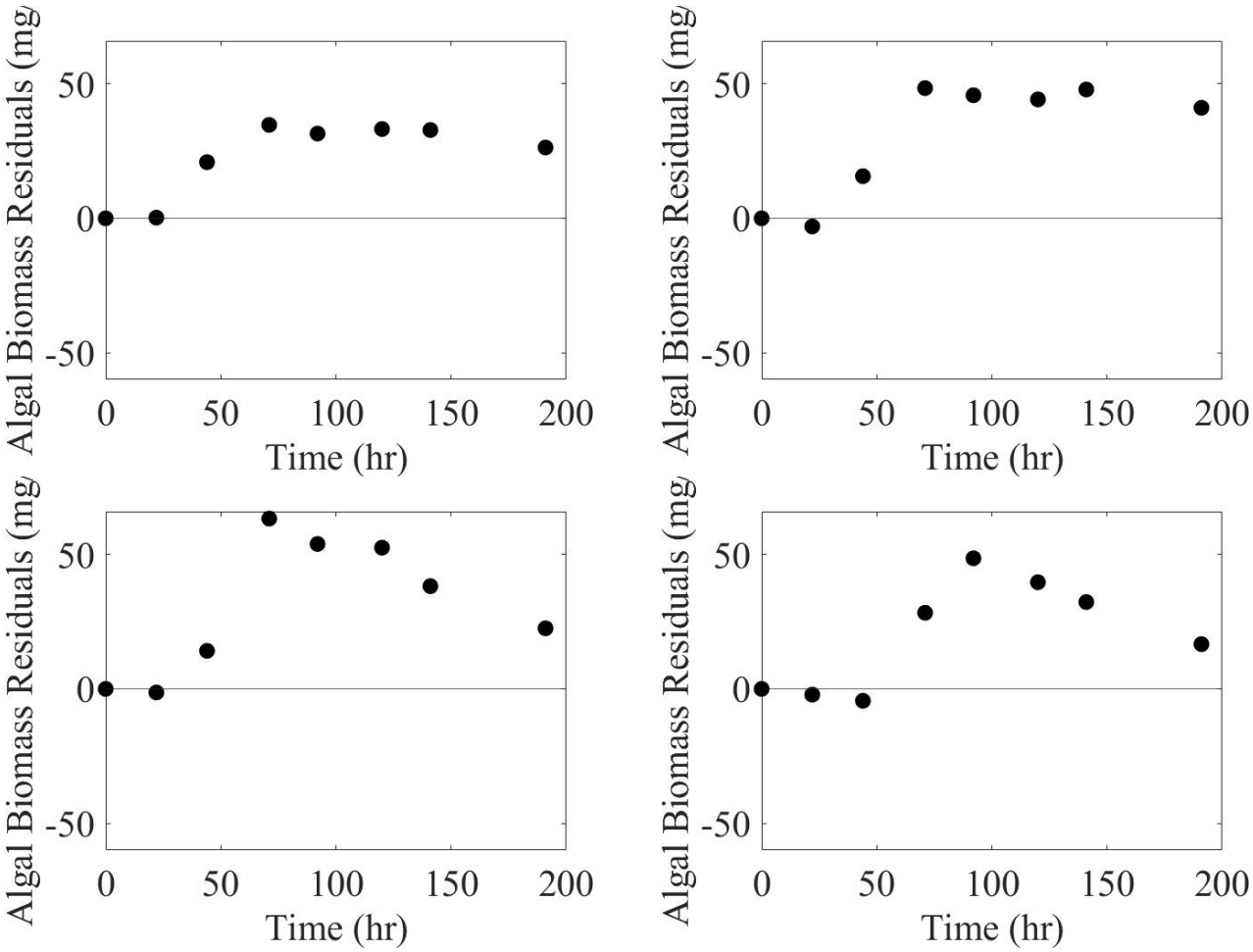

Figure A4.1: Algal Biomass TSS Residual Plots for 6, 11 (Top, Left to Right) and 17, 23 (Bottom, Left to Right) mg C L^{-1}

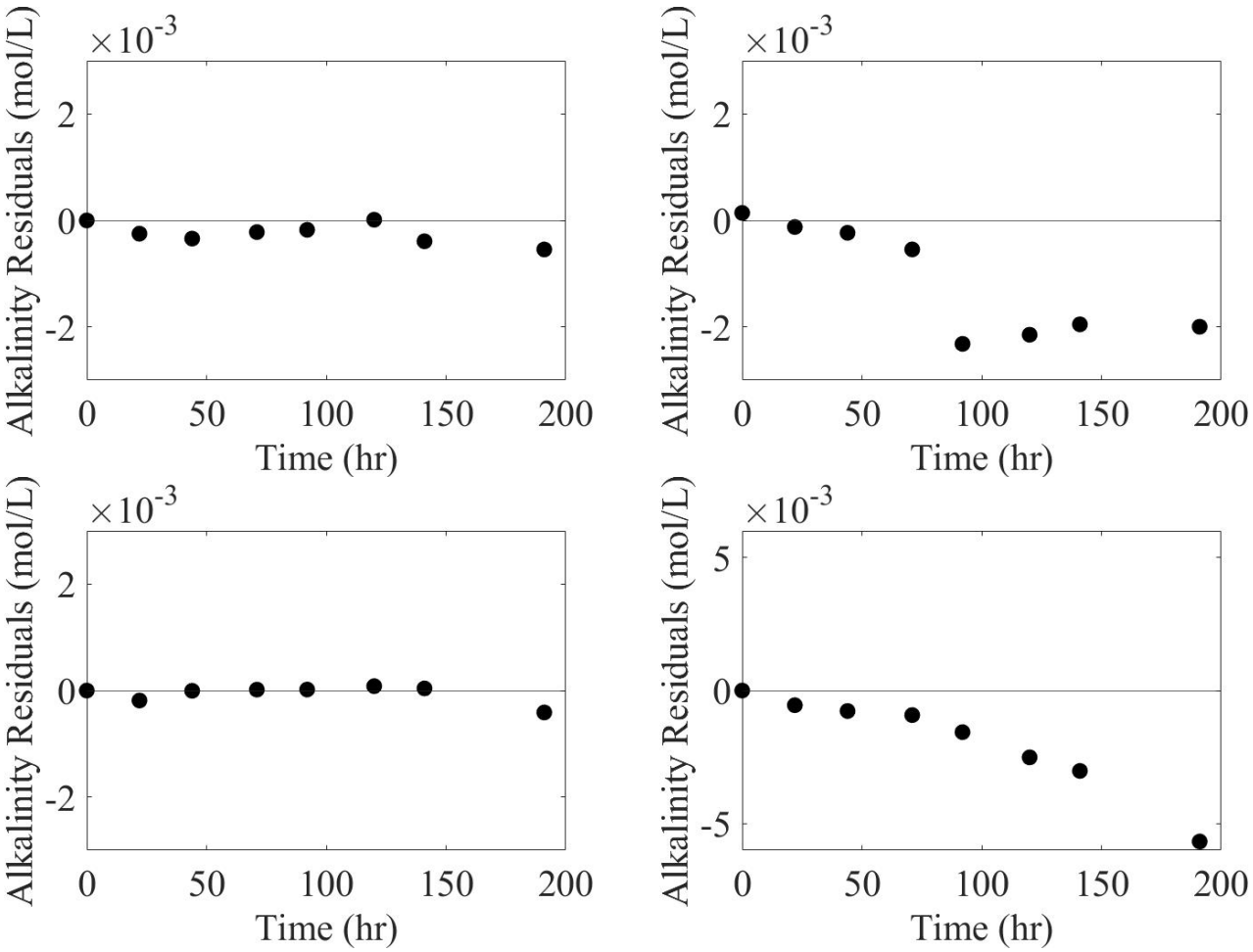

Figure A4.2: Alkalinity Residual Plots for 6, 11 (Top, Left to Right) and 17, 23 (Bottom, Left to Right) mg C L^{-1}

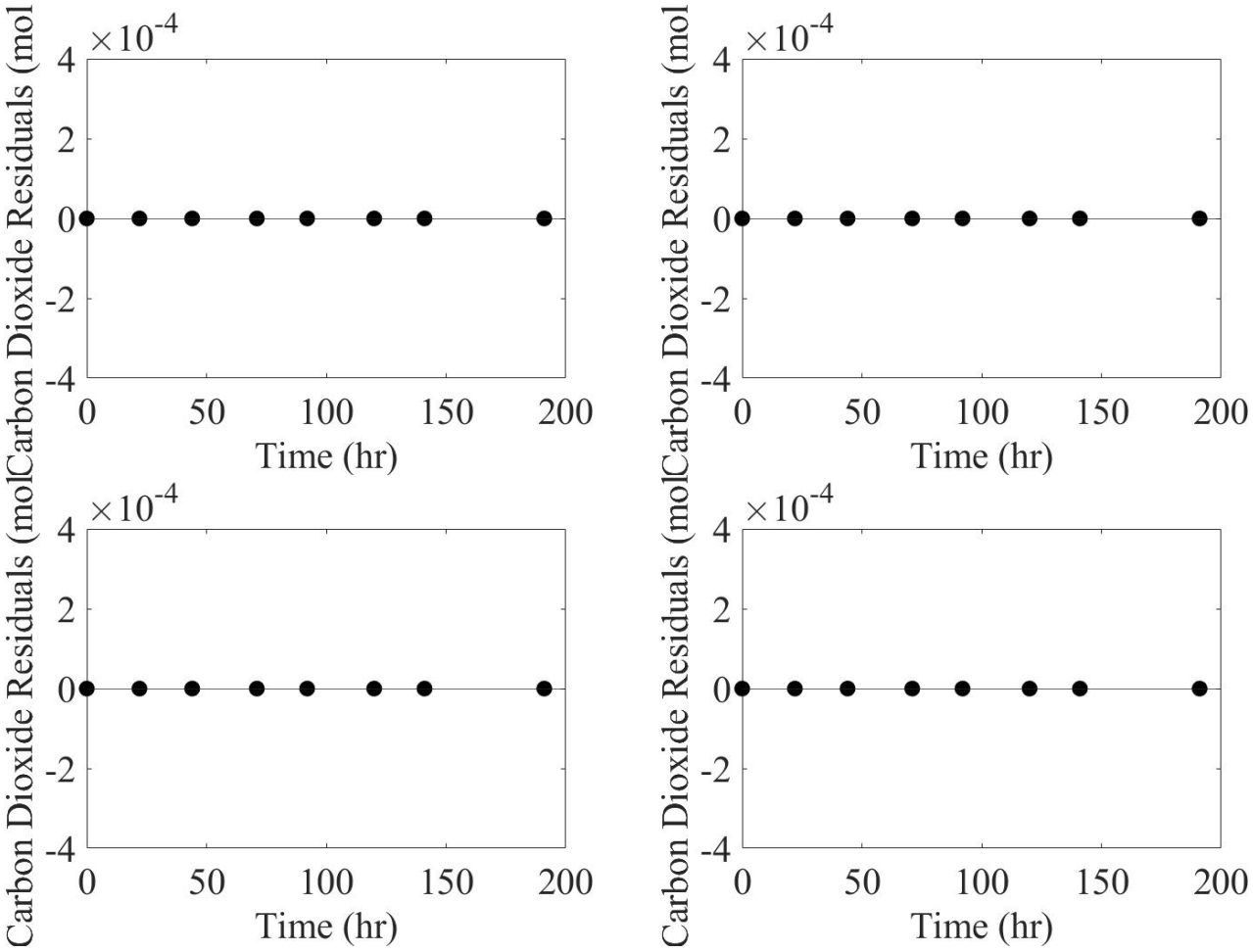

Figure A4.3: Carbon Dioxide Residual Plots for 6, 11 (Top, Left to Right) and 17, 23 (Bottom, Left to Right) mg C L^{-1}

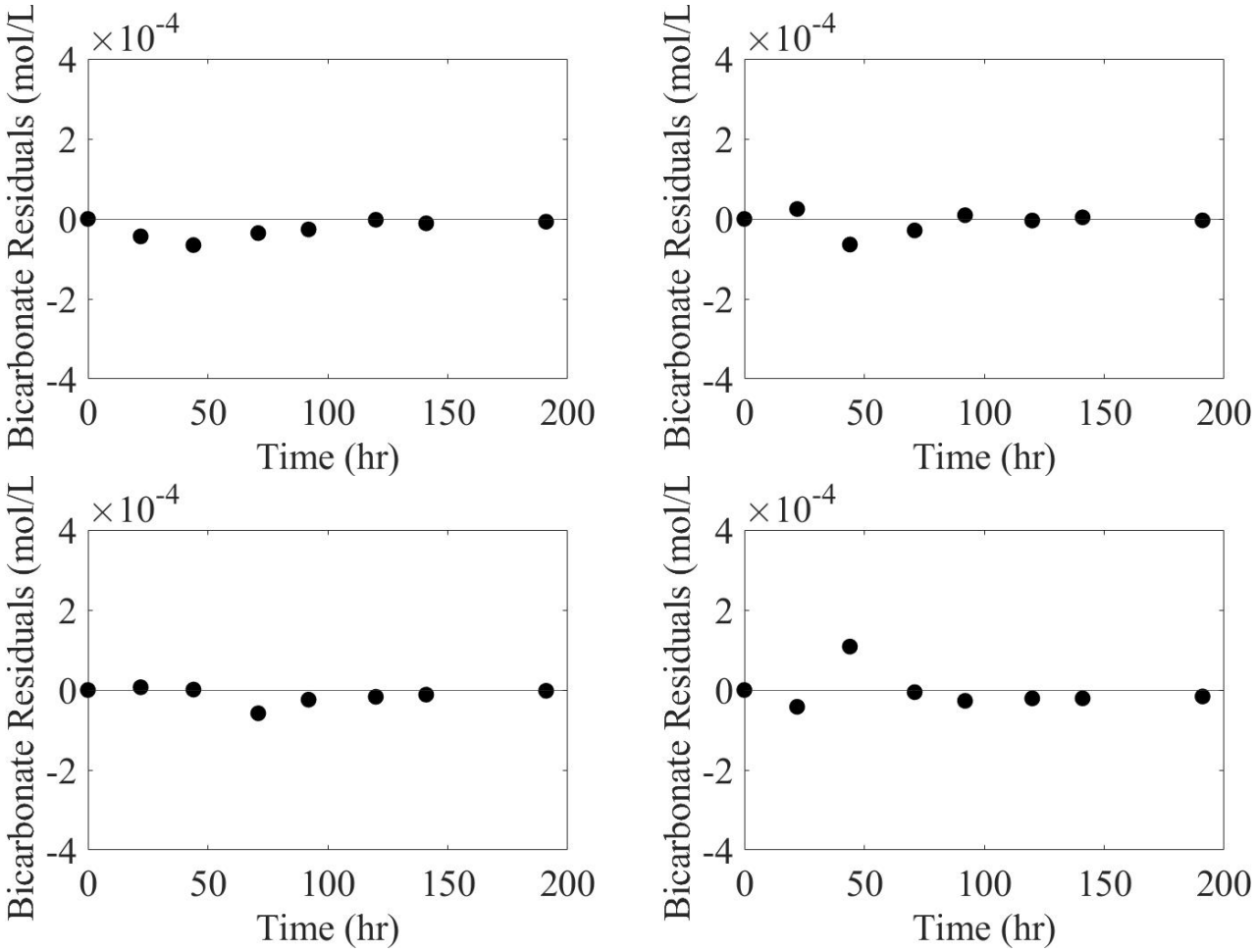

Figure A4.4: Bicarbonate Residual Plots for 6, 11 (Top, Left to Right) and 17, 23 (Bottom, Left to Right) mg C L^{-1}

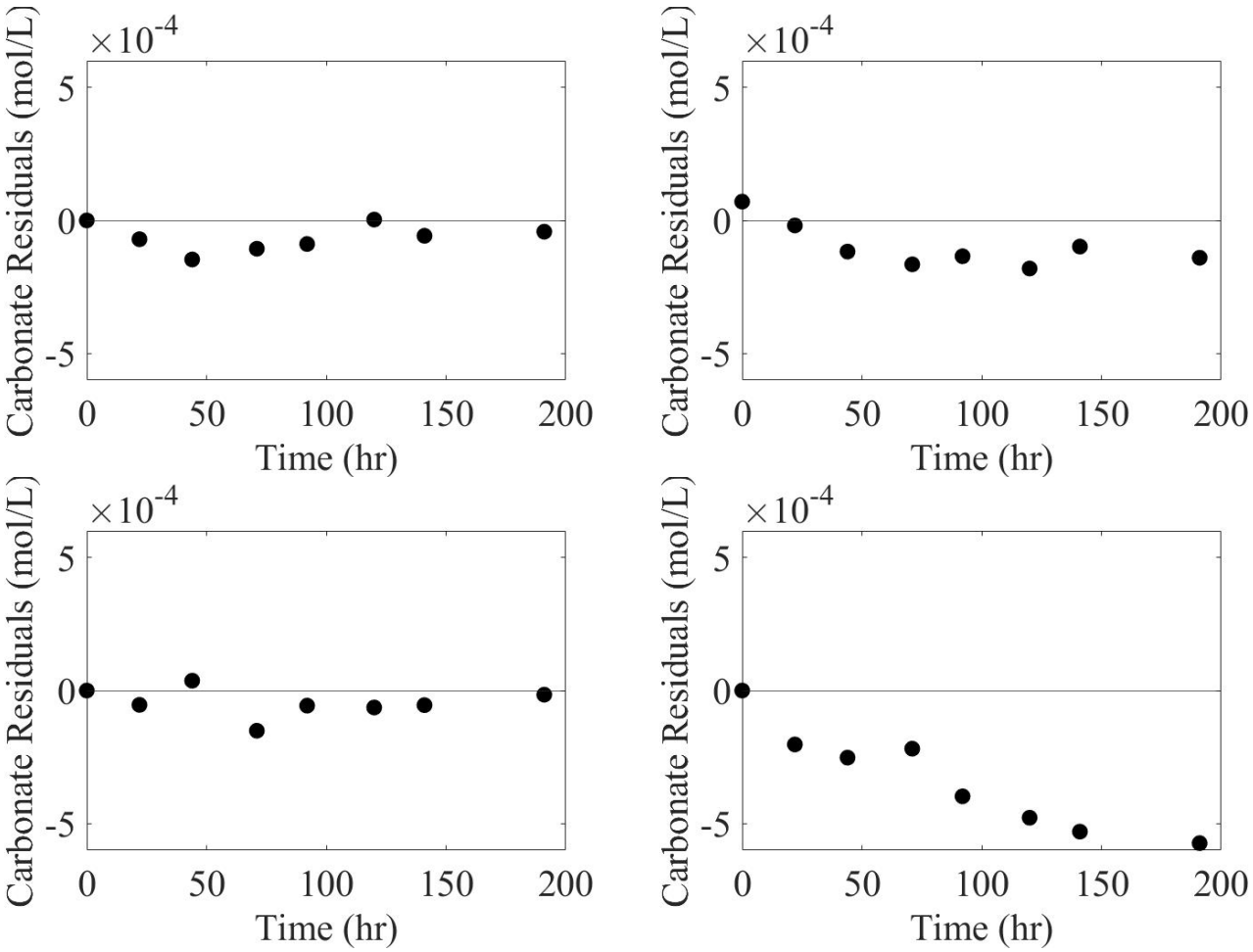

Figure A4.5: Carbonate Residual Plots for 6, 11 (Top, Left to Right) and 17, 23 (Bottom, Left to Right) mg C L-1

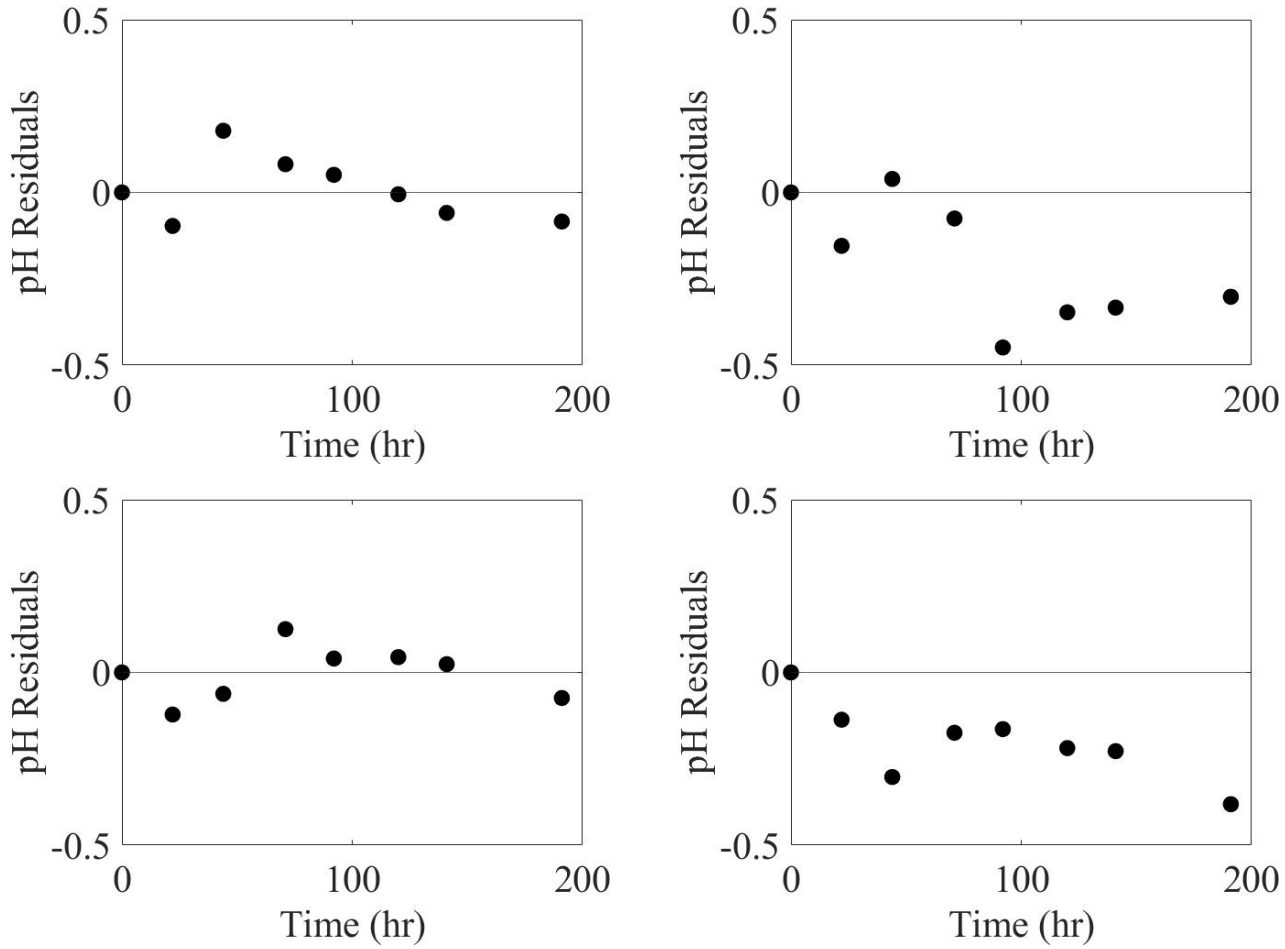

Figure A4.6: pH Residual Plots for 6, 11 (Top, Left to Right) and 17, 23 (Bottom, Left to Right) mg C L-1

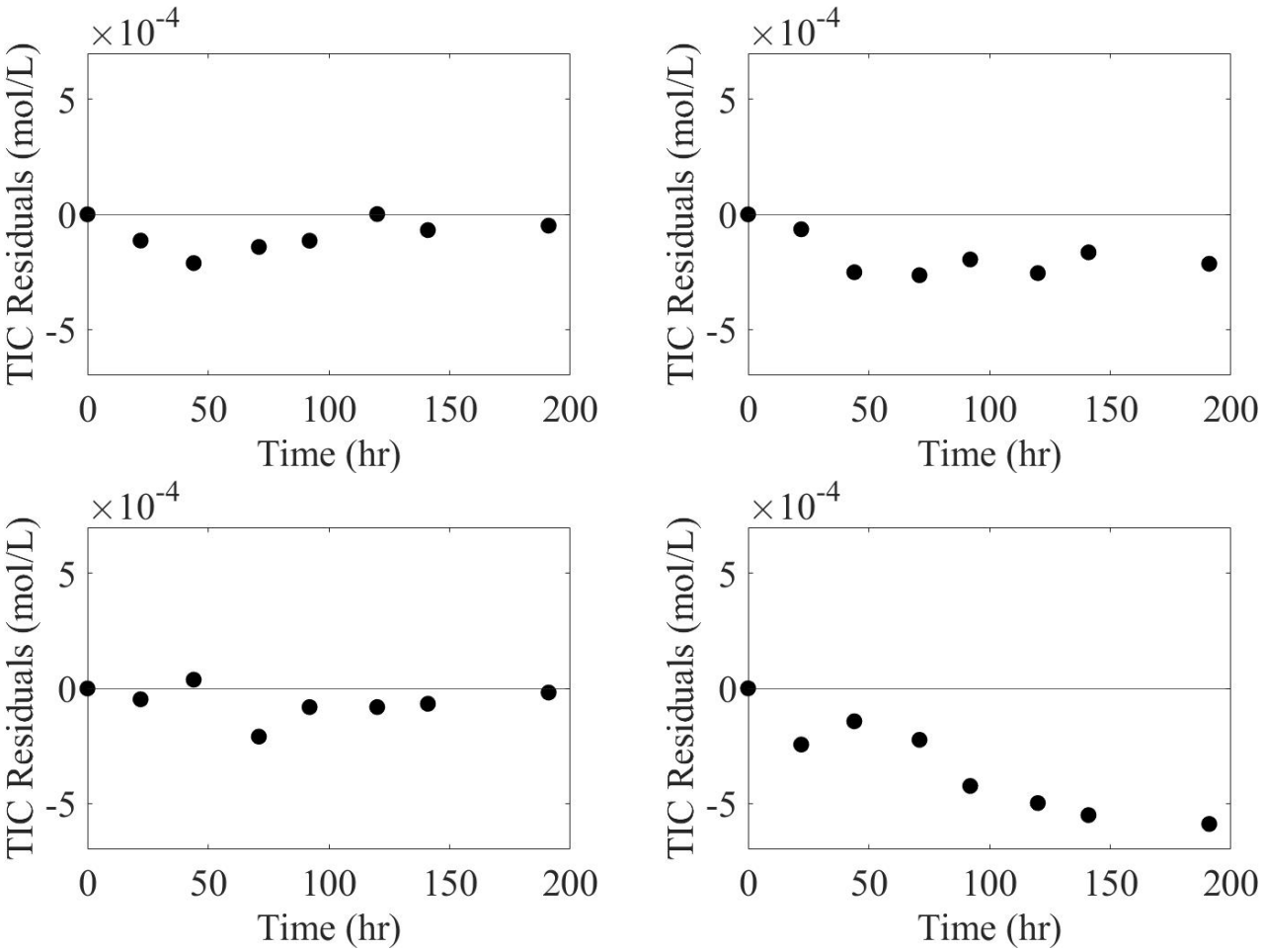

Figure A4.7: TIC Residual Plots for 6, 11 (Top, Left to Right) and 17, 23 (Bottom, Left to Right) mg C L-1

APPENDIX V: RESIDUAL PLOTS OF $CO_2/HCO_3/CO_3$ SUBSTITUTABLE MODEL

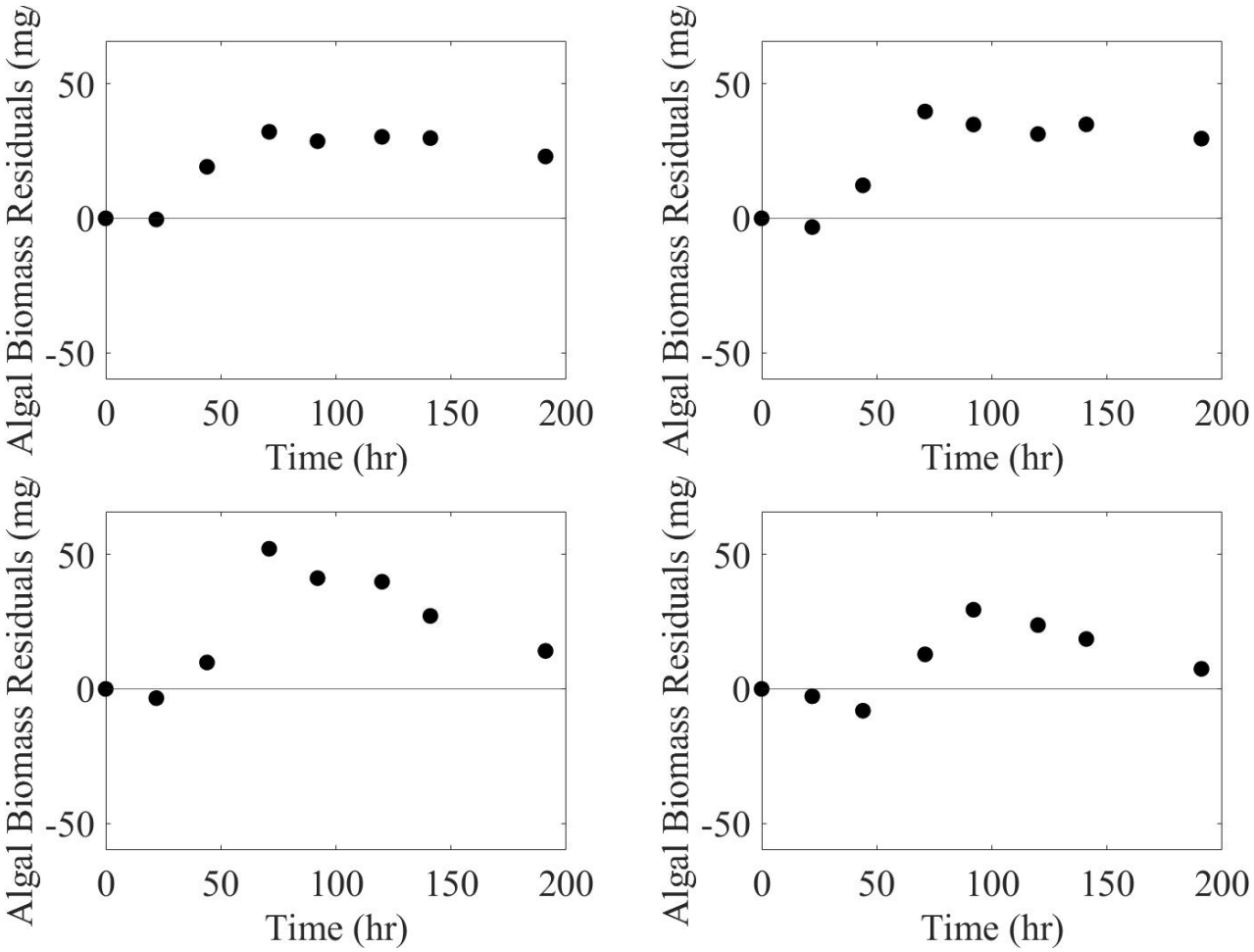

Figure A5.1: Algal Biomass TSS Residual Plots for 6, 11 (Top, Left to Right) and 17, 23 (Bottom, Left to Right) mg C L^{-1}

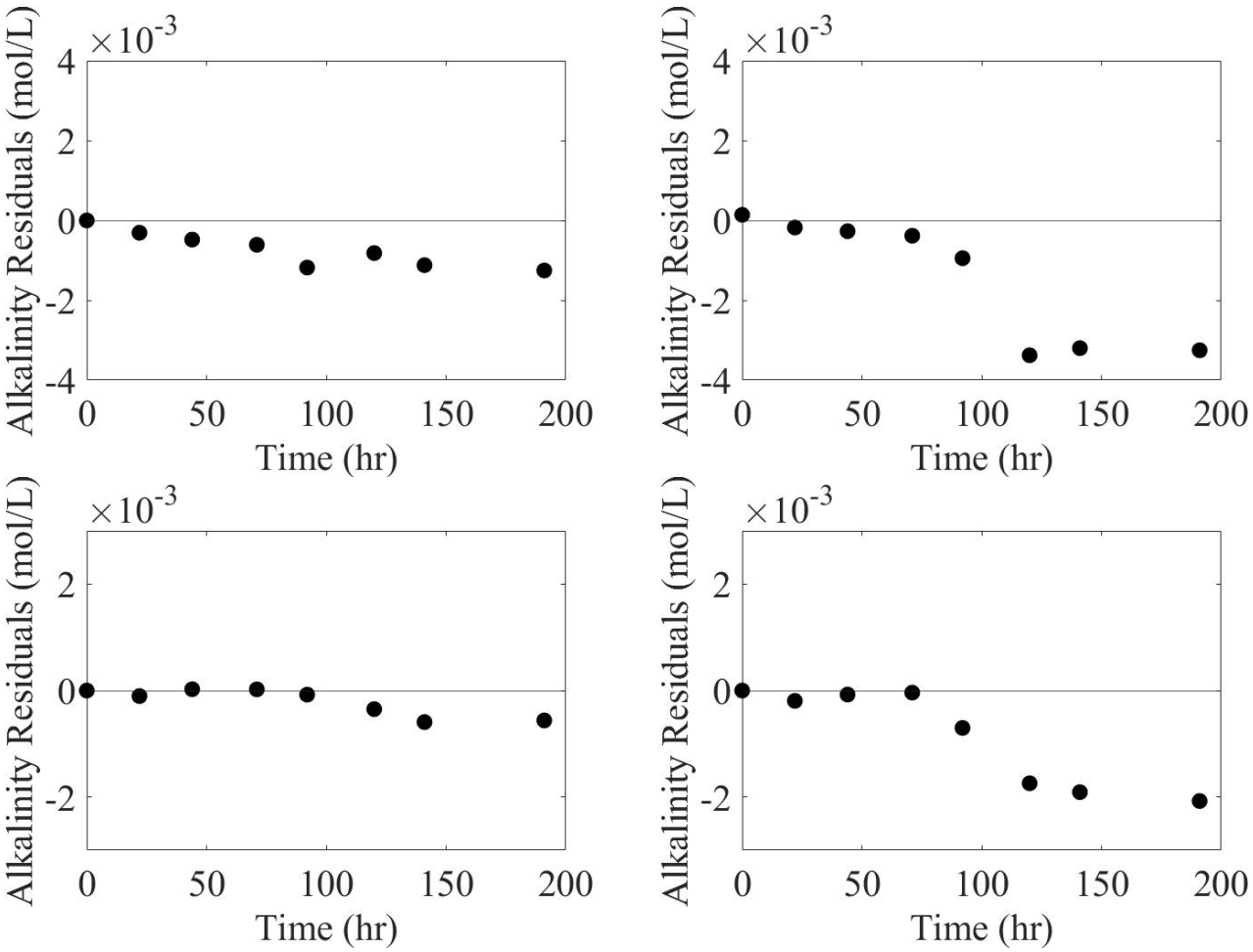

Figure A5.2: Alkalinity Residual Plots for 6, 11 (Top, Left to Right) and 17, 23 (Bottom, Left to Right) mg C L^{-1}

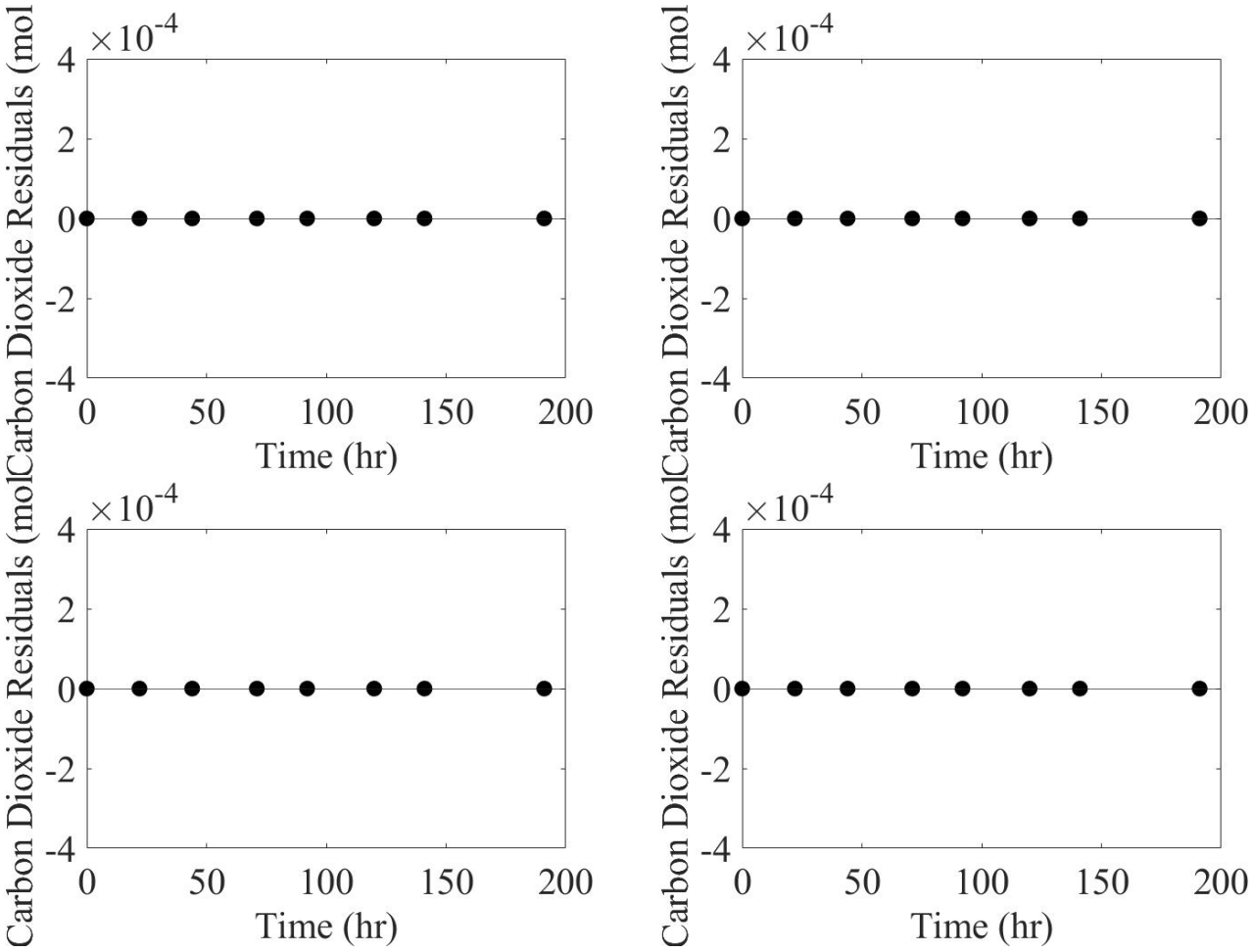

Figure A5.3: Carbon Dioxide Residual Plots for 6, 11 (Top, Left to Right) and 17, 23 (Bottom, Left to Right) mg C L^{-1}

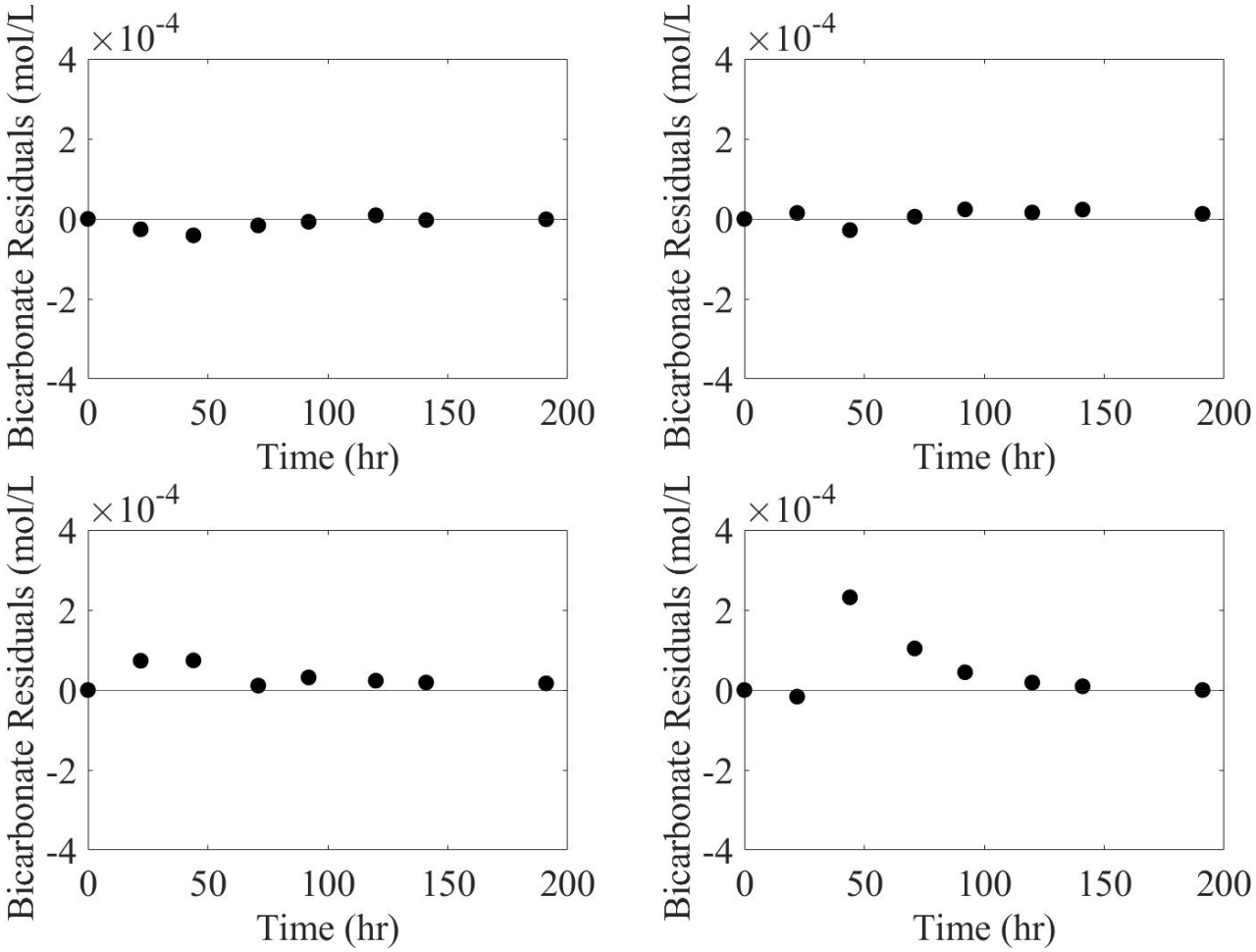

Figure A5.4: Bicarbonate Residual Plots for 6, 11 (Top, Left to Right) and 17, 23 (Bottom, Left to Right) mg C L^{-1}

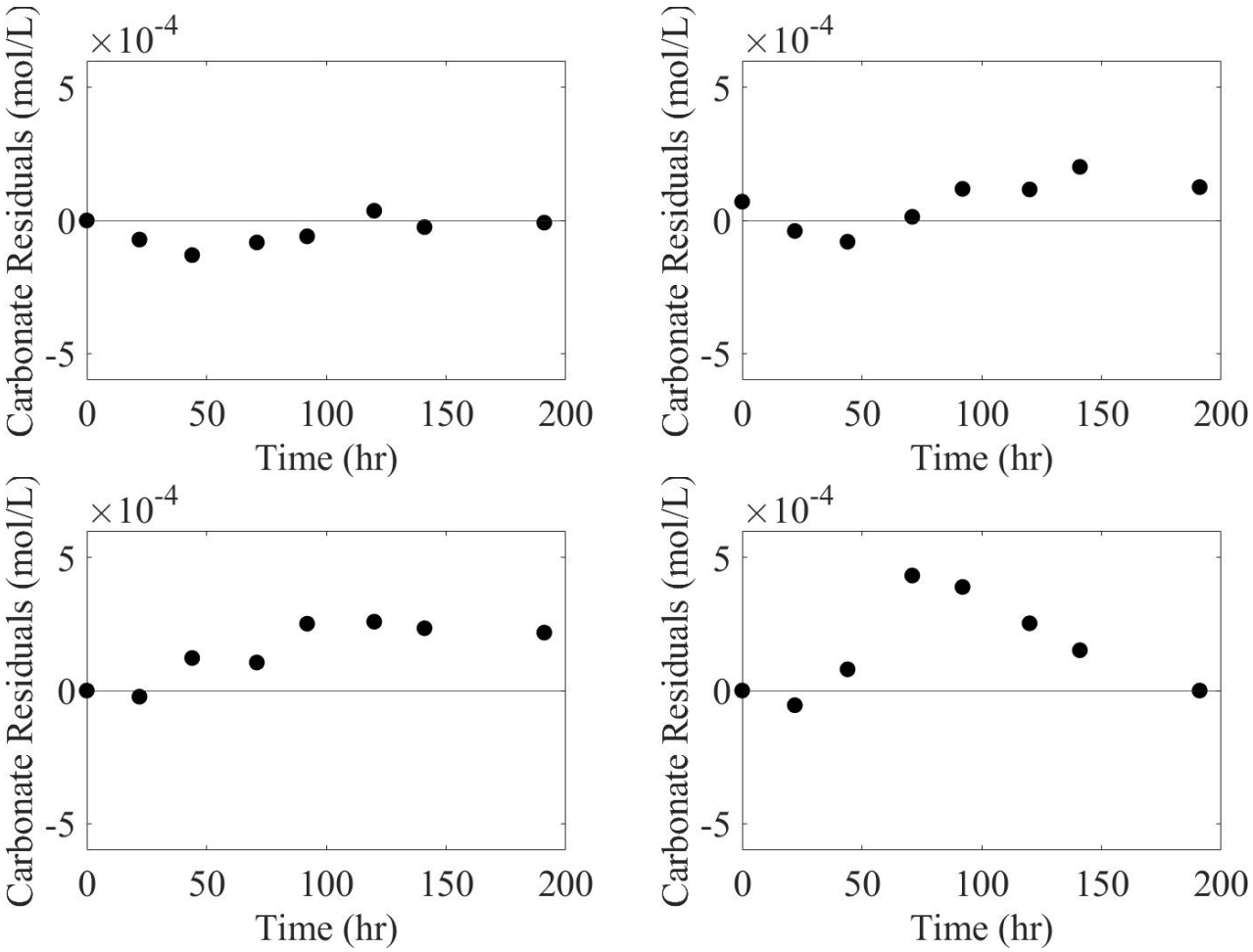

Figure A5.5: Carbonate Residual Plots for 6, 11 (Top, Left to Right) and 17, 23 (Bottom, Left to Right) mg C L^{-1}

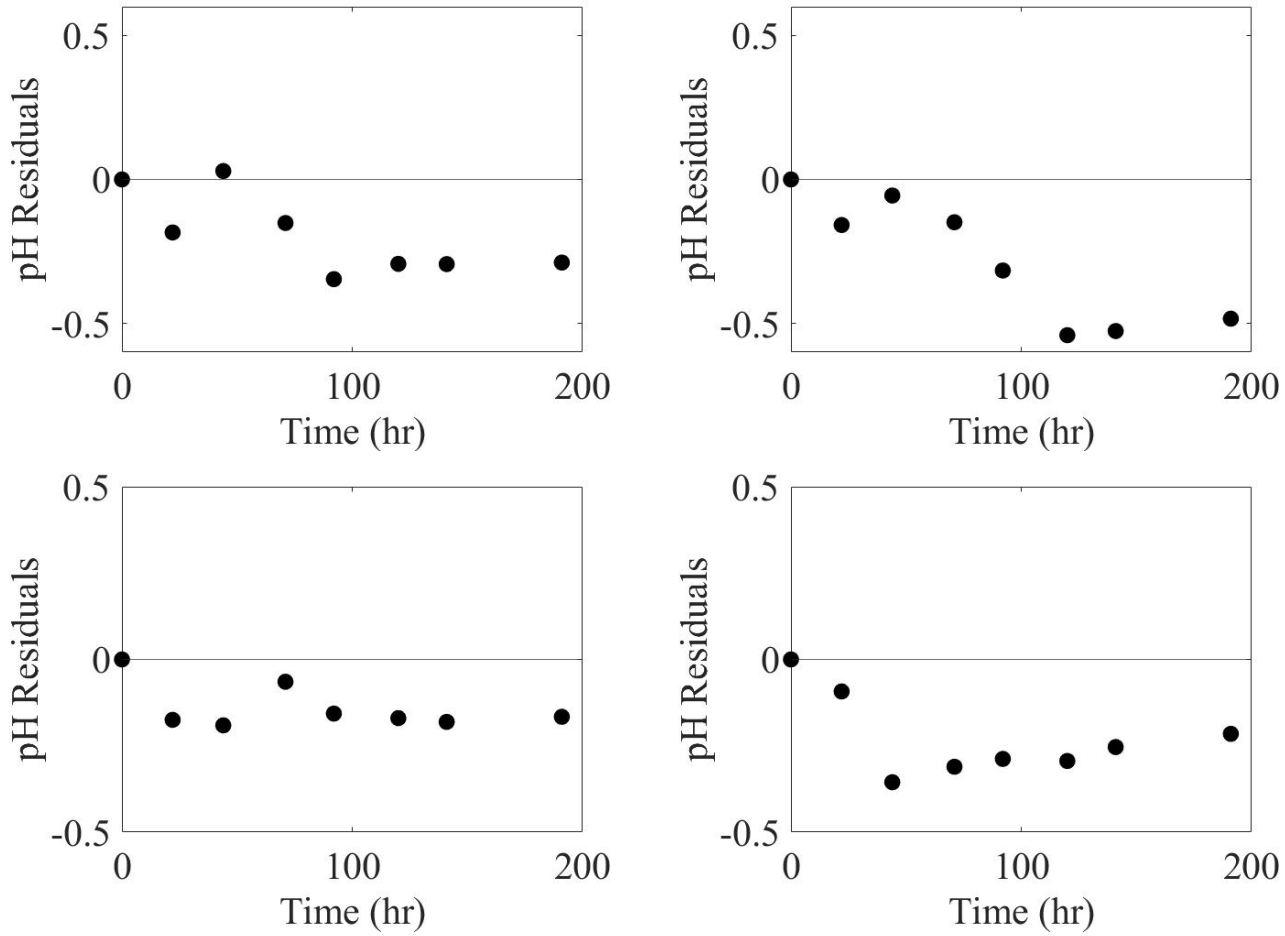

Figure A5.6: pH Residual Plots for 6, 11 (Top, Left to Right) and 17, 23 (Bottom, Left to Right) mg C L^{-1}

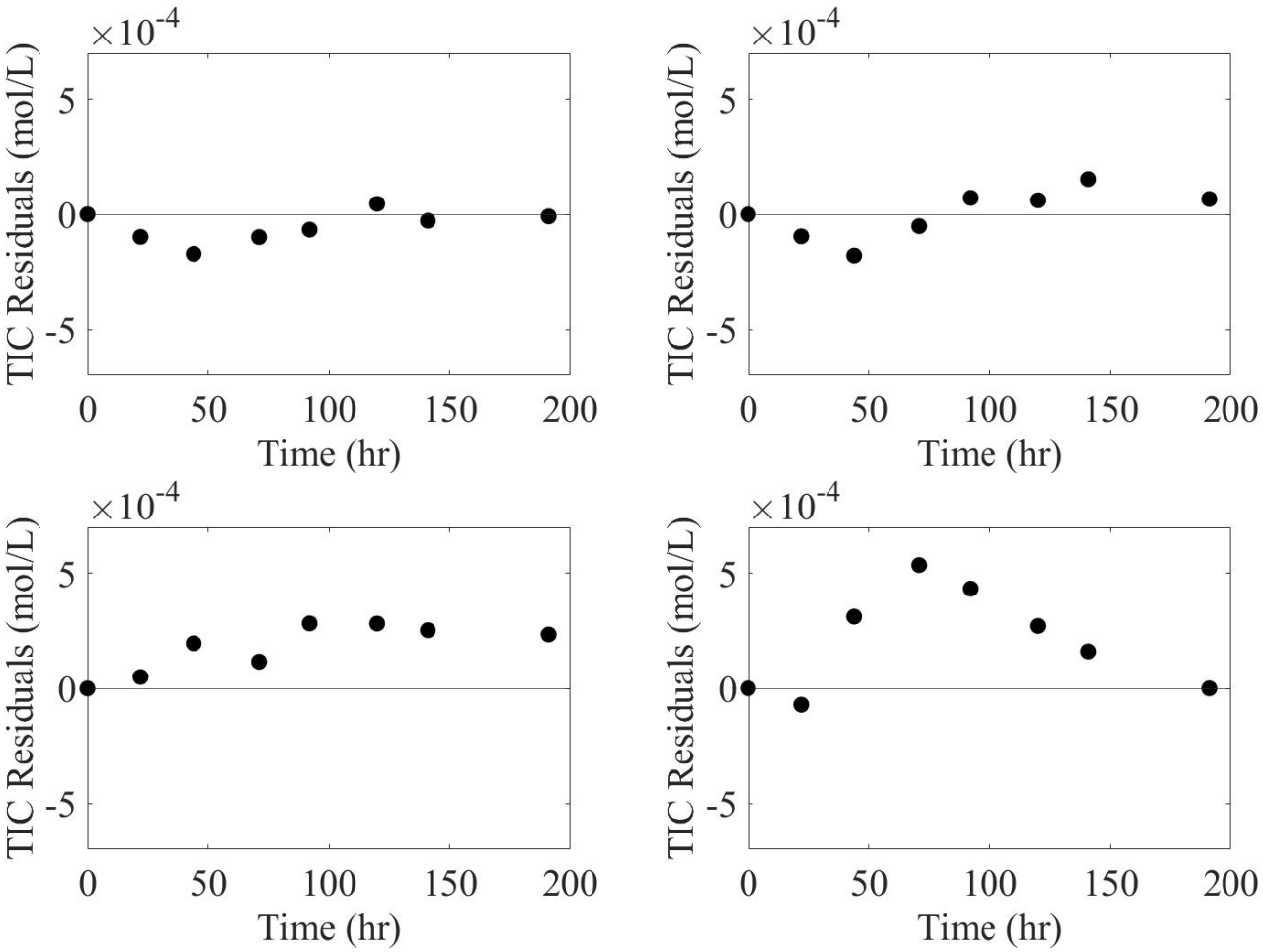

Figure A5.7: TIC Residual Plots for 6, 11 (Top, Left to Right) and 17, 23 (Bottom, Left to Right) mg C L^{-1}